2000-09

Inferring bottom acoustic properties from AN/SQQ-32 Sonar Reverberation data.

Howell, Henry R. G.

Monterey, California. Naval Postgraduate School

NAVAL POSTGRADUATE SCHOOL
Monterey, California

THESIS

INFERRING BOTTOM ACOUSTIC PROPERTIES FROM AN/SQQ-32 SONAR REVERBERATION DATA

by

Henry R. G. Howell

September 2000

Thesis Advisors: Robert H. Bourke
James H. Wilson

Approved for public release; distribution unlimited.

REPORT DOCUMENTATION PAGE		Form Approved OMB No. 0704-0188

1. AGENCY USE ONLY *(Leave blank)*	2. REPORT DATE	3. REPORT TYPE AND DATES COVERED
	September 2000	Master's Thesis

4. TITLE AND SUBTITLE: **Inferring Bottom Acoustic Properties from AN/SQQ-32 Sonar Reverberation Data**	5. FUNDING NUMBERS
6. AUTHOR(S) Howell, Henry R. G.	
7. PERFORMING ORGANIZATION NAME(S) AND ADDRESS(ES) Naval Postgraduate School Monterey, CA 93943-5000	8. PERFORMING ORGANIZATION REPORT NUMBER
9. SPONSORING / MONITORING AGENCY NAME(S) AND ADDRESS(ES) N/A	10. SPONSORING / MONITORING AGENCY REPORT NUMBER

11. SUPPLEMENTARY NOTES The views expressed in this thesis are those of the author and do not reflect the official policy or position of the Department of Defense or the U.S. Government.

12a. DISTRIBUTION / AVAILABILITY STATEMENT	12b. DISTRIBUTION CODE
Approved for public release; distribution unlimited.	

13. ABSTRACT *(maximum 200 words)*

Inversion techniques are used to infer bottom geoacoustic properties using AN/SQQ-32 Reverberation Level (RL) data gathered by USS Avenger (MCM-1) in Rhode Island Sound in February 1993. Based on the hypothesis that the magnitude of backscattered energy is directly related to the acoustic reflectivity of the seabed, a statistical analysis of beam RL time series was conducted to determine its correlation with sediment geoacoustic character.

A technique was developed using the deviation of the RL for an individual ping/beam from an area-wide average RL to generate geographic maps illustrating bottom geoacoustic characteristics. Resulting plots of "relative reflectivity" not only agreed with the existing descriptions of sediment distribution, but also provided more detailed spatial representation of bottom geoacoustic distribution. This highlighted the gross inadequacies, particularly in spatial resolution, of existing information on bottom geoacoustic distribution.

These plots, when produced using appropriately small sample intervals, have sufficient spatial resolution to expose MCM clutter density information. Geographic maps of relative reflectivity can provide an invaluable aid to planning search strategy, a surveying tool to compare clutter densities, appropriate geoacoustic parameters for accurate model (including full wave) predictions, and a means of real time performance monitoring and assessment (providing the ability to revise and modify search strategy).

14. SUBJECT TERMS Acoustics, Reverberation, Bottom Backscattering, Geoacoustics, Oceanography, Inversion Techniques, MCM Sonar Operations, AN/SQS-32	15. NUMBER OF PAGES 130
	16. PRICE CODE

17. SECURITY CLASSIFICATION OF REPORT	18. SECURITY CLASSIFICATION OF THIS PAGE	19. SECURITY CLASSIFICATION OF ABSTRACT	20. LIMITATION OF ABSTRACT
Unclassified	Unclassified	Unclassified	UL

NSN 7540-01-280-5500

Standard Form 298 (Rev. 2-89)
Prescribed by ANSI Std. 239-18

THIS PAGE INTENTIONALLY LEFT BLANK

Approved for public release; distribution unlimited

INFERRING BOTTOM ACOUSTIC PROPERTIES FROM AN/SQQ-32 SONAR REVERBERATION DATA

Henry R. G. Howell
Lieutenant, Royal Navy
B.Sc., McGill University, 1987

Submitted in partial fulfillment of the
requirements for the degree of

MASTER OF SCIENCE IN PHYSICAL OCEANOGRAPHY

from the

NAVAL POSTGRADUATE SCHOOL
September 2000

THIS PAGE INTENTIONALLY LEFT BLANK

ABSTRACT

Inversion techniques are used to infer bottom geoacoustic properties using AN/SQQ-32 Reverberation Level (RL) data gathered by USS Avenger (MCM-1) in Rhode Island Sound in February 1993. Based on the hypothesis that the magnitude of backscattered energy is directly related to the acoustic reflectivity of the seabed, a statistical analysis of beam RL time series was conducted to determine its correlation with sediment geoacoustic character.

A technique was developed using the deviation of the RL for an individual ping/beam from an area-wide average RL to generate geographic maps illustrating bottom geoacoustic characteristics. Resulting plots of "relative reflectivity" not only agreed with the existing descriptions of sediment distribution, but also provided more detailed spatial representation of bottom geoacoustic distribution. This highlighted the gross inadequacies, particularly in spatial resolution, of existing information on bottom geoacoustic distribution.

These plots, when produced using appropriately small sample intervals, have sufficient spatial resolution to expose MCM clutter density information. Geographic maps of relative reflectivity can provide an invaluable aid to planning search strategy, a surveying tool to compare clutter densities, appropriate geoacoustic parameters for accurate model (including full wave) predictions, and a means of real time performance monitoring and assessment (providing the ability to revise and modify search strategy).

THIS PAGE INTENTIONALLY LEFT BLANK

TABLE OF CONTENTS

LIST OF FIGURES

LIST OF TABLES

THIS PAGE INTENTIONALLY LEFT BLANK

ACKNOWLEDGMENTS

I would first like to thank Professors R H Bourke and J H Wilson for their guidance, encouragement, and patience in preparing this study.

Many thanks to Patrick Pitt of ARL-UT for his assistance in providing data and supporting information.

I would like to extend special thanks to both Josie Fabre of Neptune Sciences for much technical and computing support during the early stages, and to Mike Cook of NPS Oceanography Department for his considerable and invaluable advice on computer coding received throughout the whole study.

I would also like to thank Gary Heald and Patricia Thompson of DERA Bincleaves, UK, and Steve Haeger of NAVOCEANO for their support and assistance in considering other potentially suitable data.

THIS PAGE INTENTIONALLY LEFT BLANK

I. INTRODUCTION

Underwater warfare (UW) operations conducted in shallow water face a significant challenge compared to similar operations conducted in the deep open ocean. The shallow water littoral regions of the world's oceans are highly complex areas containing coastal fronts and eddies, substantial tides and currents, extensive and often steep topographic changes, abundant sea life, varied bottom sediment distributions, and high shipping traffic. Many of these features vary rapidly in time and/or space and combine to create a very complicated and challenging warfare environment, especially to acoustic sensors.

In shallow water, UW acoustic sensors are particularly influenced by geoacoustic interactive processes with the seafloor, which include transmission into the sediment, and reflection and scattering at the seafloor. Bottom reverberation, a result of the latter, is especially significant and will often severely degrade acoustic sensor performance and capability. As a result UW operations are limited in shallow water to a great extent because of their dependence on the limited information available on bottom sediment type and distribution. Bottom sediment type maps are based on large area averages (low resolution) and are typically derived from a few in-situ sample locations. Not only do they provide scarce information on geoacoustic parameters, but their spatial resolution is usually grossly inadequate for the high variability of sediment distributions common to shallow water environments.

These inadequacies in bottom sediment information are even further highlighted by the more complicated applications involved in mine countermeasures (MCM)

operations. In addition to the usual shallow water limitations faced by any other acoustic sensors (reverberation, etc.), mine hunting acoustic sensors face other limitations unique to their application. For example, the successful detection, classification and identification of mines is extremely dependant on the number of false targets, including mine-like echoes (MILECs), mine-like contacts (MILCOs), or non-mine mine-like bottom objects (NOMBOs), that may clutter the bottom and are otherwise known as "clutter density". Also, bottom types with a potential for mine burial may require acoustic sensors to have the capability to penetrate the sediment in order to detect them. This factor creates a dilemma for mine hunting, illustrated by Figure 1. While the higher frequency acoustic sensors are required for the detecting, classifying and resolving detail of small targets, lower frequency sensors are still required to penetrate the bottom in search of buried targets.

Therefore good high-resolution information on bottom sediment properties and distribution is a major requirement for all UW operations in shallow water and absolutely essential to the success of MCM operations.

The objective of this thesis is to develop a real time, high-resolution IT method for determining bottom sediment acoustic properties and discrete clutter densities in a shallow water environment. This study sought to determine those properties through the analysis of an acoustic sensor's individual beam reverberation level (RL) related to the statistical analysis of many such RL beam time series from the same area.

The use of RL data is practical not only because a large amount of data is available for research, but because the RL data is gathered (but currently discarded) by

active fleet assets rather than an oceanographic research vessel. In this study, the RL data was gathered during an experimental trial, aboard an Avenger class minehunter, using the AN/SQQ-32 advanced minehunting and classification sonar system.

A. HIGH FREQUENCY REVERBERATION IN SHALLOW WATER

1. MCM Sonar

MCM sonars operate at much higher frequencies, thus much shorter ranges, than their ASW equivalents. Most MCM sonars employ a dual-frequency capability; operating at lower frequencies (20 to 50 kHz) to search and detect at a safe stand-off range (several hundred meters) and higher frequencies (200 to 500 kHz) to identify and classify targets at shorter range (Friedman, 1997; Lathrop, 1995).

Dedicated US MCM vessels in use today are the Avenger (MCM-1) class minehunter and the Osprey (MHC-51) class coastal minehunter, both equipped with the AN/SQQ-32 variable depth sonar (VDS). The Royal Navy's (RN) MCM vessels are the Hunt class minehunter/sweeper with the hull mounted sonar (HMS) Type 2193 and the Sandown class minehunters fitted with the VDS Type 2093 (Jane's Underwater Warfare Systems, 2000-2001).

2. Shallow Water Acoustics

Factors that affect the transmission of underwater sound include the structure of the water column, the interaction at the boundaries (surface and bottom), and the background noise. In shallow water, it is the interactive processes at the sea bottom that particularly affect sound transmission, and often severely. These processes include reflection at the seafloor, transmission into the sediment, and perhaps the most

significant, scattering at the seafloor. Scattering is the random re-radiation (reflection) of a portion of the acoustic energy by the surface, volume, and/or bottom (Urick, 1983).

3. Reverberation

Unlike scattering, which is random in direction, backscatter is that component which is re-radiated (reflected) back towards the direction that it came from. The combination of all backscattering mechanisms (surface, volume, and bottom) received, both directly and indirectly, by the acoustic monostatic (co-located transmitter/receiver) sensor of origin is known as reverberation. Although subtly different in their definition, backscattering and reverberation are directly related and often considered the same.

Sea surface reverberation is due to backscattering from a roughened air-ocean interface, a function of wind-driven wave heights, and therefore directly related to wind speed. Volume reverberation occurs due to the backscattering from marine life or other suspended material within the water column and from inhomogeneities in the ocean thermal/density structure. Bottom reverberation is typically the most dominant and variable component of reverberation in shallow water, and is due to the backscattering from the ocean-bottom interface.

In shallow water, the effects of the bottom become particularly significant due to the nearness of the seabed. The reflective nature of the overlying sediment, and sometimes the underlying material, can exert a significant effect on active sonar performance. Resulting reverberation levels (RL) can be overwhelming to the point that a target's echo level (EL) is saturated or masked by the RL, and hence not detected. Acoustic sensor operations in the shallow water environment are further complicated by the high spatial variability of sea bottom composition. Clearly, a detailed knowledge of

the bottom environment in shallow water and how it effects bottom reverberation is critically important and essential to detection ranges and their accurate prediction. Bottom backscattering processes, and hence bottom RL, are complexly inter-dependent on frequency, grazing angle, and the nature of the bottom (both grain size and surface roughness).

*a) **Backscattering Strength (S_b)***

The intensity of the backscattered energy from the sea floor that arrives at the sonar receiver is parameterised as the bottom backscattering strength (S_b) (Urick, 1983, pp. 238-239);

$$S_b = 10 \log \frac{I_{scat}}{I_{inc}} .$$

where I_{scat} is the intensity of the scattered sound per unit area at a unit distance and I_{inc} is the incident plane wave intensity impinging on the scattering area.

*b) **Grazing Angle (θ)***

Grazing angle is the horizontal arrival angle measured from the seabed (whereas the incident angle is measured from normal to the seabed). Figure 2 illustrates the scattering strength (S_b) as a function of grazing angle. It indicates that scattering strength tends to be independent of grazing angle at small angles, with increasing slope from 8° to 20° where Bragg-type scattering occurs, and then rising steeply as the scattering approaches coherent reflection from the seafloor.

*c) **Frequency***

Backscattering coefficients are independent of frequency when the spatial scale of bottom roughness is large compared to the wavelength. However when the scale of bottom roughness (appreciable roughness at small spatial scales) is small compared to the wavelength, the scattering strength increases with frequency. Thus variation of

bottom backscattering with frequency is highly complex because it is influenced by both bottom composition and bottom roughness (AOMC Training Publication).

d) Grazing Angle (θ) and Bottom Type (Roughness)

Measurements of RL and S_b arising from seabed backscattering have indicated that S_b is a function of grazing angle (θ) and bottom type. Backscattering strength from acoustically rough topography is traditionally represented using a Lambert's law relationship;

$$S_b = 10 \log \mu + 10 \log \sin^2\theta,$$

where μ, Mackenzie's constant, represents the degree of reflectivity of the sediment interface. Based on the deep water data of Mackenzie (1961) and others, Urick (1983, pp. 271-273) reported that over moderately rough topography of varying sediments and small to intermediate grazing angles, Mackenzie's constant ($k = 10 \log \mu$) averaged about -29 dB, and was essentially invariant with frequency and grazing angle. More recent shallow water experiments (south of Long Island) have indicated an association of Mackenzie's constant to the bottom sediment type and that grazing angle dependence may be scaled as $\sin \theta$ over muddy, absorptive bottoms where volume reverberation from the upper layers of the sediment may be important (Scanlon et al, 1995; McCammon, 1993). Exercise LWAD 99-1 reproduced these relationships, with measured bottom backscattering strengths over a silty clay bottom having a $\sin \theta$ relationship and that over a sandy bottom exhibiting a $\sin^2\theta$ relationship (Schalm, 1999). These findings suggested a direct correlation exists between backscattering strength and sediment type, and with this knowledge, Schalm (1999) used inverse techniques to infer the nature of the sediment type as a function of its reflectivity from RL data.

e) Grain Size

The surface sediment type can also be characterised by its grain size. Various texts and papers outline such classifications, all having similar categorisations, for example Komar (1998). Although a relationship between grain size and S_b of graded sands has been demonstrated in the laboratory (Nolle, 1963), a corresponding relationship has not been verified in the field (Figure 3). Statistical examination of most available data suggests that there are at least two independent scattering processes; a scattering process that is driven by grain size and another mainly the result of scattering from gas bubbles trapped within the sediment (Chotiros, 1992).

B. GEOACOUSTIC PREDICTION

1. Traditional Approach

Traditionally in deep water where bottom sediment properties are relatively constant spatially, bottom backscatter coefficients have been determined from measured data at single locations (Gomes et Al., 1998; Urick, 1983; Boehme et al., 1988; Boehme et al, 1985; McKinney and Anderson, 1964; Jackson et al., 1986; Stanic et al., 1988; Stanic et al., 1989; Urick, 1954; Hamilton, 1980; Turgut et al., 1990; Nolle, 1963; Medwin, 1977). Estimates of bottom backscatter coefficients, derived from these spot measurements, have then been applied over large geoacoustic provinces in "look up tables" for application in deep water acoustic propagation models.

In shallow water this application is particularly inappropriate as the bottom sediment types and clutter densities are extremely variable on spatial scales of hundreds of meters, not hundreds of miles. Scanlon et al. (1996) showed that the spatial scale can grade from hard sand to mud/silt clay sediments over distances less than 500 m. This has

been supported by numerous very high frequency side scan sonar (SSS) measurements using the AQS-14 or Klein 5000 SSS (Null et al., 2000). Thus averaging sonar data over large areas in shallow water to determine an average bottom backscatter coefficient produces gross inaccuracies in bottom effects and hence unreliable predictions of sonar performance.

Another limitation to this approach, of using backscatter coefficients, is the assumption that, at the high frequencies associated with MCM sonars, the scattering occurs at the sediment-water interface. Recent studies (Neumann et al., 1999) show that the scattering occurs from inhomogeneities in the sediment sub-bottom for slow (i.e., clay, mud) sediments at low grazing angles.

2. Alternative Approach

Although widely spaced, single-point bottom backscattering measurements cannot accommodate or resolve the high spatial sediment variability inherent in shallow water, acoustic inverse techniques (IT) can be developed to estimate this variability, based upon an analysis of MCM sonar bottom reverberation observations. The IT is first used to determine the type and spatial distribution of sediments on small spatial scales, as well as discrete clutter (MILECs, MILCOs, and/or NOMBOs). A bottom loss model can then be "matched" to the highly variable bottom in the shallow water area "surveyed" with the IT estimate derived from the acoustic data.

If SSS bottom mapping data are available, then the lower frequency search sonar IT estimates can be fused with the SSS data. High frequency SSS data provide a very high spatial resolution of bottom surface features, but contain little information regarding buried features such as mines and/or buried clutter (MILECs, MILCOs, and/or

NOMBOs), not to mention the vertical gradient of sediment properties. As Figure 1 shows schematically, lower frequency MCM and ASW sonars can provide sediment-penetrating capabilities, but have less seafloor surface resolution than higher frequency SSS data. Although multi-sensor data fusion capability is still in development, "surveying" the same bottom area with more than one sonar is highly desirable.

Once the IT-derived sediment type and clutter objects are mapped (and archived), one may perform propagation and sonar performance modelling in one of two ways. The classical bottom backscatter "look up tables" can be input into the propagation model based on IT results or one can use a full wave propagation model without look up tables.

C. INVERSION TECHNIQUES (IT)

In ocean acoustics the "forward problem" addresses those methods which predict the acoustic propagation characteristics based on a knowledge of the relevant oceanic parameters (e.g., sound speed structure, sea surface roughness, geoacoustic properties, etc.). An "Inverse" (or inversion) technique is the exact opposite such that one infers one or more oceanic parameters through the analysis of acoustic propagation data. (Medwin et al., 1998).

Inverse techniques have a wide variety of applications including the simulation of broadband signal propagation (Westwood et al., 1987) and high-resolution geoacoustic modelling (Osler et al., 1997). ITs have also been used to identify features in reverberation data from which acoustic properties such as sound speed structure, surface roughness, and geoacoustic properties can be determined. Schalm (1999) used such an

IT to infer bottom sediment characteristics from analysing beam reverberation level (RL) data by an active ASW sonar (AN/SQS-53C).

A similar IT is used in this study to identify features in beam reverberation level (RL) time series of active MCM sonar (AN/SQQ-32) data from which the bottom acoustic properties are deduced. Specifically, features of the RL time series and statistical analysis describing the character of the RL time series are analysed to identify a correlation to sediment type.

As previously discussed (Chapter I B.2), reverberation is a combination of backscattered energy from the sea surface, within the water column (volume), and the sea floor. For this study it is assumed that the volume and sea surface components of reverberation were constant within the temporal and spatial scales involved. Therefore, it is hypothesised that for a single ping from the AN/SQQ-32 sonar , the individual RL beam (bearing) time series should only differ, from beam to beam, because of variations in backscattered energy from different bottom types. This hypothesis is further extended to encompass a number of pings (as many as 442 pings were used in one combined data set), as long as they occur in the same general area, and that any changes to the ping type or mode of operation (source level, pulse length, etc.) are accounted for.

The following assumptions were made to support this hypothesis:

(1) The sound speed profile in the area around the source (within ~3 km) was constant over the period of observations (12 minutes).

(2) For each ping transmission the output source level (SL) from the AN/SQQ-32 in any direction did not vary (i.e., the SL was independent in azimuth).

(3) There were no major bathymetric or topographic changes that would significantly change the RL curve (i.e., no upslope/downslope effects).

THIS PAGE INTENTIONALLY LEFT BLANK

II. DATA

A. DATA COLLECTION

The full resolution reverberation level (RL) data examined in this study was collected by the Applied Research Laboratory - University of Texas (ARL-UT) aboard USS Avenger (MCM-1) on 19 February 1993 in Rhode Island Sound over the New England continental shelf (Figure 4). The Avenger operated within an exercise minefield approximately 8 km SE of Newport, RI, in 25-27 m depth of water (Figure 5). The minefield consisted of 15 exercise mines of varying types, both bottom and moored (Figure 6). Over 600 pings from USS Avenger's AN/SQQ-32 Mine-Hunting sonar were recorded between 11:02 and 13:07 (Eastern Time) over two identical navigational tracks (course approximately 270°), within the vicinity of the minefield (Figure 6). These pings were transmitted along a distance of 1500 m on Track 1, and 900 m on Track 2. The orientation was such that the ping locations from the last 400 m of Track 1 overlapped the ping locations of the first 400 m of Track 2 (Figure 7).

1. Weather and Oceanography

All acoustically relevant meteorological and oceanographic parameters were reported as relatively invariant for the exercise, making for near-laboratory conditions. The wind speed was less than 5 ms^{-1} from the NW, the sea surface was smooth with a significant wave height of less than 0.3 m (Pitt, 2000). However, meteorological observations from two buoys in the vicinity of Rhode Island Sound (Table 1) showed that the mean wind speed gradually decreased from 4-6 ms^{-1} to 3-4 ms^{-1} over the two hour duration of the exercise (NDBC, 2000). Such a reduction is unlikely to have affected

acoustic conditions within the duration of each track, but the decrease could have been sufficient to make a significant difference to the sea state (surface roughness) experienced between tracks one and two (separated by over 1.5 hours).

Buoy Location	Buzzard's Bay		Long Island Sound	
Local Time 2/19/1993	Wind Direction	Wind Speed Mean/Gusts (ms^{-1})	Wind Direction	Wind Speed Mean/Gusts (ms^{-1})
11:00	330	5.8 / 7.5	332	4.3 / 5.6
12:00	334	4.9 / 5.4	318	4.1 / 5.6
13:00	332	3.7 / 4.2	311	4.0 / 4.9

Table 1. Meteorological Data from Buoys in the Vicinity of Rhode Island Sound.

Climatological data suggests that the mixed layer extended to the seabed and this was confirmed by observation taken on 19 February (Pitt, 2000). The temperature profile was essentially isothermal representing typical oceanic-atmospheric forcing for these waters during winter. Little spatial or temporal deviation is expected within the confines of the study area. The resulting positive sound speed profile (SSP) provides a slight upward refractive effect to sonar transmissions, which can be considered negligible within the depths and ranges of this study. The wave-guide is so shallow (25-27 m) that the declination angle rays essentially interact with the boundaries, reflecting from the sea surface and ocean bottom. Direct paths within the water column at declination angles existed only for very short ranges and large incident angles. Their grazing angles ranged from approximately 1° at 1100 m range to approximately 15° at 80 m range, all defined as shallow angles from Chapter 1.

2. Sediments and Geoacoustics of Area

a) The New England Continental Shelf

Most of the continental shelf south of New England is covered with sands and locally gravelly sands (Figure 8). The finer-grained materials in these sediments have been winnowed out and transported either shoreward into estuaries or off the shelf and into canyons onto the continental slope (Tucholke, 1987). Studies by Milliman et al., (1972) found most of the coarse fraction (125-250 mm) is comprised of quartz and feldspar, although there are local concentrations of glauconite and phosphorite. Rivers draining from the eastern part of North America carry little sediment to the continental shelf (Milliman et al., 1983); most of that sediment is trapped in estuaries or coastal marshes (Tucholke, 1987). Relict sediments, those left from a glacial deposition cycle, are concentrated on the continental shelf and consist of fluvial and carbonate detritus and glacial outwash.

In summary shelf sediments of this region are generally comprised of mixed subarkosic to arkosic sands of glacial origin with 10-25% feldspar / feldspar and quartz (Tucholke, 1987).

b) Rhode Island Sound and the Area of Study

An extensive survey of Rhode Island Sound surface sediments by McMaster (1960) revealed that the region, in which the area of this study is located, consists of well-sorted fine sand. A large area of silty sand occurs adjacent to the Rhode Island mainland and a tongue of this finer sediment lies approximately 3 km WNW of the study area. The MIW pilot (NAVO) described the area as "...covered by irregular interwoven patches of gravel, sand and mud. It is often strewn with rocky outcrops that sometimes contain

boulders. Seaward of the sounds, the bottom is smoother and consists of sand and sand/gravel mixes."

Spatially detailed sediment information for the specific area of study was unavailable. However, two sources did provide some indication of the spatial variability. The 'Bottom Materials' chart from the NAVO MIW Pilot (2000) of this region (Figure 9) implies that most of the area is comprised of mixed sand, gravel and rocks, but may include mud and sand in the northeast part of the study area. It also suggests that the far west of the study area is more likely to be just sand. The 'nature of the bottom' descriptors, detailed on the navigational chart (#13221) of this area (Figure 10), generally supports this picture with sands throughout, rocks and pebbles in the eastern half of the area, and an adjacent area to the north is described as 'hard'. In addition, high-resolution bathymetry obtained for this area (Figure 11) shows little depth variation (< 1 m) implying that the bottom geomorphology is relatively featureless especially in the west. However, an area in the middle appears relatively more erratic and could certainly be accounted for by rocks or rock outcrops implied in the descriptors above.

Unfortunately, there were no sediment cores available for this particular area, with the nearest such cores all over 5 km away.

3. Description of AN/SQQ-32 Reverberation Data

The beam-formed sonar reverberation level data used in this study was recorded in full resolution from USS Avenger's Raytheon / Thomson Sintra AN/SQQ-32 sonar. Operation was in an experimental search mode at a frequency range of 35 to 36 kHz. The search mode has a 90° azimuthal transmit coverage (Pitt, 2000). The receiver employs 28 beams, each with a 2.5° beamwidth giving an azimuthal receive coverage of 70°. This

azimuthal beam pattern is duplicated vertically to produce two different azimuthal coverage sectors at upper and lower depression angles. The depression angles throughout this exercise were set at 4° and 12°, respectively (Pitt, 2000). Data from the lower depression angle of -12° was used for analysis in this study to ensure strong bottom interaction of the acoustic signal despite the slight upward refractive effect of the water column.

During the exercise the SQQ-32 sonar used all three of its transmission power modes: low, medium and high. The low and medium power transmissions, 210 dB and 215 dB source levels, respectively (peak re μPa @ 1 m), had an experimental pulselength of 11 ms LFM, while the high power transmission (220 dB) had an experimental pulselength of 2 ms. All three modes of operation had a bandwidth of 9 kHz. Pings were transmitted at a rate of approximately one every 2 seconds along Track 1 and one every second along Track 2 (Pitt, 2000).

Track	Event	Start Time	End Time	Number of Pings	Pulse Length	Power Setting	Source Level
1	1	11:02:15	11:05:26	109	11ms	Medium	215dB
1	2	11:05:26	11:12:20	228	11ms	Low	210dB
1	3	11:12:20	11:14:53	88	11ms	Medium	215dB
2	4	12:45:09	12:49:36	156	2ms	High	220dB

Table 2. Details of Recorded AN/SQQ-32 Transmissions on 19 February 1993.

Each period for which pings were transmitted at a particular power setting is referred to as an event. These events are detailed in Table 2. Events 1 through 3 occurred on Track 1; Event 1 (Medium Power) included 109 pings covering the first 400 m, Event 2 (Low Power) included 228 pings covering the central 800 m, and Event 3 (Medium Power) included 88 pings covering the last 300 m (Figure 12). Event 4 (High

Power) included 156 pings and exclusively occurred along the entire 900 m of Track 2. Throughout all events the sonar heading was the same as ship's head (~270°T), with the exception of some 45 pings at the end of Event 4 which progressively veered from ~270°T to ~300°T as the sonar was trained to starboard. The approximate range of coverage for the pings analysed in this study was 1100 m giving a total study area approximately 3000 m long and 1000 m wide.

4. Description and Preparation of Data

The beam-formed sonar reverberation data from all 601 pings was originally recorded at a sample rate of 18 kHz and supplied in binary format, along with ASCII log files, all on 9 CD ROMs. Positional information was not included, but was obtained by matching ping times to the ship's GPS navigation-track log output supplied separately in ASCII format. The data was first converted from binary to ASCII files ('.mat') for analysis using Matlab®. For each ping the data was then processed to convert from a complex measure of intensity (I) in volts (v) to reverberation level (RL) in decibels (dB re 1 μPa @ 1m). This was achieved using the following equation (Pitt, 2000):

$$RL = 10 \times \log10(Abs(I)) - TVG - RS$$

where TVG = time varying gain, and RS = receiver sensitivity (-69dB re 1 μPa @ 1m). The Time Varying Gain (TVG), applied at the preamps before recording, is detailed in Table 3 and illustrated in Figure 13. It was removed (subtracted) from the data in the same way it was applied.

Range (yds)	Gain (dB)	Range (yds)	Gain (dB)	Range (yds)	Gain (dB)
85 – 95	-5	280 – 325	13.0	705 - 750	28.0
95 – 115	-2	325 - 360	14.5	750 –805	29.5
115 - 130	-0.5	360 - 390	16.0	805 - 870	31.0
130 - 150	1.0	390 - 425	17.5	870 - 915	32.5
150 - 160	2.5	425 - 455	19.0	915 - 965	34.0
160 - 195	5.5	455 - 490	20.5	965 - 985	35.5
195 - 215	7.0	490 - 575	22.0	985 - 1030	35.5
215 - 230	8.5	575 - 605	23.5	1030 - 1095	37.0
230 - 255	10.0	605 - 655	25.0	1095 - 1165	38.5
255 – 280	11.5	655 – 705	26.5	1165 - end	40.0

Table 3. Gain vs Range of TVG Function. (From Pitt, 2000)

For each ping the processed data consisted of 56 time series, one for each of the 28 beams at both upper and lower declination angles. For each beam the time series contained approximately 25,000 sample points, which translates to about 1.5 seconds in time or 1100 m in range (assuming two-way travel at 1500 ms^{-1} sound speed). Figure 14 displays a typical processed RL time series from a single beam (beam 14). The significant change in slope of RL, which occurs at approximately 0.2 seconds, represents the transition from spherical to cylindrical spreading due to boundary interaction. The relatively unchanging slope of RL beyond 0.2 seconds implies that the RL decays with range at a fairly constant rate due to cylindrical spreading, suggesting that there is little change in the environment over this range.

B. PROCESSING METHOD

An example of how the sediment effects reverberation can be seen by comparing two different RL time series in which distinctly different characteristics can be seen. The single beam (beam 14) RL time series in Figure 14 shows that the RL curve, beyond 0.2

seconds decays at a fairly constant rate due to cylindrical spreading. In contrast, Figure 15, another single beam (beam 21) RL time series from a different ping, shows significant changes in the slope of RL at 0.6 and 0.75 seconds, well beyond the spherical to cylindrical spreading transition range (~0.2 seconds). In fact, it is clear that the RL actually increased during this period. This would imply that the environment changed significantly and this heightened degree of backscatter is due to the presence of a more reflective bottom.

The inversion technique (IT) proposed for RL curve analysis is as follows: (1) determine a characteristic RL curve for an area determined from the average of many pings and (2) compare individual beam data to determine its difference from the area-wide mean.

A variety of statistical parameters derived from the beam RL time series can be examined to determine if the characteristics of the RL curve bear any correlation to sediment type. Schalm (1999) investigated the mean slope, standard deviation, skew, and excess kurtosis, but only was only able to show promising results with the mean slope due to time and funding limitations. Therefore the mean RL and the slope of RL were investigated here to build on Schalm's work.

Before continuing, some background about the statistical method used in this study is required. The statistics calculated are not based on the entire time series but rather upon segments of the time series partitioned into intervals of 50, 100, 200, 500, or 1000 sample points corresponding to 2, 4, 8, 20, or 40 meters range spacing, respectively. In addition, a degree of overlap of the data is often useful, e.g., 25, 50 or 75% of the interval and, based on the results of Schlam (1999), a 75% overlap was used. The

statistics derived from the overlapped segments are referred to as "moving" statistics (moving average or mean). For example, a 1.4-second time series, with 18,000 data points per second, contains 25,200 data points. With an interval/overlap combination of 1000/75% the first data point of the moving mean would be the mean of points 1 to 1000, the second point would be the mean of points 251 to 1250, the third would be the mean of points 501 to 1500, etc. Selection of interval entirely depends on the degree of smoothing desired and the spatial size of the features of interest. Based mainly on limited data capacities an interval of 1000 was selected and used as the standard throughout the analysis. Figure 16 shows an individual single beam (beam 14) RL time series (black) overlaid by the 1000/75% moving mean (white) RL curve.

1. Example Using RL Data at 1000/75% Moving Mean

From the 88 pings of Event 3 an 'Event-wide' average RL curve is calculated by first taking the 1000/75% moving mean for all of the beams (28) in each transmitted ping to smooth the curve. (The slope of each beam can be determined by calculating the gradient (d/dt) of the smoothed RL curve). These smoothed curves from each beam are then used to calculate the mean RL curve for that particular ping. This process is repeated for all the pings in Event 1 generating 88 individual mean RL curves, each representing 1 ping over the 70° sector width. The 'Event-wide' RL curve is then calculated from all the pings' individual mean RL curves. Figure 17 shows all the ping's individual mean RL curves for Event 3 (black) overlaid by the Event-wide mean RL curve (white). Calculating the mean from all (24x88) RL data sets from Event 3 generates an Event-wide average RL curve based on over 2000 individual RL time series. This process was performed on the data sets of each of the four separate events.

Figure 18 shows the smoothed RL curve for a single individual beam (beam 14) (dashed line) along with its appropriate Event-wide average RL curve (solid line). Each point along the smoothed single beam RL curve has an associated range and bearing which corresponds to a geographic position. By determining the difference between the area-wide average RL curve and the individual smoothed beam RL curve, a geographic contour plot can be generated to display the anomaly from the Event-wide mean (Figure 19). Subsequently, different pings can be compared to determine if any geographic correlation exists between sets of pings to identify a unique but consistent area exhibiting similar RL characteristics. In Figure 19, red and yellow represents areas of relatively high reflectivity while green and blue are relatively low reflectivity areas.

III. ANALYSIS

A. ANALYSIS OF RL DATA

1. Analysis of Single Pings

Through the comparisons of single ping RL data to RL averaged over the entire event area, various features can be seen that are consistent in their geographic location. The resulting backscatter features from Ping 107, shown in Figure 19, exhibit RL characteristics that are common in all pings in the data set and are discussed in detail below. Figure 19 is a geographic contour plot displaying deviation of beam RL from the event-wide mean RL for each of the 28 azimuthal beams of ping 107. It is anticipated that regions where the deviations (from the average RL curve) are positive correspond to seafloor areas exhibiting more reflective characteristics than the area-wide mean, while regions with a negative deviation are less reflective. For example, Figure 20 (top) shows the RL and smoothed RL curve of ping 107, beam 21. At approximately 0.7 s a region of increased (>5 dB) RL is observed in both the raw and smoothed curves. Figure 21 depicts this region of ping 107, beam 21, enlarged to show the area of heightened RL (2550 m east, 800 m north). As a result, the deviation of beam RL from the event-wide mean RL is referred to as 'relative-reflectivity'. The same geographic region of increased relative-reflectivity can be seen on other contour plots using different pings. For example, Ping 97 (Figure 22) transmitted about 20 seconds (~ 35 m) earlier, and ping 117, (Figure 23) transmitted about 20 seconds (~ 35 m) later, both demonstrate that the region of increased reflectivity (increased RL) is consistent in its geographic location

(2550 m east, 800 m north). This indicates that the high backscatter or reflectivity is due to a geographic feature, and is not a random occurrence.

Alternatively, this feature can be identified by a comparison between different pings, by overlaying contour plots from a set of pings from the same event. Figure 24 shows the sector areas covered by such a sequence (pings 59,86,113,140,167, and grouped as Set 1), while their contour plots (Figure 25) illustrate how the same high backscatter or reflectivity (discussed above) appears consistently in the same geographic location in a number of pings, despite the varying transmission range as the ship moved progressively closer towards the features.

2. Analysis of Events

A thorough analysis of all the RL curve plots from each event was first conducted to create a geographic representation of various sediment types based on consistent spatial variations in the RL curves within that event.

a) Overlays of Ping Sequences

Within an event a continuous sequence of pings, equally spaced at approximately 100 m (4-9 pings depending on ship's speed during an event), was used to produce a display of overlaying contour plots that represents the geographic area covered by that particular event, as previously illustrated in Figures 24 and 25. For each event this procedure was repeated four times, each time with a different set of pings, to produce five completely independent geographic representations of the area covered by each event. Figures 26-27 show two such sequences (pings 60,87,114,141,169; Set 2, and pings 61,88,115,142,170; Set 3, respectively) both from Event 1 which demonstrate their consistency in portraying features evident in all five representations. A comparison of

the five displays from each event reveals that the same spatial RL anomalies are displayed consistently in the same geographic location regardless of the sequence of pings used. A similar degree of consistency was demonstrated for other spatial RL anomalies in the study area using such sequences of RL ping data from the other events (Events 2, 3 and 4). For example, the large area of heightened backscatter spanning north-south across the sonar swath at 1800-2000 m east in Event 2 (Figure 28), is not only consistently displayed across all the pings of that event, but can also be seen at the end of Event 1 (Figure 27, left) and just at the beginning of Event 3 (Figure 29, right). In Event 4 (Figure 30) several spatial RL anomalies consistently occur near the beginning of the track (1300-1500 m east), but RL variation from the mean appears consistently very low in the western end of the area (0-1200 m east). Figure 30 (left) also demonstrates spatial consistency of RL features between pings which progressively vary in centre beam heading as the sonar was trained to the right near the end of the event.

b) Composite Plots

Figure 31 is similar to those of Figures 25-27 but is a composite plot derived from combining the data of all 5 pings from that particular sequence. For each defined geographic location covered by the sequence, the average deviation of RL from the event-wide mean RL (relative-reflectivity) was calculated and then displayed.

Because this is an average of relative-reflectivity for a number of pings, this plot will show RL features that have geographic consistency, while eliminating those features that are not geographically consistent but only appear in single pings. As a result, the composite plot appears to lose some of the detail present in the single and overlay plots (Figures 21-27), but the significant features are still exposed.

In addition, because each ping from the sequence was transmitted at a progressively shorter range from each defined geographic location, the resulting relative-reflectivity has been calculated from a well distributed range of grazing angles; from about 1° to 15° (for direct path transmissions) as discussed in Chapter 2 (A.1). This effectively averages out any effect of varying grazing angle, and the result, for each geographic location of the composite plot, is a generic value of relative-reflectivity, independent of grazing angle (over this range).

Composite plots of the other three events (Events 2, 3 and 4), displayed in Figures 32-34, also manifest the more relevant spatial RL features that were previously displayed in their appropriate sequence overlay plots (Figures 28-30). It should be noted that most of the RL features observed in these composite plots display nearly the same level of relative-reflectivity as they did in the single ping plots indicating that grazing angle plays only a minor role in the variation of RL (over the range of shallow grazing angles (1° to 15°) analysed in this study). This is in agreement with established theory as seen in Figure 2.

3. Combining Events

In order to analyse the entire area of study as a whole, the RL statistical data from the different events were combined to produce an 'area-wide' mean RL curve. However, RL statistical data from one event to the next can only be combined once the difference between the modes of operation (transmission power and pulse length) and their implications on the RL statistics is completely understood.

When combining events that employ the same operating modes, such as Events 1 and 3, all the RL statistical data from both events can be used to simply calculate an

overall mean RL curve that represents the average for both areas covered. However, events which employ different operating modes must be treated differently. For example, a decrease in transmission power, or source level (SL), would result in a corresponding decrease in RL (Urick, 1983). This means that a difference in SL, such as that between Event 1 and 2 (5 dB), has to be taken into account when calculating the combined mean RL for all events. This involved applying an adjustment (adding 5 dB logarithmically) to the mean RL data of Event 2, which normalised the data (to medium power) so that it was equivalent to that of events 1 and 3, before calculating an overall mean.

The non-normalised event-wide mean RL curves for Events 1, 2 and 3 are shown in Figure 35 together with a fourth which is the mean of all three mean RL curves calculated, as discussed, from all the RL data of events 1, 2 and 3. Notice that they all have similar shape and rate of decay, an observation reflected by the correlation coefficients between one another that range from 0.99813 (Events 1 & 2) to 0.9998 (Events 2 & 3). This similar shape and rate of decay is a mean representation of the environment and is applicable independent of operating mode (transmission power). The displacement or offset between the mean RL curve of Event 2 and those of the other events is primarily due to a difference in transmitting power. However, any RL level difference between events which had the same operating mode (transmitting power), such as Events 1 and 3, can only be attributed to a difference in the environment (sea floor characteristics).

The RL statistical data of Event 4 was not combined with that of the other events as their relationship was more complicated. Event 4 not only employed a different SL

(220 dB), but also employed a different pulse length, 2 ms as opposed to 11 ms. The influence of pulse length on RL can be seen from the following equation (Urick, 1983):

$$RL = SL - 2TL + S_{s,v} + \log A,V$$

where TL = transmission loss, $S_{s,v}$ = scattering strength (surface and volume), and A,V = the reverberating area or volume, respectively. A is specifically given by:

$$A = c\tau_{/2} \times \Phi r$$

where c = sound speed, τ = pulse length, Φ = beam width, and r = range. Thus a decrease in pulse length (τ) such as that between Events 3 and 4 could result in a corresponding decrease in RL, despite the increase in SL. In addition, there was a delay in time between these events (an hour and a half), in which the wind experienced a small but significant decrease of 2-3 ms^{-1} (Table 1). The resulting decrease in surface roughness almost certainly decreased the surface component of reverberation, thus compromising one of the fundamental assumptions (stationary surface reverberation over the duration of the experiment), discussed in Chapter 1, on which the IT analysis of these combined events depends.

This complication and resulting outcome were confirmed when a number of pings from Events 3 and 4, transmitted over the same geographical area, were compared. The 88 pings of Event 3, transmitted at medium power (215 dB), were compared to the 60 pings of Event 4 (referred to as Event 4a), transmitted at high power (220 dB), which all covered the same geographical area. The event-wide mean RL curves for these two events are displayed together in Figure 36 where their shape and rate of decay appear identical, with a correlation coefficient of 0.99994. However the mean RL curve for Event 4a is displaced approximately 2 dB below that of Event 3, contrary to what might

be expected based on SL considerations alone! Although the mean RL from Event 4a, transmitted at a higher SL, would be expected to be above that of Event 3, the effects of both reduced pulse length and reduced surface reverberation clearly had an opposite and overriding effect on the result.

Analysis of these event-wide statistics confirms that RL statistical data for pings from different events can be combined to produce results applicable for the entire area. However, if the resulting measure of deviation (of single ping beam RL from mean RL) is to have any validity, each ping analysed must use the appropriate event-wide mean RL curve for the event from which the ping in taken.

4. Overlay and Composite Plots of Entire Study Area

Figure 37 is an overlay of the contour plots of a sequence of pings (Set 1 from Events 1, 2 and 3) covering most of the study area. The values of relative-reflectivity have been calculated from a single normalised area-wide mean RL curve calculated, as discussed above, from the RL statistics of Events 1, 2 and 3. Theses contour plots appear to combine well, in that overlapping plots from adjacent events appear to produce similar levels of relative-reflectivity over the same geographic areas. Figure 38 is a composite plot of the same sequence, which is produced as previously discussed, but again employs the single area-wide mean RL curve (Events 1, 2 and 3) in calculation. This plot was primarily used for the following comparison to known sediment ground truth.

5. Comparison to Existing Information on Sediments

The previous sections have demonstrated that RL features consistently appear on all of the single ping, sequence overlay, and composite contour plots produced. Two composite contour plots, one from combining Events 1, 2 and 3 (Figure 38) and the other

from Event 4 (Figure 34), cover the entire area and are used in the analysis below for comparison to the (little) known sediment distribution of the area. However, it must be emphasised that the values of relative reflectivity from Figures 34 and 38 cannot be compared directly to each other, as the values are relative to separate area/event mean RL curves, as previously explained. This is confirmed by observing the difference in appearance, and different values of relative reflectivity, of an area observed in both figures (34 and 38) at 1300 m east and 800 m north.

Despite the lack of spatial detail in all of the existing sediment distribution sources, analysis of the contour plots show clear similarities to the general sedimentary characterisation of the area. There are three distinct geographic areas or domains observed in Figures 34 and 38, similar to that described in Chapter 2.

The first of these distinct domains is the most significant feature in the area covered by Figures 34 and 38, namely the somewhat featureless area west of 1200 m east and south of 1200 m north. This area displayed the least variation in relative-reflectivity, as illustrated by a dynamic range of less than 1 to 2 dB. This implies a relatively homogeneous surface/subsurface sediment spatial distribution, and is most likely the result of a fairly uniform surface sediment cover of mainly sand, just as the information from Figure 9 suggests. The relatively smooth bottom that the bathymetry implies in Figure 11 also supports this conclusion.

The second area is the region that extends from 1200 to 3200 m east, although is interrupted by the third area, a band between 1800 m to 2100 m east. This second area has a high variability in relative-reflectivity (dynamic range as much as 10 dB), and is characterised by areas of fairly low relative-reflectivity (0.5 to 2 dB below the mean)

interspersed by irregular patches of quite high relative-reflectivity (2 to 5 dB above the mean). This region appears anything but homogeneous and implies a bottom of different sediment types. The patches of high relative reflectivity, such as that around 2400-2600 m east and 600-900 m north, and the group around 2700-3100 m east and 400-700 m north, all appear to be quite localised sharp features of increased reflectivity, some of which appear inter-connected. It is suggested that these highly reflective zones could be uncovered (or thinly covered) rock, rocky patches, or gravel/pebble fields, whereas the less reflective areas may be due to depressions or basins filled with finer grained sediments. The few small areas displaying minimum relative reflectivity (-3 to -4 dB), for example 1600 m east and 900 m north, are quite likely to be flat areas of fine sediment or mud. This all closely follows the bottom type descriptions of this area, especially those from the MIW pilot (Chapter 2), and is indicative of the glacial origin (mixed moraine) of sediments in this area.

The third area is by far the most prominent feature in terms of relative reflectivity. The 200-300 m wide band previously referred to, transects the entire swath of coverage north-south between 1800 m to 2100 m east, and stands out as an extremely reflective feature. The reflectivity and size of such a large feature suggest that it is either an exposed rock outcrop or (ancient) reef, or more likely a particularly large linearly oriented field of mixed rock and gravel (moraine). Although no such feature is specifically described in the sources of sediment distribution, the general descriptions of mixed sediment with glacial origin certainly make such a feature a credible possibility. Interestingly enough, this is somewhat supported by the fact that the location of this feature is approximately coincidental with the area of greatest variation in bathymetry

(Figure 11), thus confirming that this band has a particularly erratic or rough bottom. The AN/SQQ-32 penetrates sediment up to approximately 1.5 acoustic wavelengths (Null, 1996), or up to 6 cm. Thus partially buried rocks or outcrops could cause some of the high reflectivity.

In summary, the resulting geographic contour plots of relative reflectivity not only agreed with the broad picture painted by the various existing sources of information on sediment distribution, but also provide far more detailed spatial representation of sediment distribution. This served to highlight the gross inadequacies, particularly in spatial resolution, of the existing information available on bottom sediment distribution and geoacoustics.

B. DISCUSSION

1. Choice of Sample Interval

All of the analyses described thus far were carried out with RL data smoothed with a sampling interval of 1000 data points. Although this interval is equivalent to a range spacing of 40 m, this does not correspond to the actual spatial resolution, as the latter is more complicated parameter which is also dependent on the overlap (75%)! The interval of 1000 data points was by no means meant to reflect the optimum choice, but, as mentioned in Chapter 2 (B), was a compromise between maintaining sufficient detail (spatial resolution) in the time series data and keeping the data sizes manageable within the capabilities of the PC equipment available to this study. The optimum choice of interval would actually require further investigation, and also depend upon the required application and the data management available. However, in partial response to the

question of optimum interval size one single ping data set was analysed using a range of different intervals.

As the sampling interval is directly related to the spatial resolution (and overlap), the particular ping used for this brief investigation was selected because it included a target of opportunity of known size. Ping 211 of Event 2 was selected because a Mark 36 mine (a cylinder 2.2 m long and 0.4 m in diameter), indicated as mine #13 in Figures 6 and 7, had been detected in this particular ping during previous analysis (Wilson et al., 1996). It can be seen in Figure 39 at a range of 300 m, predominantly manifested in beam 1.

A series of contour plots of ping 211 were produced and then examined using a progressively smaller interval each time. The intervals employed included 2000, 1800, 1600, 1400, 1200 ,1000, 900, 800, 700, 600, 500, 400, 300, 200, 100, 50, and 26, which corresponded to spatial intervals of 80 m to 1 m. Examination of the resulting contour plots revealed that even at an interval as large as 2000 (corresponding to 80 m range interval), the broad picture of relative reflectivity was still very much evident. As the interval was decreased, the resulting contour plots progressively revealed smaller features and more detail, much as expected. For example, in Figure 40 the contour plot of ping 211 produced at an interval of 1200 (~50 m) was the first plot of the series to reveal an area of high relative reflectivity (~2 dB) at 2100 east, 500 north. This particular feature of heightened reflectivity is almost certainly associated with the quite significant bathymetric feature, possibly a pinnacle or rock outcrop of some kind, located in approximately the same position observed in Figure 11. Mine 13 is first observed, at

2400 m east, 470 m north, in the contour plot of ping 211 produced with an interval of 200 (8m) (Figure 41).

Figure 42 shows the contour plot of ping 211 produced using an interval of 26 (1 m), the smallest interval used. This figure demonstrates the detail and high level of spatial variation that can be achieved using a fine scale interval, a capability that would prove most useful in archiving clutter densities and NOMBO fixes.

2. Analysis of RL Curve Data versus Analysis of RL Slope Data

The same method of analysis used on the RL curve data was also carried out on the RL slope data, following the procedure outlined by Schalm (1999) for use on SQS-53C data. However complications in removal of the TVG created an (artificial) artefact within the RL slope data. This artefact corrupted the results, as illustrated in the contour plot of Figure 43, (although the most significant geographically consistent features were still revealed). This corruption only occurred in the analysis of RL slope data, and was due to the way in which the TVG specifically affected the slope calculations. The RL curve data analysis was completely free of such corruption as its method involves calculations that actually cancel out the artefact. As a result the analysis of RL slope data was put aside in favour of the more successful analysis of RL curve data. Although the TVG artefact was the prime motivation in focusing effort on the analysis of RL curve, it was firmly believed that this method actually provided superior results anyway, even if the TVG problem had not been present. This however did prevent any direct comparison of the two methods (RL curve and RL slope).

Comparisons between the results of Schalm's AN/SQS-53C work (1999) and this study are complicated due to the difference in sensors, applications and the environments

involved, and thus one can only make qualitative comment. Notwithstanding significant differences in parameters including frequency, pulselength and sector coverage, one of the fundamental differences between the two applications is that of spatial scale; the SQQ-32 extends a 70° sector of coverage out to a range of approximately 1 km, while SQS-53C extends a 120°or 360° sector of coverage out to a range of approximately 19 km. Clearly the scale of area covered is vastly different. Further investigation involving direct comparison of the two methods (RL curve and RL slope) applied to one or both applications (MCM and ASW) is needed, but it is expected that the RL curve analysis will be superior to the RL slope analyses for both MCM and ASW applications.

3. Implications of Horizontal Orientation

As the data used was opportunistic and not gathered as a dedication effort for this study, there were some limits to the way in which it could have been exploited. One very desirable aspect of this study was not covered because of this aspect. Virtually the entire area studied was acoustically surveyed from the same direction (transversing east to west). This prevented comparison of results using this IT method over the same piece of bottom but from different transmission directions. It might be expected that certain types of bottom, particularly those with highly oriented features, such as sand ripples or waves, would provide different results depending on the azimuthal orientation of the sensor. To investigate this aspect would require with tracks arranged in such a way as to obtain transmissions over the same geographic location from different directions, before any conclusions could be made.

4. Tactical Implications of the Plots of Bottom Relative Reflectivity

The high variability of bottom sediment type and clutter density in shallow water presents a strong tactical significance because it can unexpectedly, and often times adversely, affect the results of an acoustic search, especially when executed under the assumption that the bottom sediment is homogenous. Figure 44(A) is indicative of a typical MCM search plan that was executed assuming that detection ranges were constant (regardless of sediment type). This "mowing the lawn" technique can result in lower or higher probability of detections (PDs) than anticipated. This is due to regions where detection ranges are degraded or improved because more or less reflective areas are encountered (along the search pattern), respectively. Implications are two fold: If the PD along the search track is lower than predicted the resulting search swath is narrower than the line/track spacing planned for. This potentially results in gaps, known as "holidays", between the search lanes, giving over-optimistic confidence levels and inaccurately low risk estimates. Conversely, if the PD is higher than predicted, the resulting search swath is wider than the line/track spacing planned for, giving a level of redundancy, and meaning that the planned search takes longer than necessary. The overall implications to a larger naval mission, highly dependent on the timely execution of such a (MCM) search, are that it proceeds at an unnecessarily slow rate, so much so that it may be delayed or cancelled, or worse, that it proceeds at under-estimated levels of risk, and thus (unknown) inadequate levels of safety!

Prior to an acoustic search a rapid environmental update could be conducted which includes an IT survey of relative reflectivity, from which a sediment map, similar to the one in Figure 38, could be used to modify or dictate the search plan. Such a

survey, run at the appropriate spatial resolution (sample interval), as discussed in Chapter 2.B.1, could also include assessments of clutter density and even NOMBO fixes. The search plan could then divide the area into sub-divisions differentiated by PD, with the line/track spacing and orientation within each sub-division dictated by the PD of that particular sub-division (Figure 44B). This selective approach, "searching by sediments", would optimise the efficiency of such a search, and areas of particularly high reflectivity (very low PD) or high clutter density, which might be considered too time intensive to search, could be simply cordoned off and discarded in the overall search.

In addition, or alternatively, an IT analysis run during the actual search would provide a very useful means of real time performance assessment and monitoring.

This technology could be further exploited by populating databases, such as the Route Survey Data Base (RSDB), with the actual processed IT data, either as composite plots of relative reflectivity or in actual data form such that their plots can be regenerated. In either case this information would then be available to aid planning as discussed above, but ahead of the arrival of fleet assets. Such databases would also facilitate the means of comparing how bottom reflectivity and clutter densities may have changed between such surveys, a particularly useful attribute in respect to clutter densities and NOMBO fixes. This information, available to populate such databases, is gathered, and currently wasted, whenever a platform sensor is operating. This IT would ensure that all such data and information is used to its potential whenever possible. Subsequent processing and database population could be made an automatic process.

THIS PAGE INTENTIONALLY LEFT BLANK

IV. CONCLUSIONS AND RECOMMENDATIONS

USS Avenger (MCM-1) conducted an experimental sonar trial in Rhode Island Sound on 19 February 1993, which included collection of reverberation level data from the ship's AN/SQQ-32 sonar. The reverberation level data was used to investigate the possibility of employing inversion techniques to infer bottom geoacoustic properties.

The hypothesis presented in this thesis was based on the assumption that the magnitude of backscattered energy (and its rate of spatial decay) was directly related to the acoustic reflectivity of the seabed. By examining the character of RL curves from various sedimentary provinces, one should be able to identify and associate various reverberant areas with unique sediment or geoacoustic types. This study examined the statistics of both the RL curve and its slope, to test this hypothesis.

A. CONCLUSIONS

Of the two statistical parameters the RL curve was found to be most clearly aligned with the degree of bottom reflectivity. Over less reflective (mud/silt) bottoms a decrease in RL deviation from the area-wide mean RL curve (relative reflectivity) was noted while acoustic interactions with a more reflective bottom (gravel, pebbles and rocks) cause an increase in relative reflectivity. Based on this finding, a technique was developed using the deviation of the RL for an individual ping/beam from an area-wide average RL to generate geographic maps illustrating bottom acoustic characteristics.

Through the comparisons of different plots displaying the same geographically located features of reflectivity, it was noted that grazing angle plays only a minor role in

the variation of RL (over the range of shallow grazing angles (1° to 15°) analysed in this study), as in agreement with established theory.

Resulting geographic maps of relative reflectivity not only agreed with the existing descriptions of sediment distribution, but also provided far more detail in spatial representation of the bottom geoacoustic distribution. This served to highlight the gross inadequacies, particularly in spatial resolution, of the existing information available on bottom sediment distribution and geoacoustics.

In addition, geographic maps of relative reflectivity can be produced, when using an appropriately small sample interval, at sufficient spatial resolution to expose clutter density information (MILECs, MILCOs, NOMBOs etc.).

The resulting geographic maps of relative reflectivity can provide the following:

1 A means of real time performance assessment and monitoring that enable more accurate PDs and line/track spacing, and the ability to revise and modify search strategy.

2 An invaluable aid to planning a search strategy, optimising resources based on "searching by sediments", either from in-situ IT surveying or from archived IT derived data.

3 A means of comparing clutter densities (MILECs, MILCOs, NOMBOs etc.) from different surveys.

4 Appropriate geoacoustic parameters for propagation models (including full wave) to provide more accurate predictions.

B. RECOMMENDATIONS

It is recommended that the RL method of this inverse technique analysis for generating sediment maps be used by fleet assets as part of efforts to develop both in-situ and archived databases of bottom properties, and that these results be incorporated into shallow water MCM (and ASW) search planning.

In addition, further research into the nature of RL IT statistics and its impact on sonar system performance should be undertaken and include the following:

1 Investigation of different sample intervals in respect to optimum spatial resolutions for both broad geoacoustic distribution and clutter densities.

2 Investigation of IT results performed on the same geographical area but from different azmuthal directions to determine any directional dependence.

3 Comparison of this IT using both RL analysis method (Howell, 2000) and slope of RL analysis method (Schlam, 1999) in respect to optimising both ASW and/or MCM applications.

4 Multi-sensor data IT fusion algorithms from various sonars operating over the same bottom area, but at vastly different frequencies, should be developed. For US sonars the AN/SQS-53C, AN/SQQ-32, and a high frequency side scan sonar (SSS) all contain different information about the bottom sediments, and their IT data must be fused to optimise the 3D description of the bottom. This equally applies to UK sonars including Sonar Types 2050 and 2093.

It is emphasised that high quality and accurate ground truth information is essential in validating future IT analysis results.

APPENDIX A. FIGURES

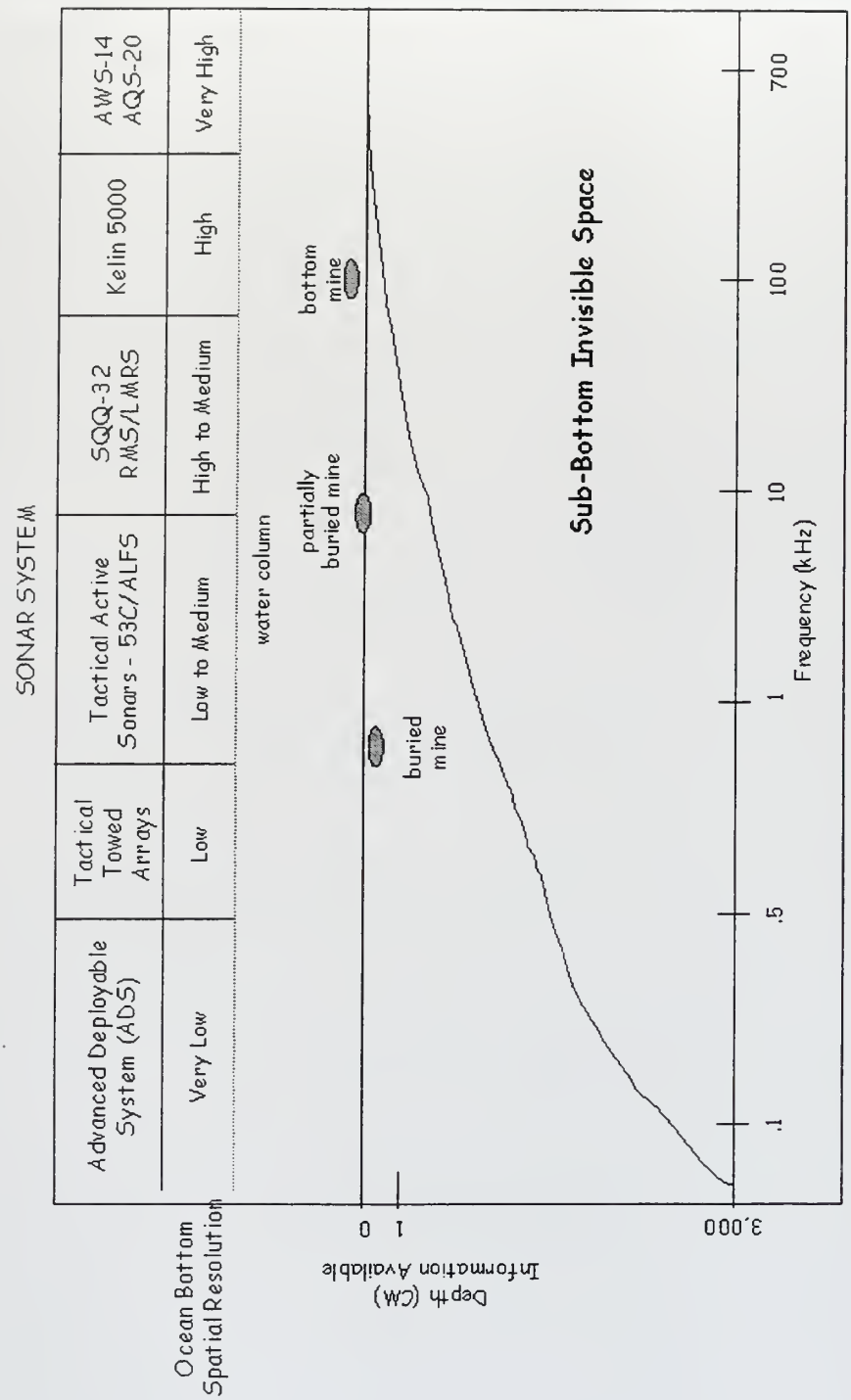

Figure 1. Spatial Resolution in 3D using MIW and ASW Sonar Systems (from Null, 1999),

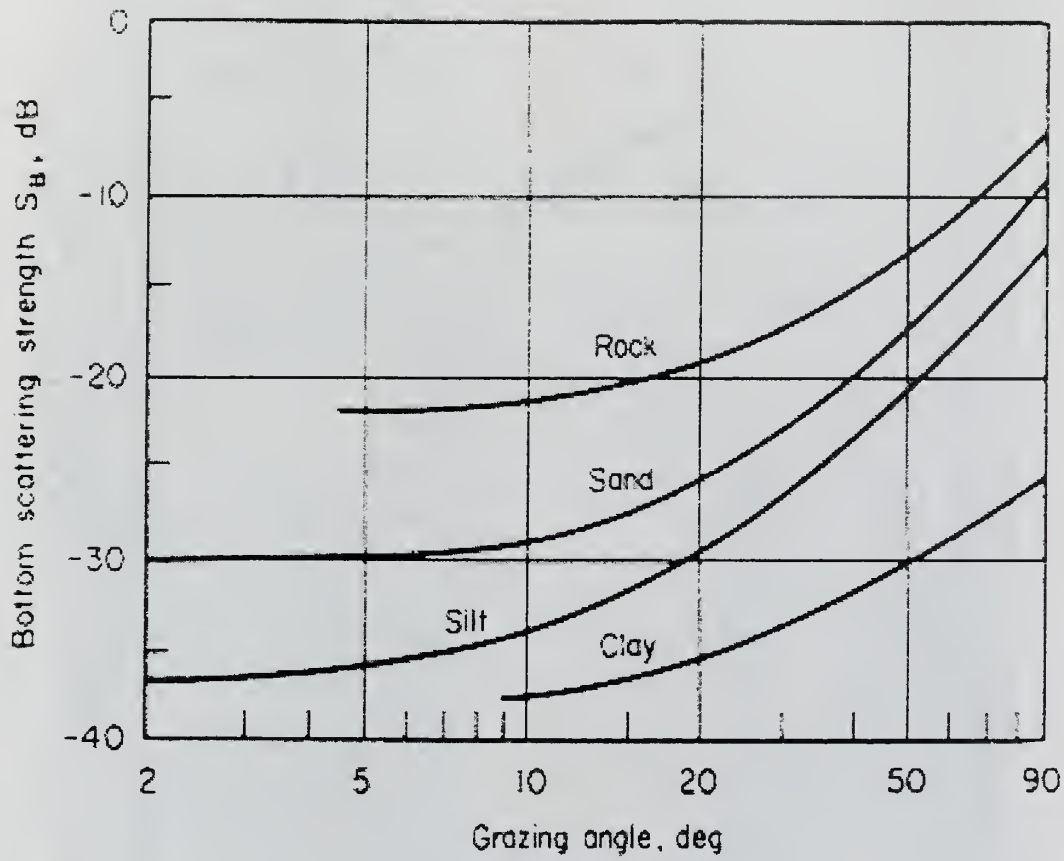

Figure 2. Bottom S_b as a function of grazing angle illustrating (from Urick, 1983).

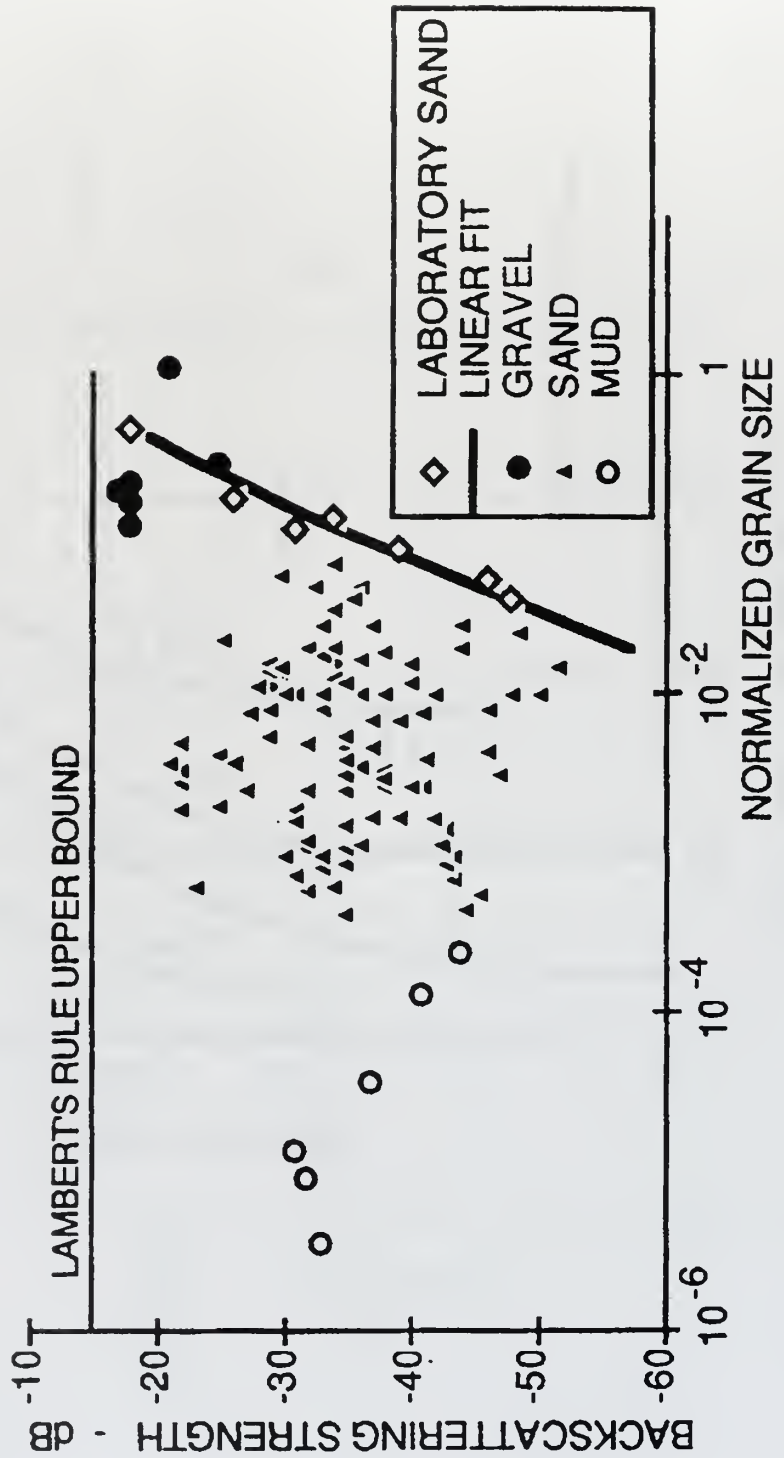

Figure 3. Bottom backscattering strength as a function of normalised grainsize at 10° (from Chotiros, 1992)

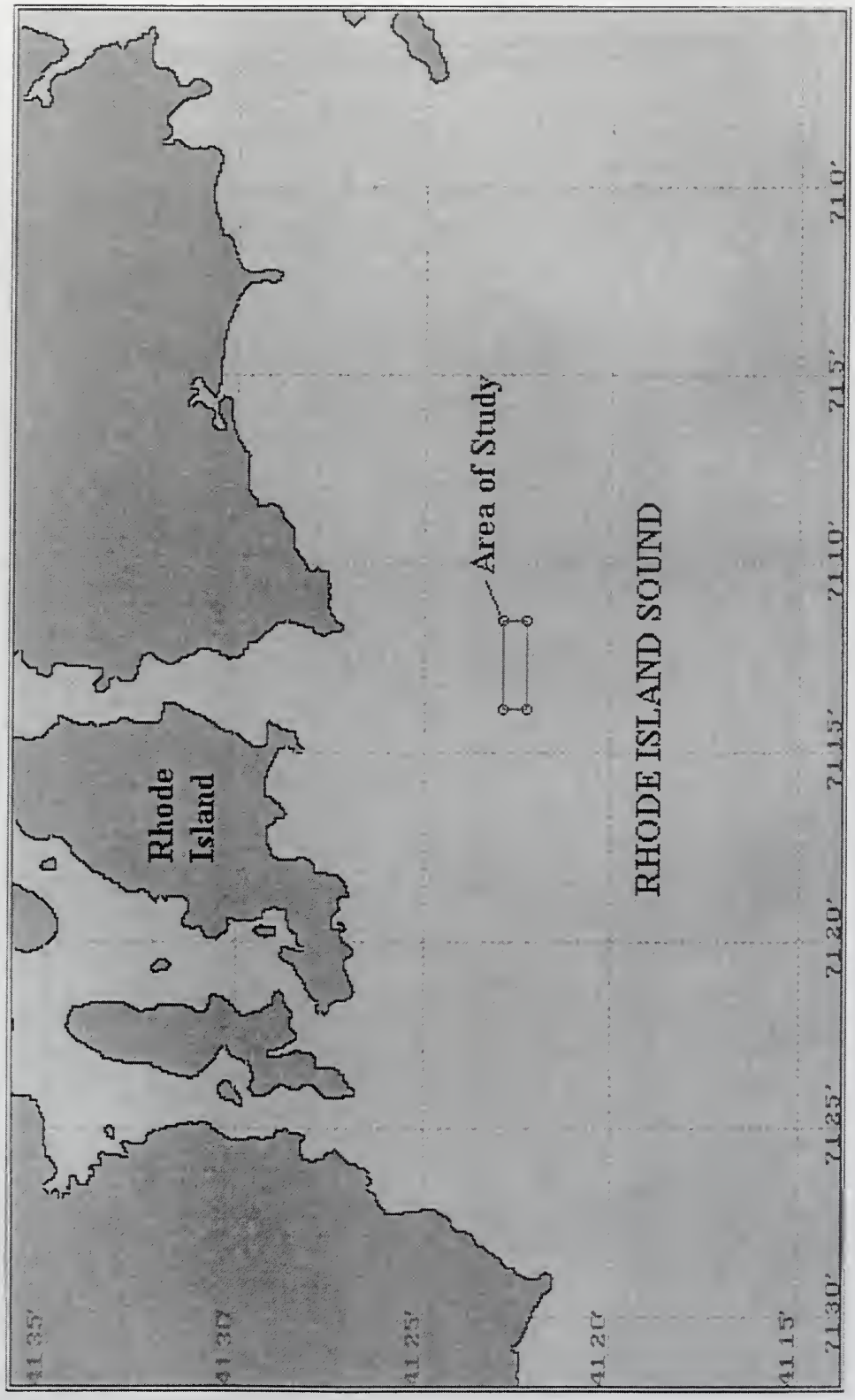

Figure 4. Map of Rhode Island Sound displaying area of study.

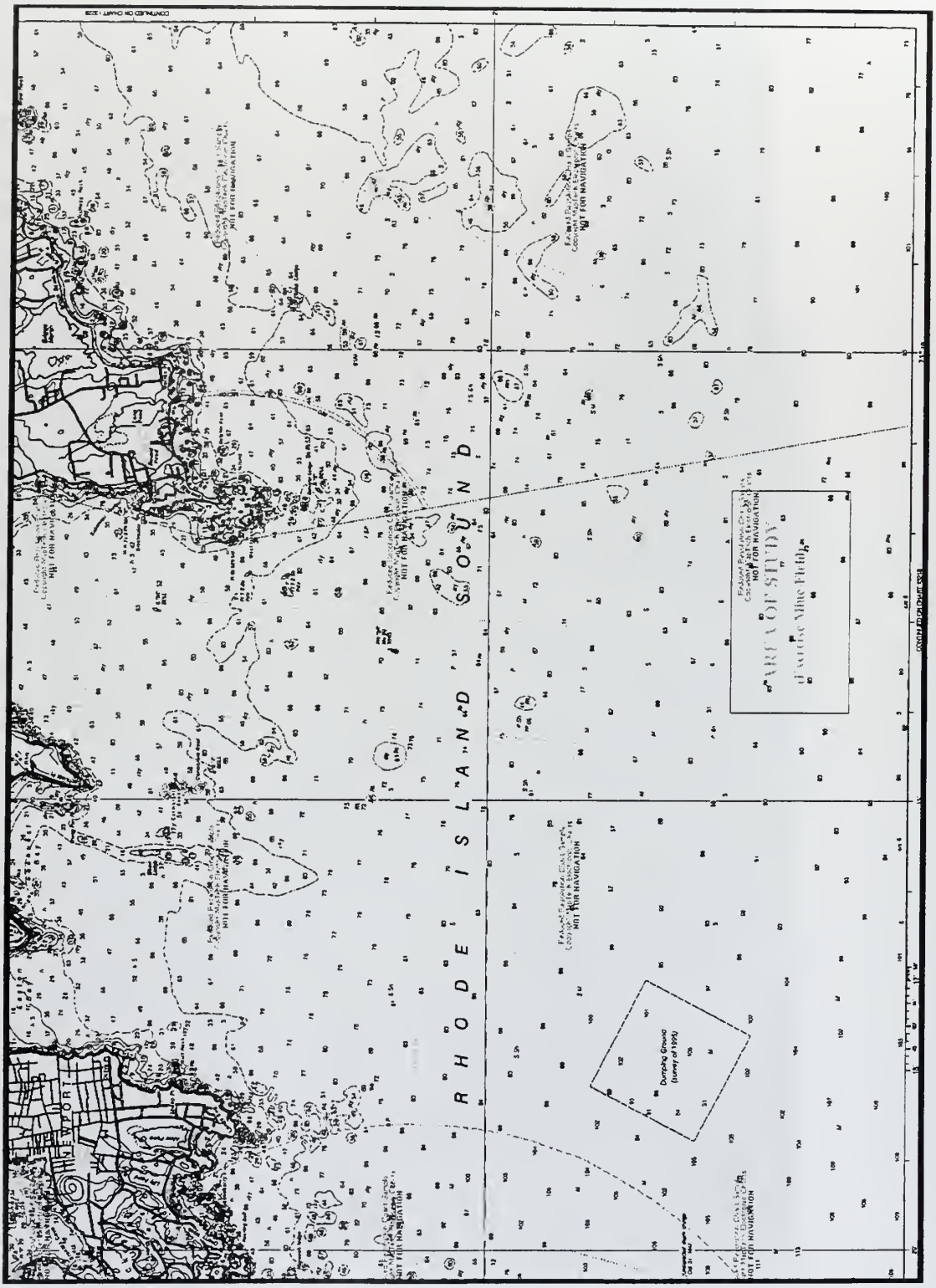

Figure 5. Chart of Rhode Island Sound displaying the MIW exercise area (after NOAA, 1998).

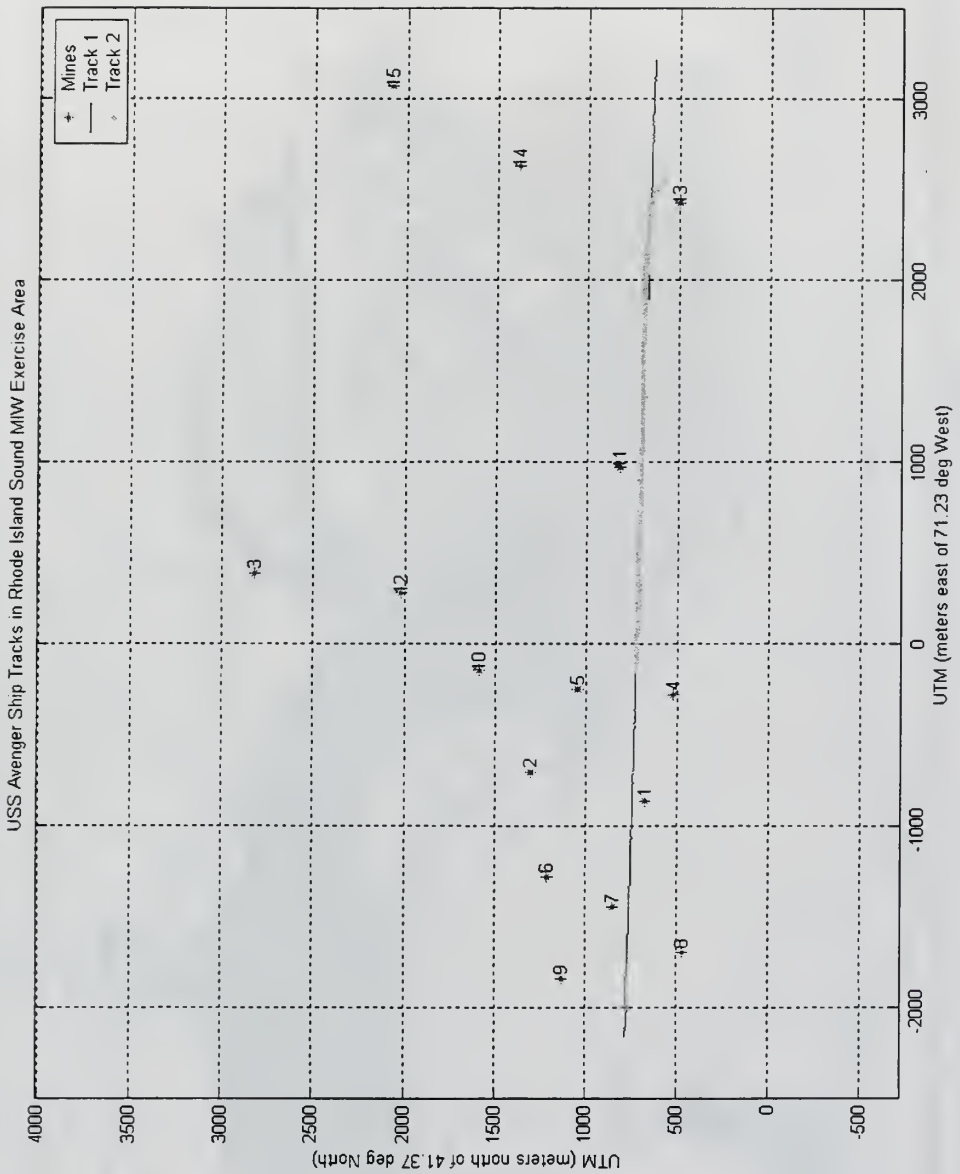

Figure 6. Ship's tracks in Rhode Island Sound MIW exercise area.

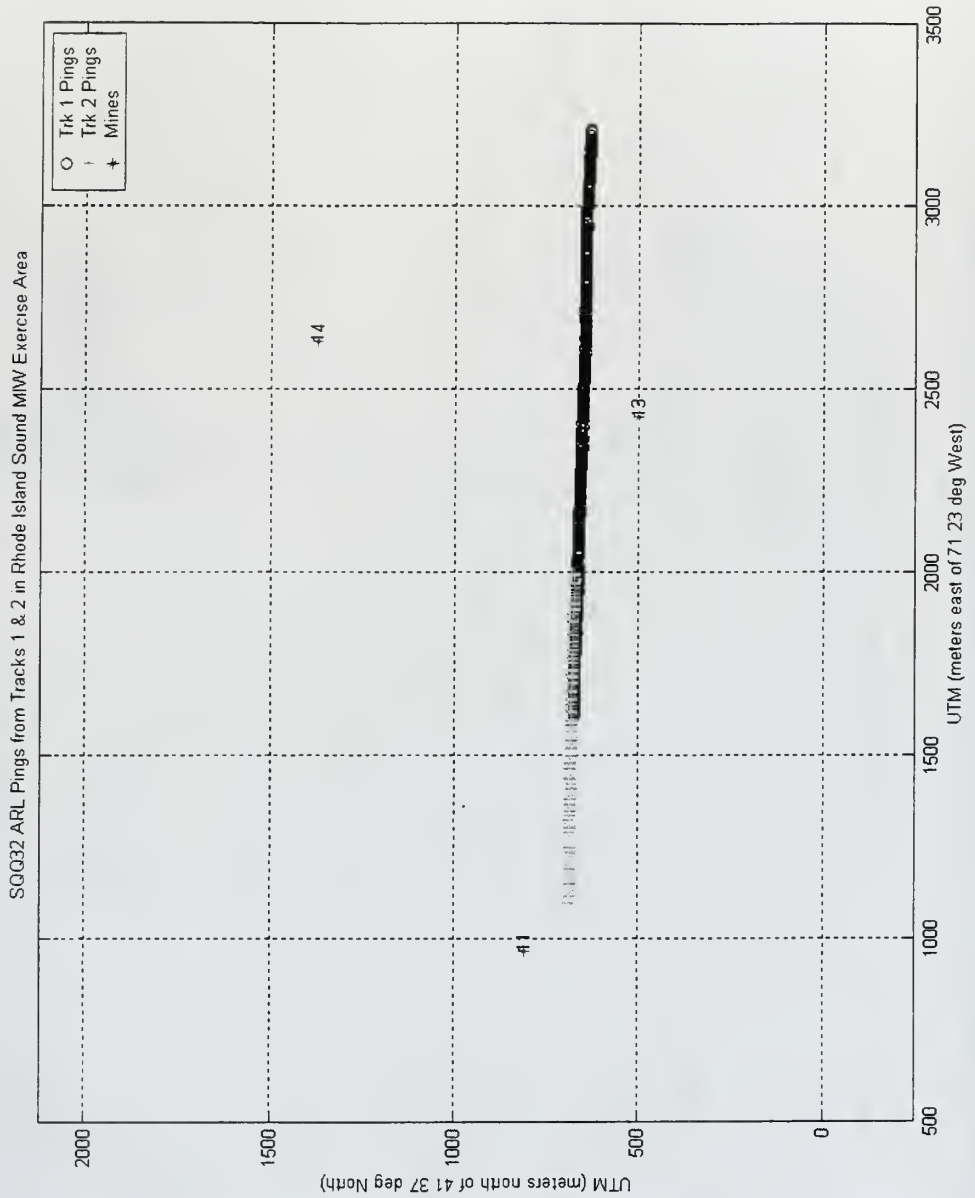

Figure 7. Ship's ping coverage in Rhode Island Sound MIW exercise area.

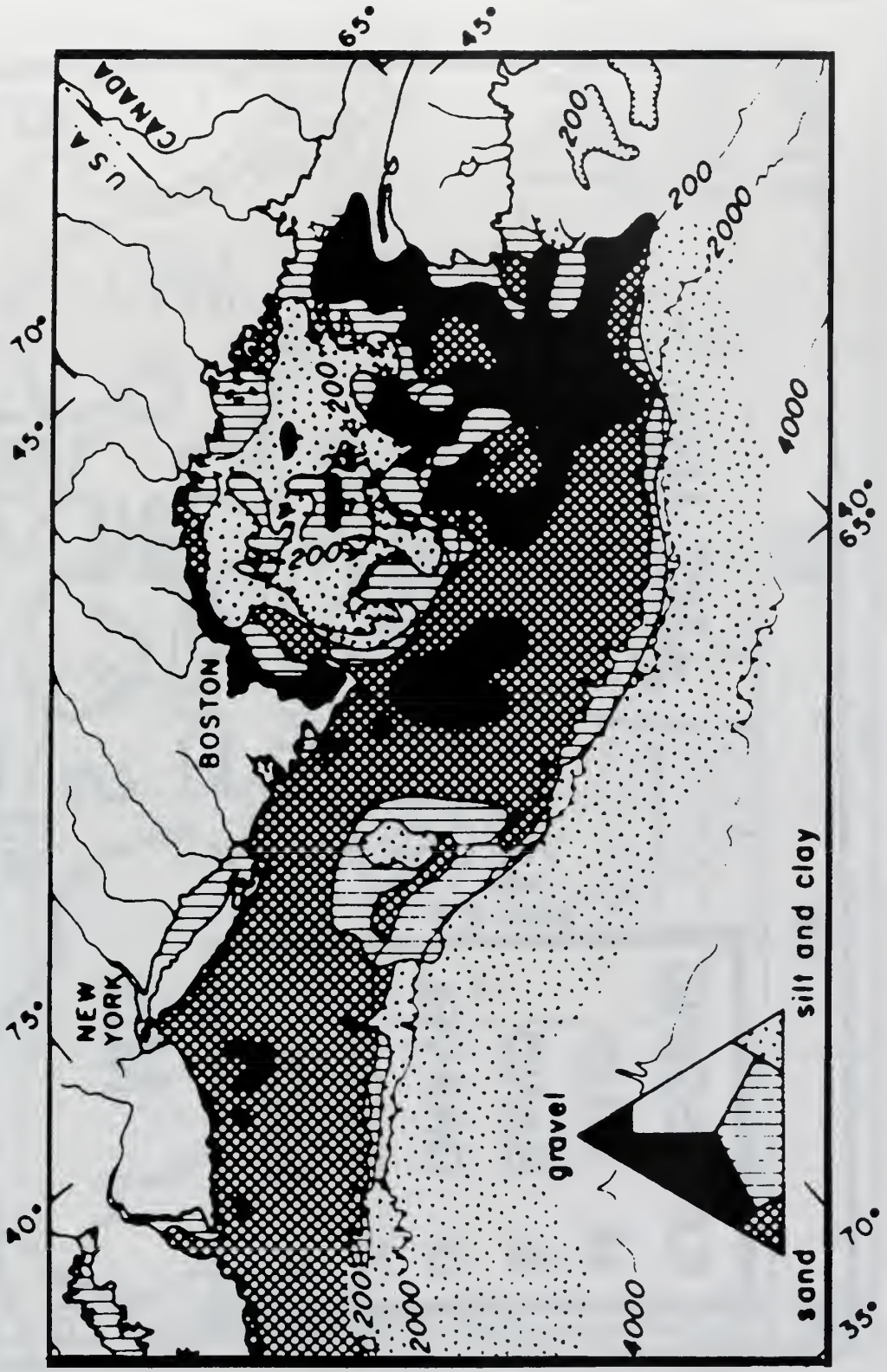

Figure 8. The sediment distribution off the New England continental shelf is comprised mostly of sand (after Milliman et al., 1972).

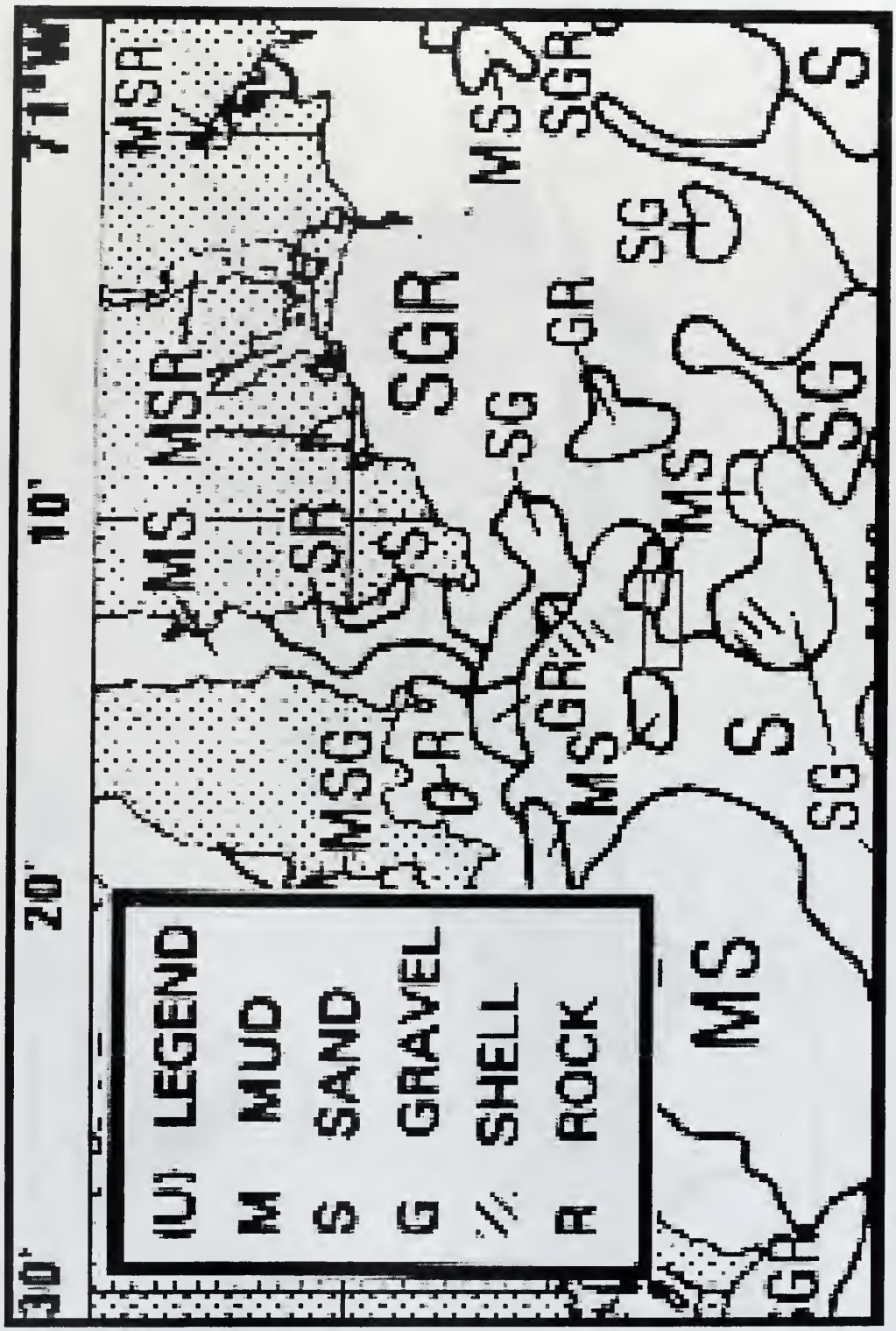

Figure 9. Sediment distribution in Rhode Island Sound (after NAVOCEANO MWP, 2000).

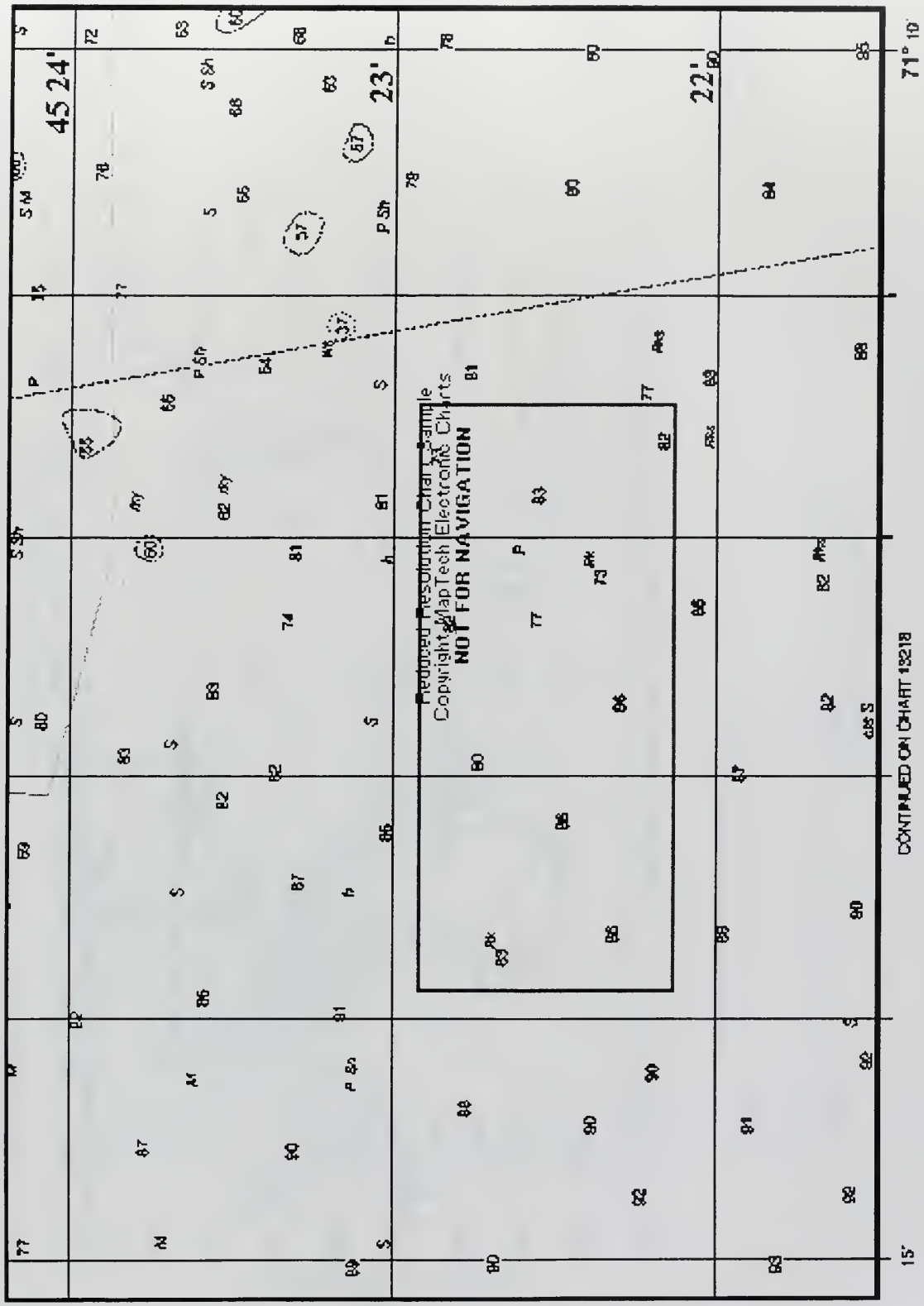

Figure 10. Close-up of navigation chart displaying 'Nature of Bottom' descriptors showing sand throughout (after NOAA, 1998).

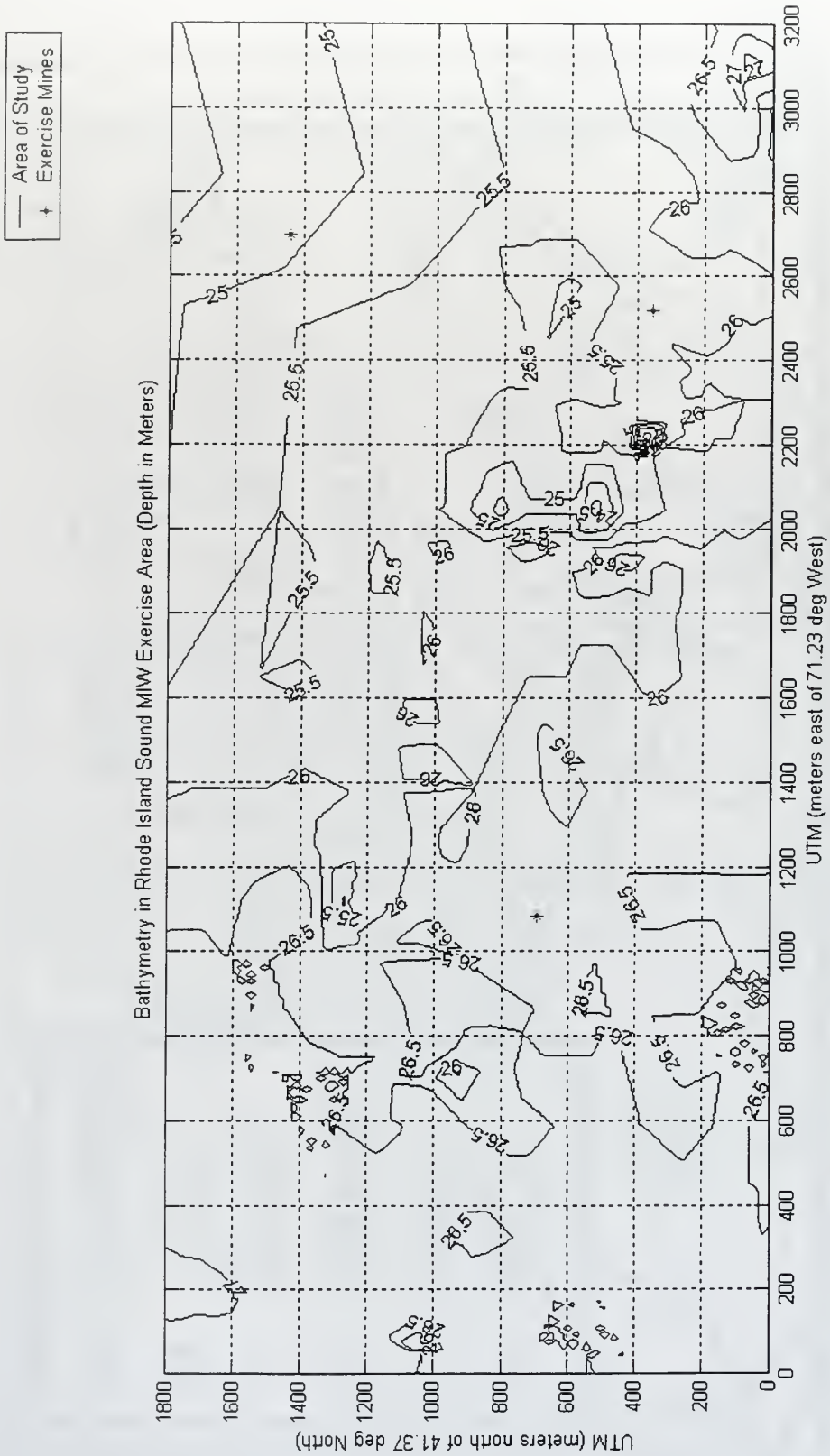

Figure 11. High Resolution Bathymetry of Area of Study (bottom contours in meters)

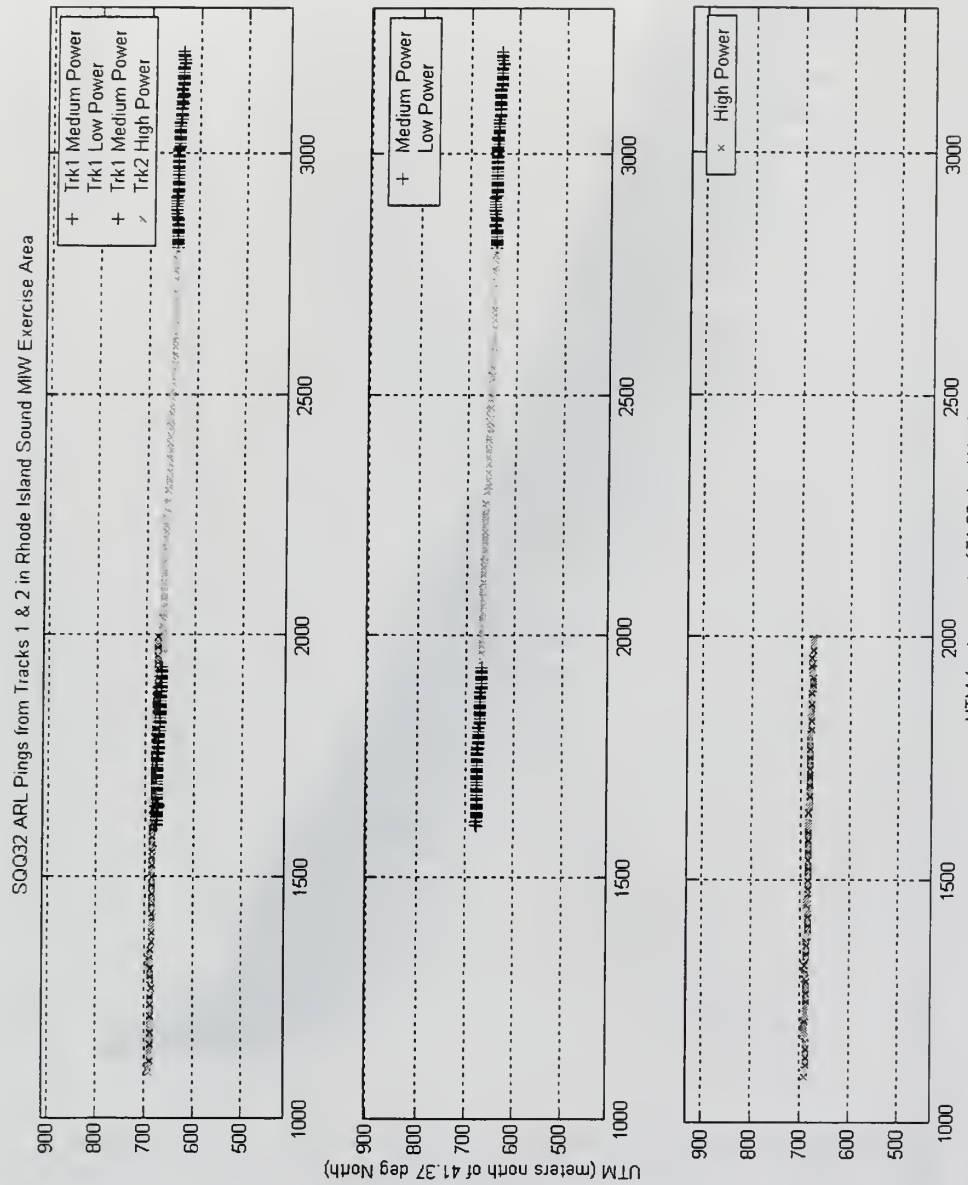

Figure 12. Ship's ping distribution detailing different operating modes.

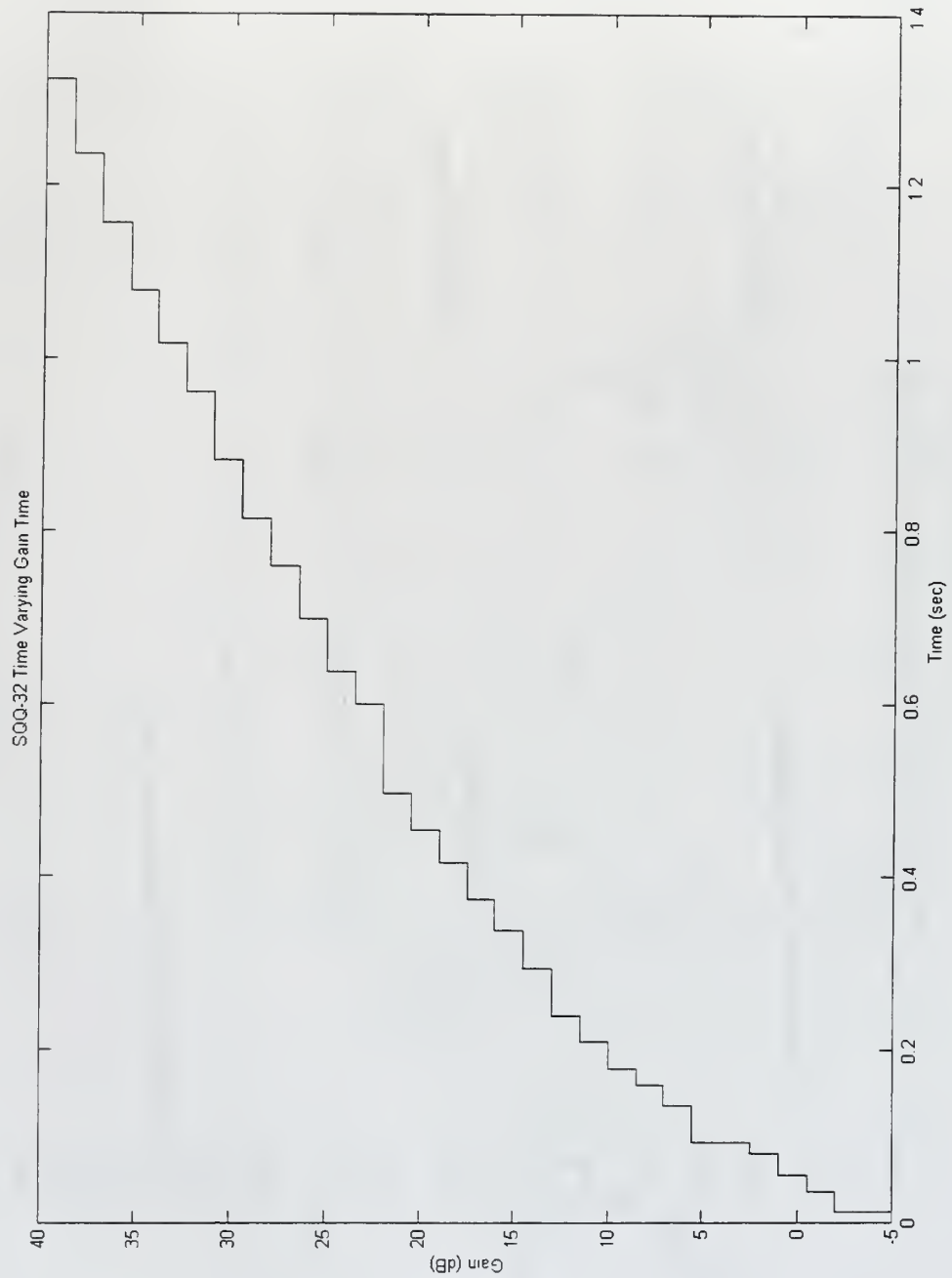

Figure 13. AN/SQQ32 Time Varying Gain

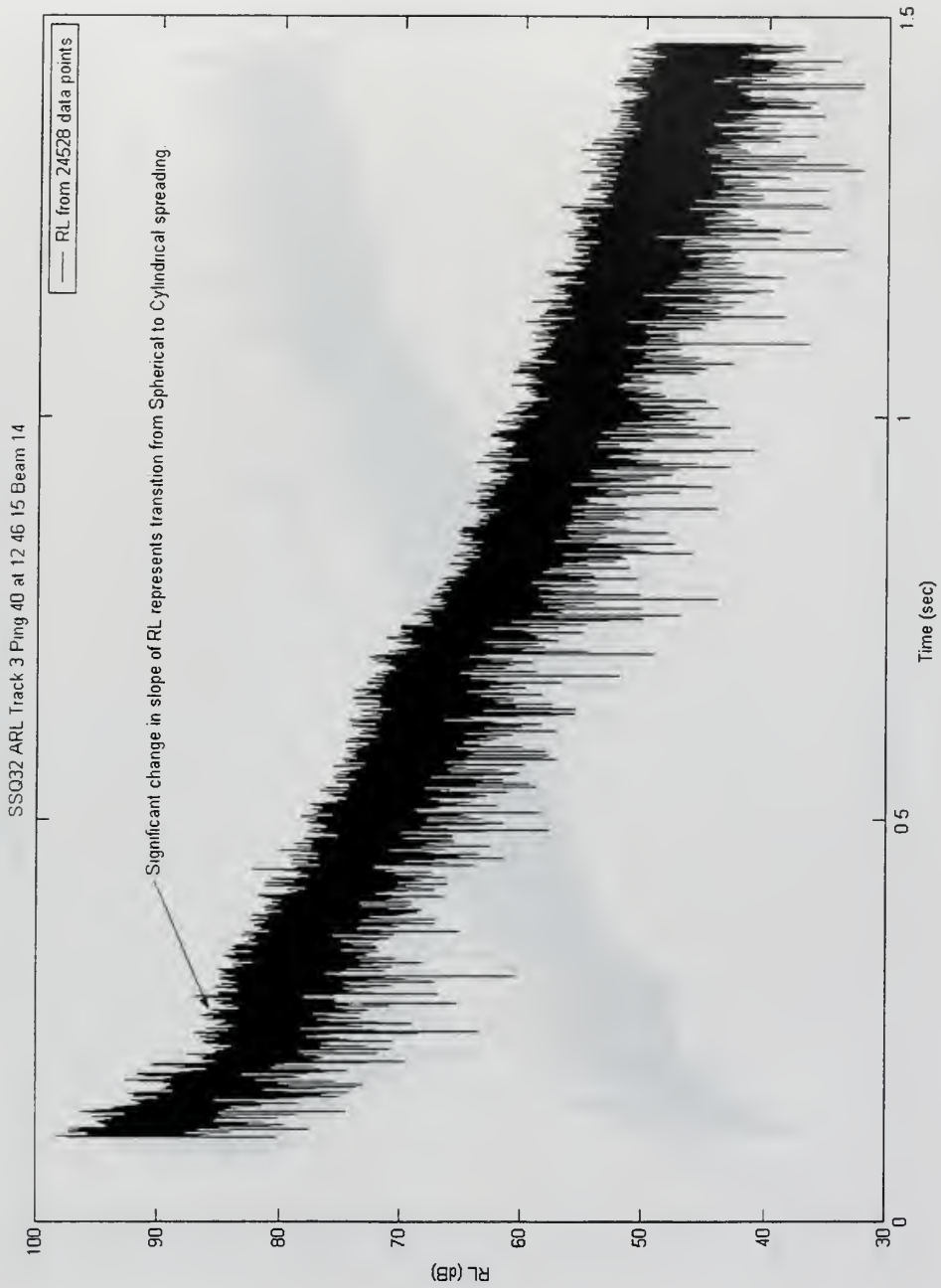

Figure 14. Typical single ping's time series of RL from a fairly homogeneous bottom.

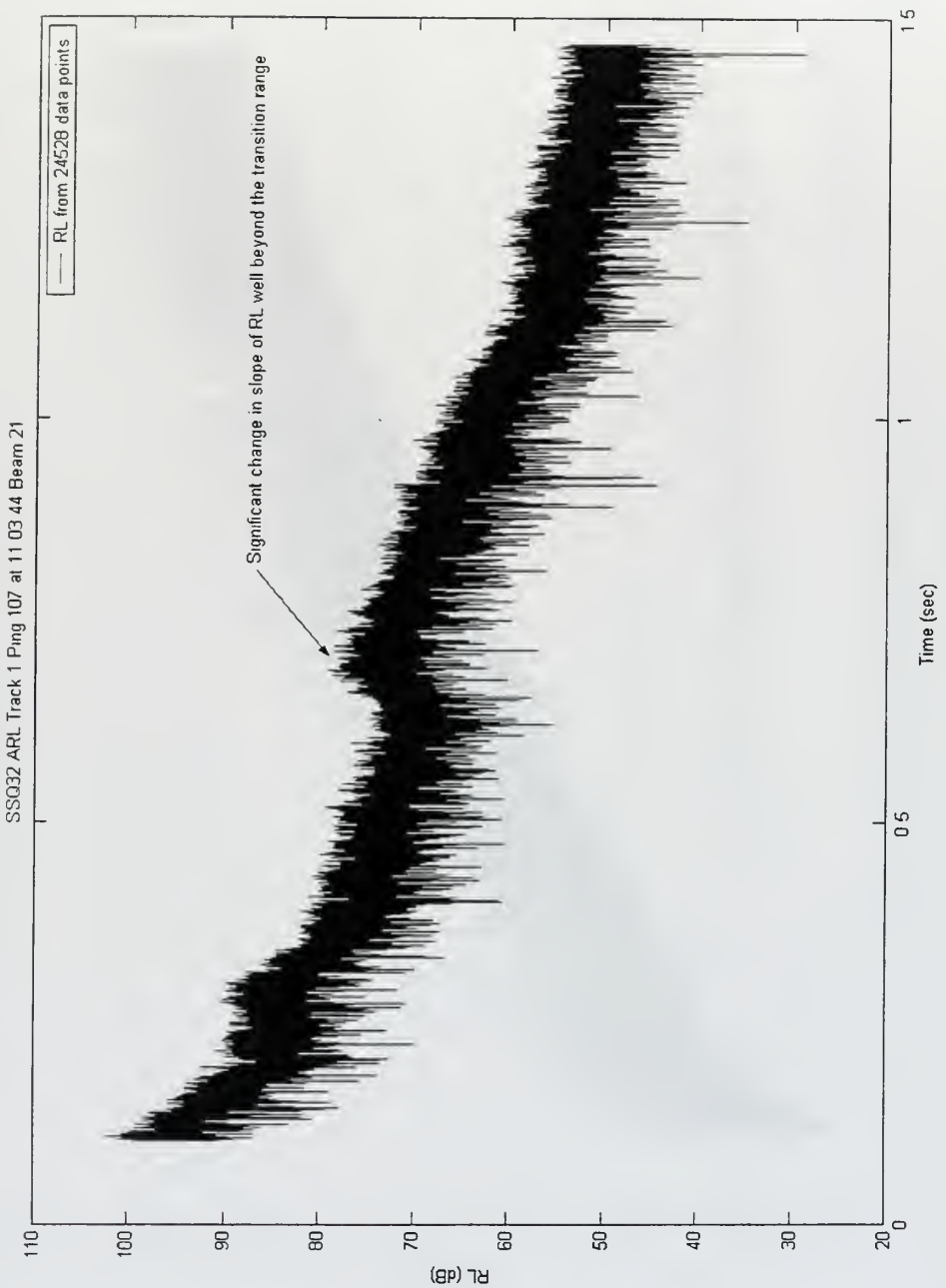

Figure 15. Single ping time series of RL from a non-homogeneous bottom.

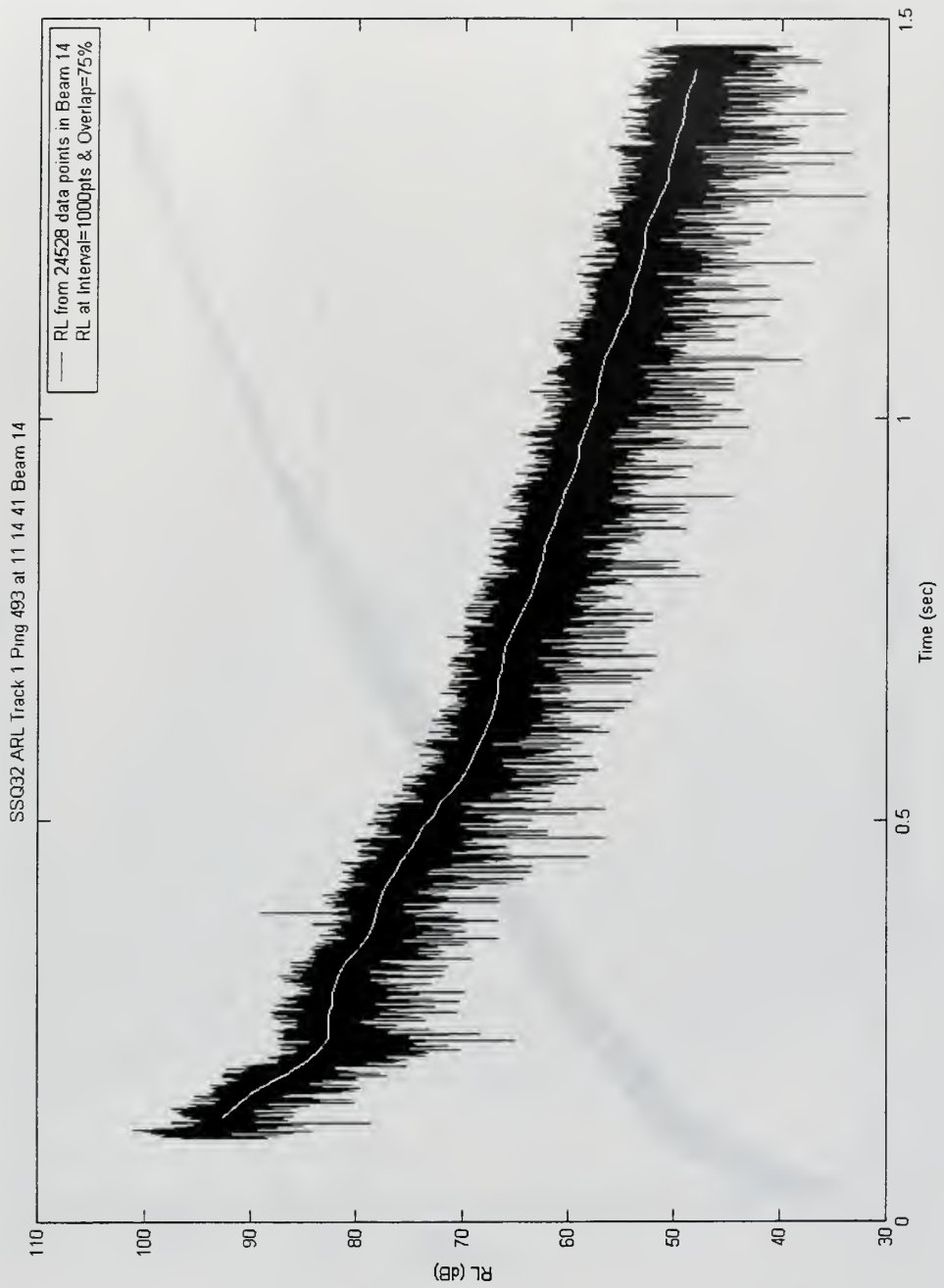

Figure 16. Typical single ping time series of RL and its smoothed (1000/75%) RL curve.

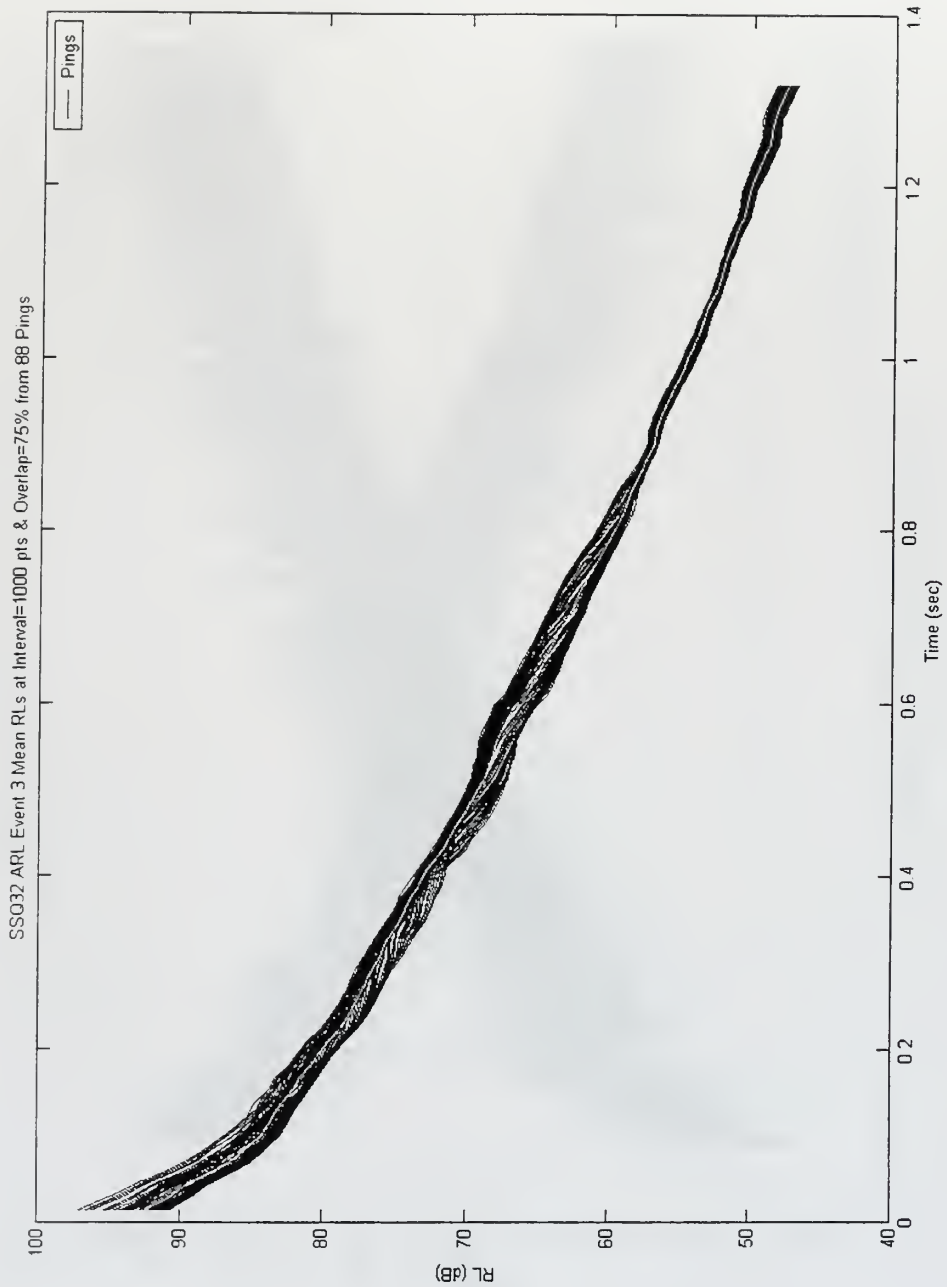

Figure 17. Individual mean RL curves of Event 3's pings (Black) overlaid by Event 3's mean RL curve (White).

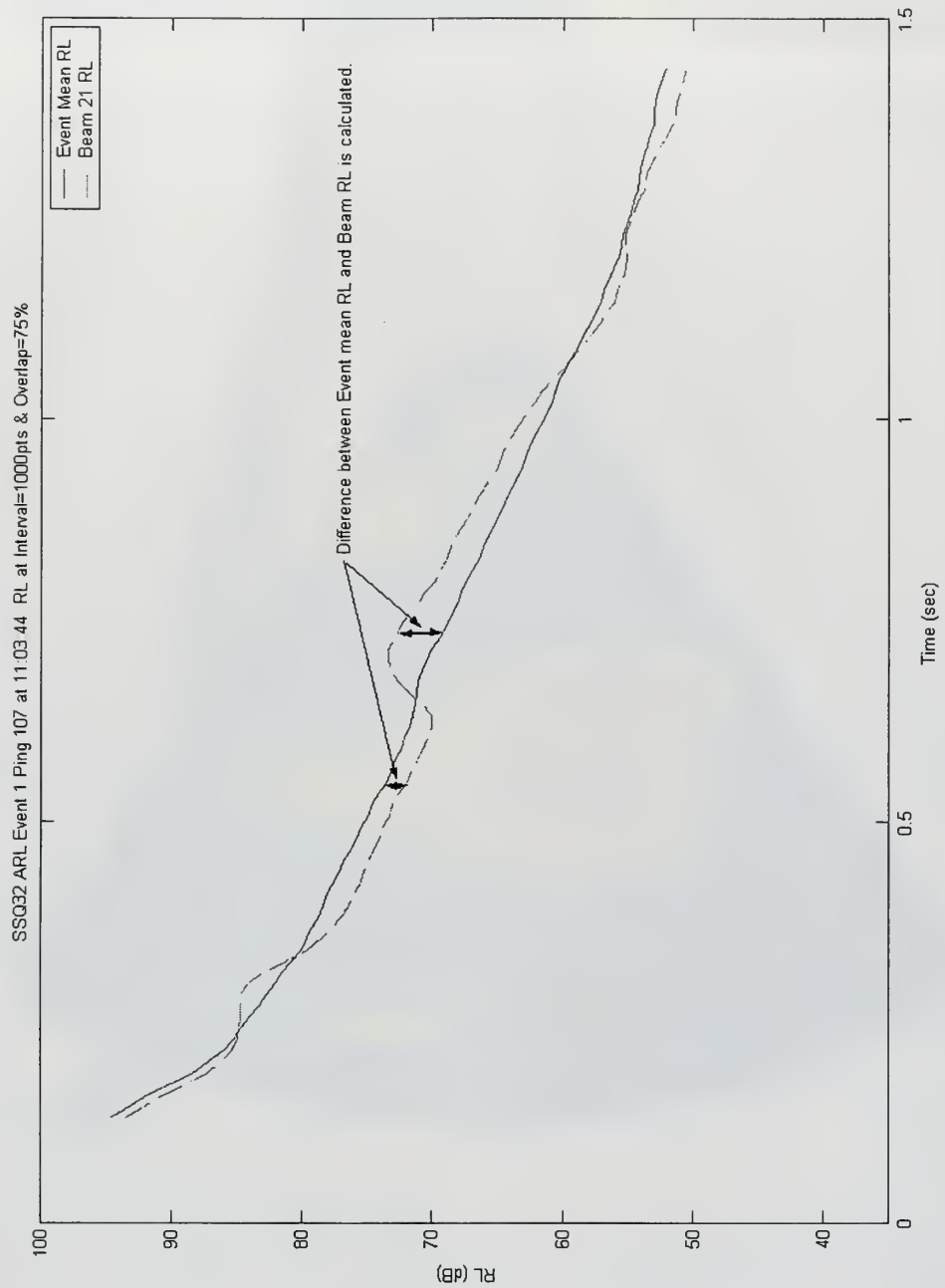

Figure 18. Smoothed RL curve for Beam 14 (dashed) with its event-wide mean RL curve (solid).

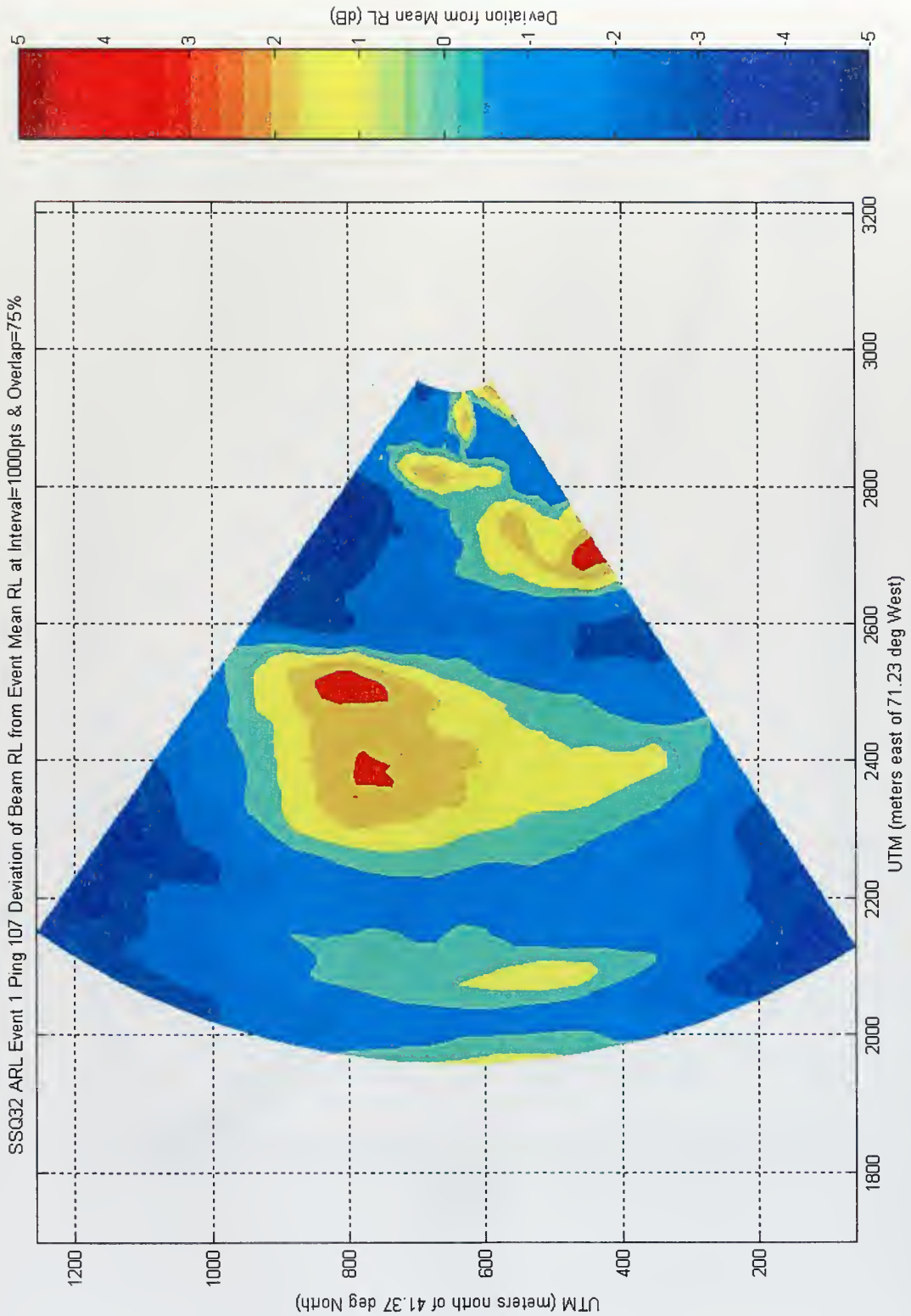

Figure 19. Contour plot of Ping 107's RL deviation from event-wide (Event 1) mean RL.

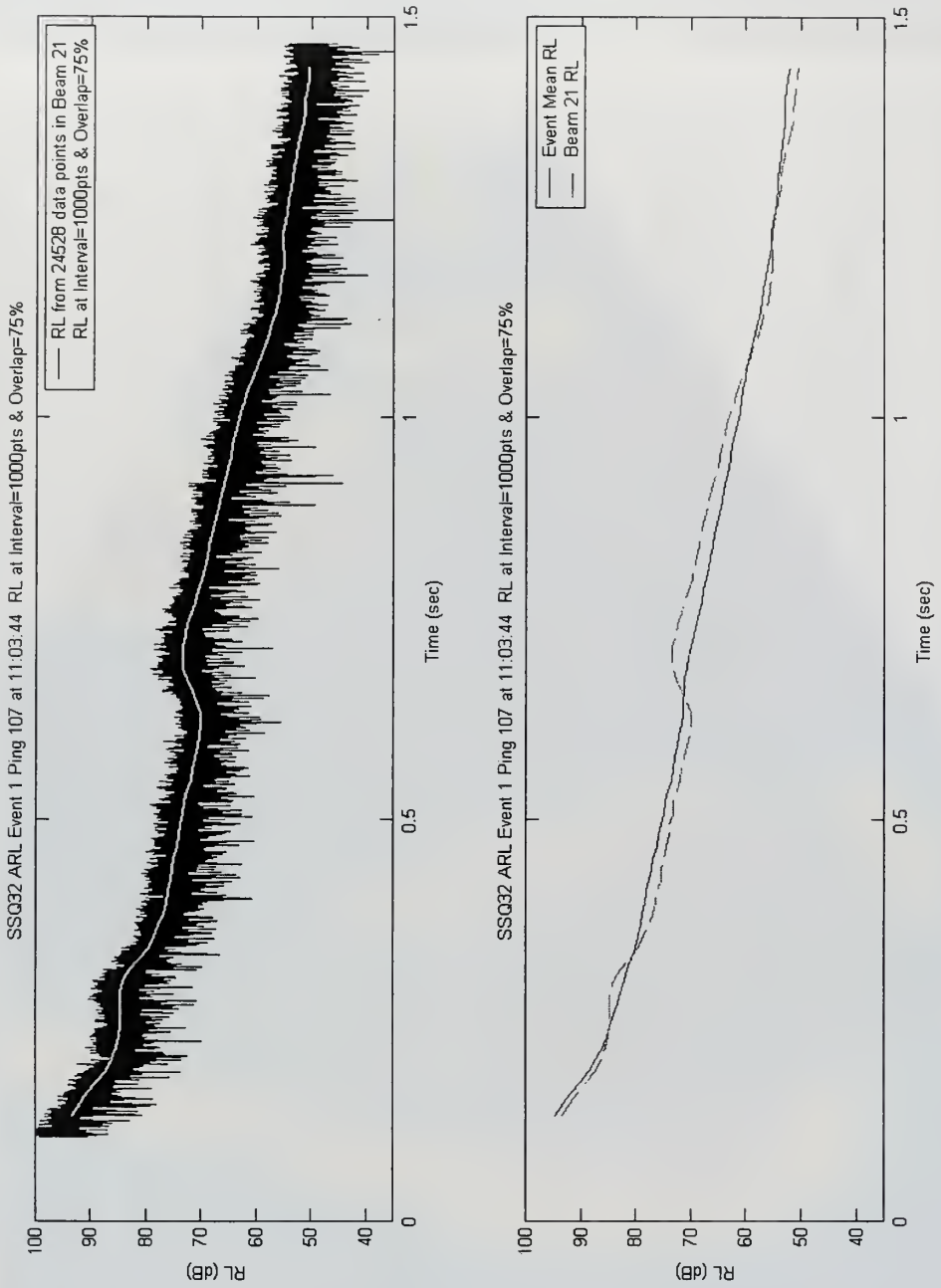

Figure 20. RL and smoothed RL (top) for ping 107, beam 21, and smoothed RL (dashed) with event mean RL (solid) (below).

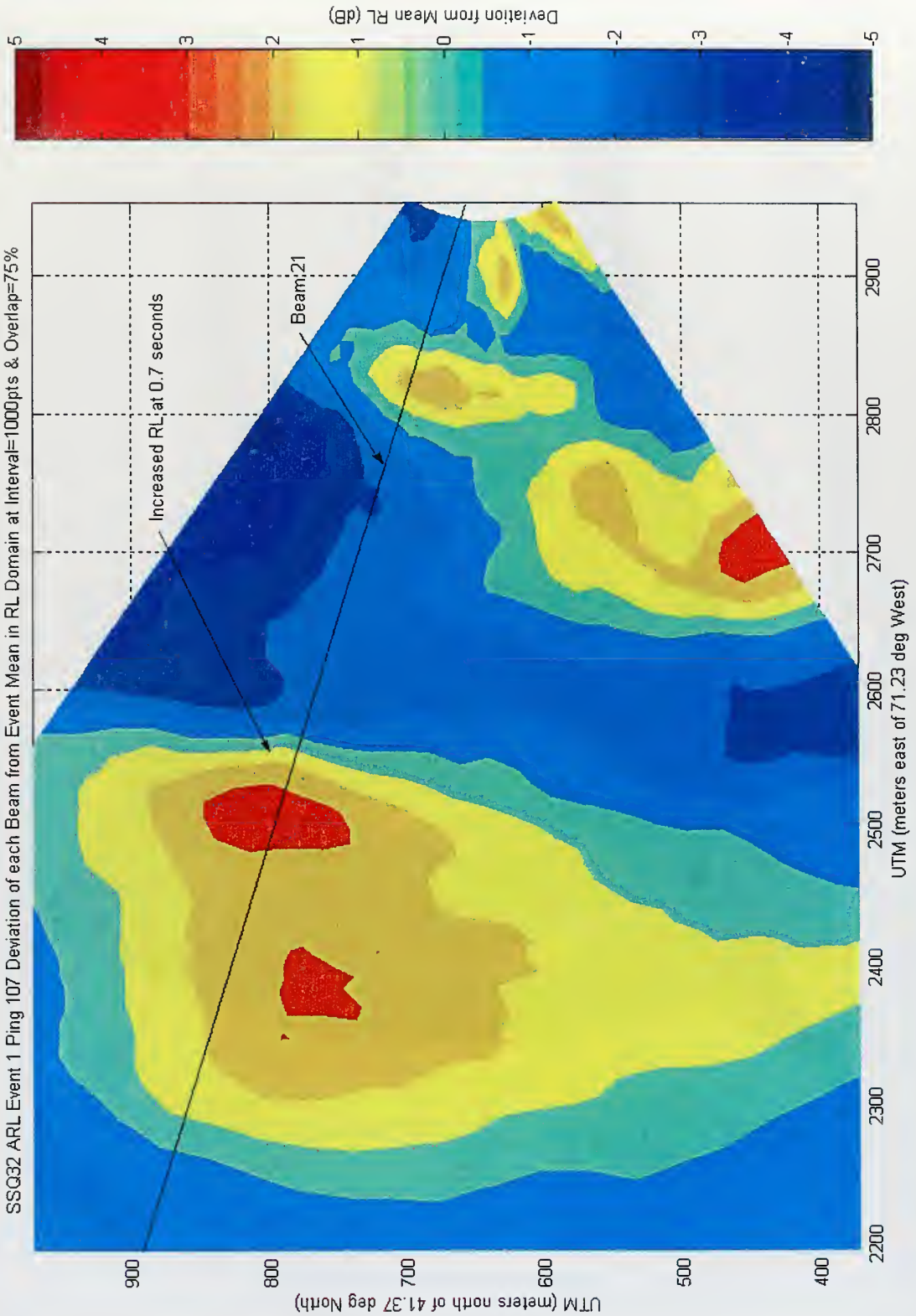

Figure 21. Region of ping107 beam 21 (enlarged) to show the RL curve details.

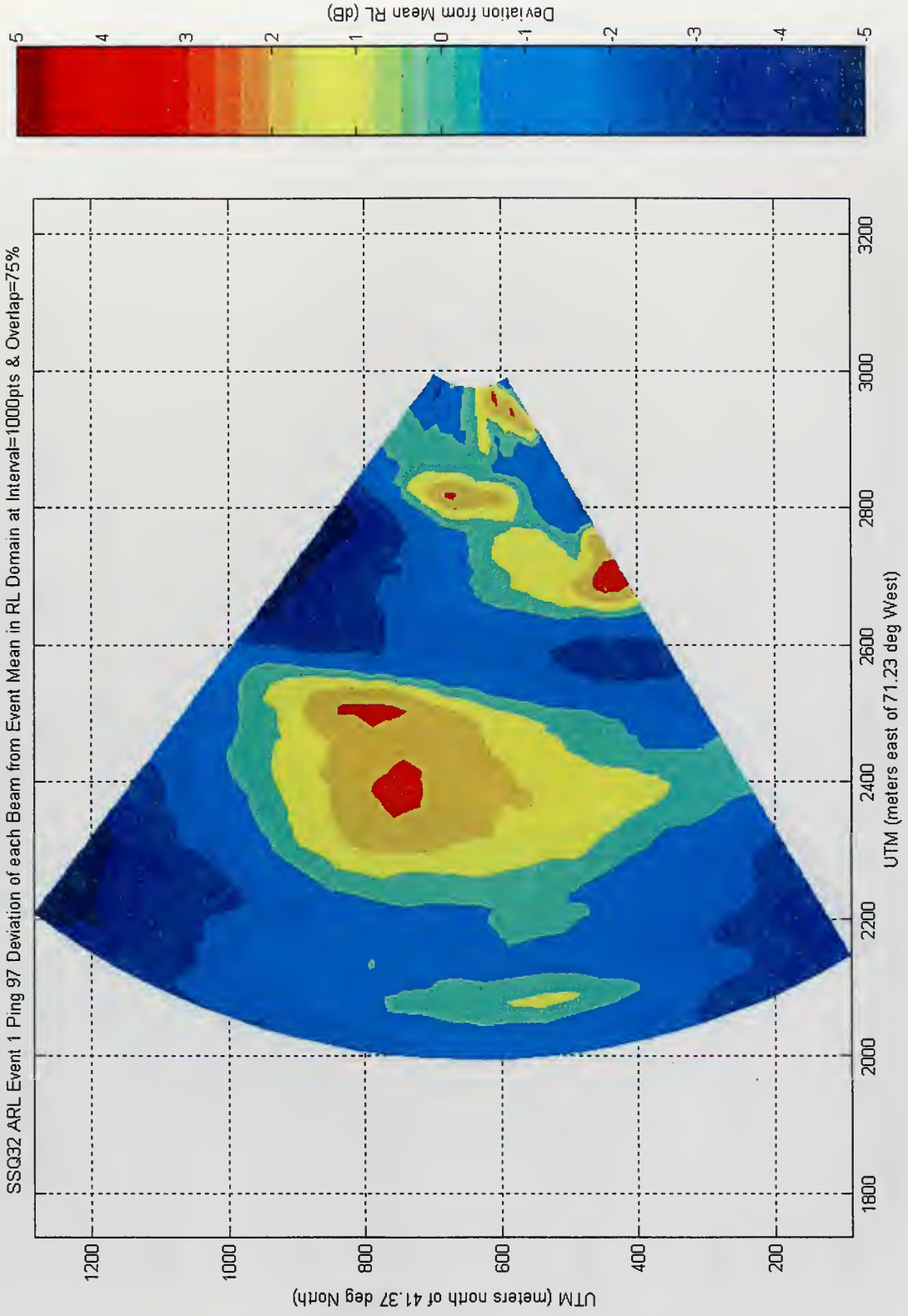

Figure 22. Contour plot of Ping 97's RL deviation from event-wide mean RL.

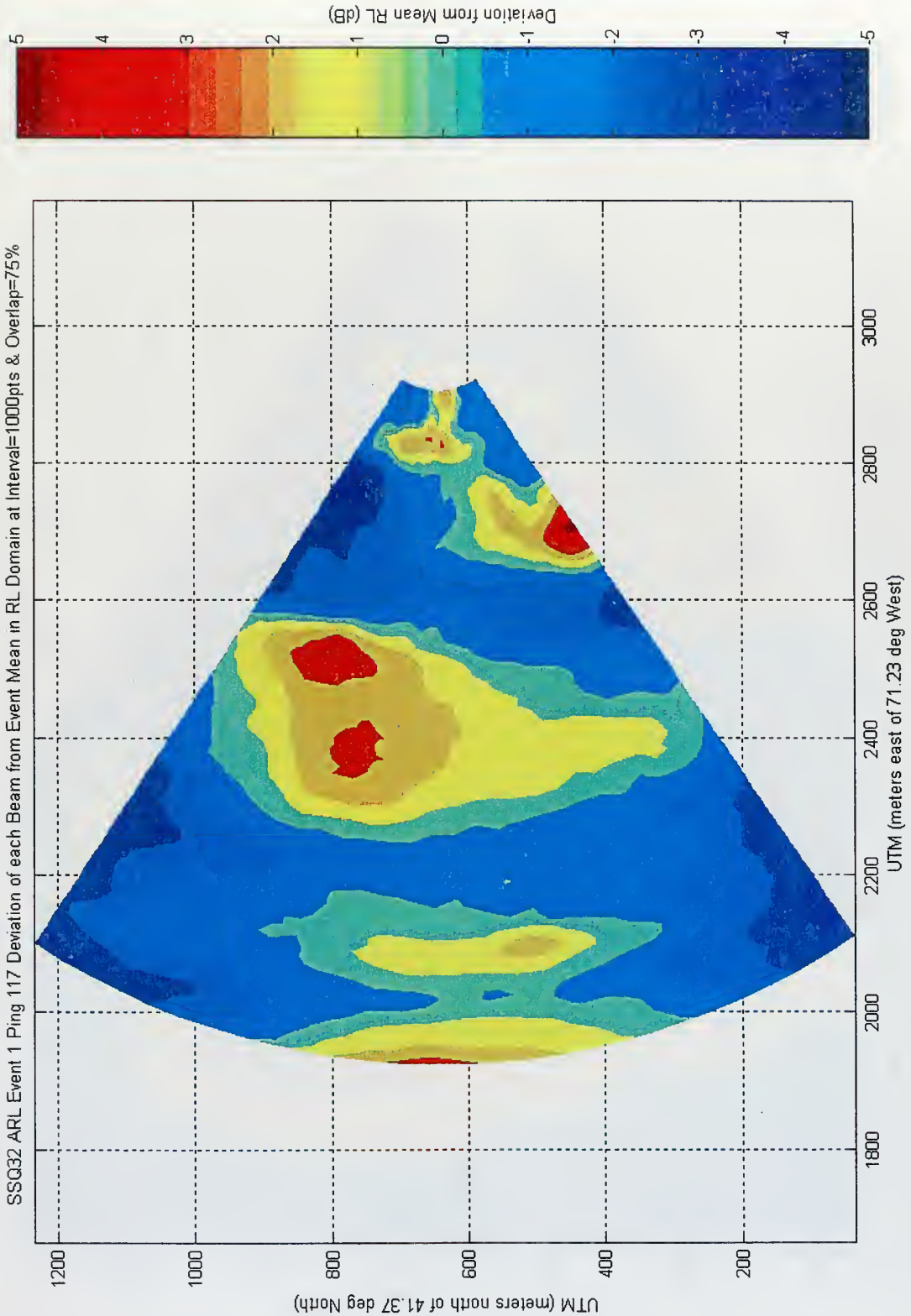

Figure 23. Contour plot of Ping117's RL deviation from event-wide mean RL.

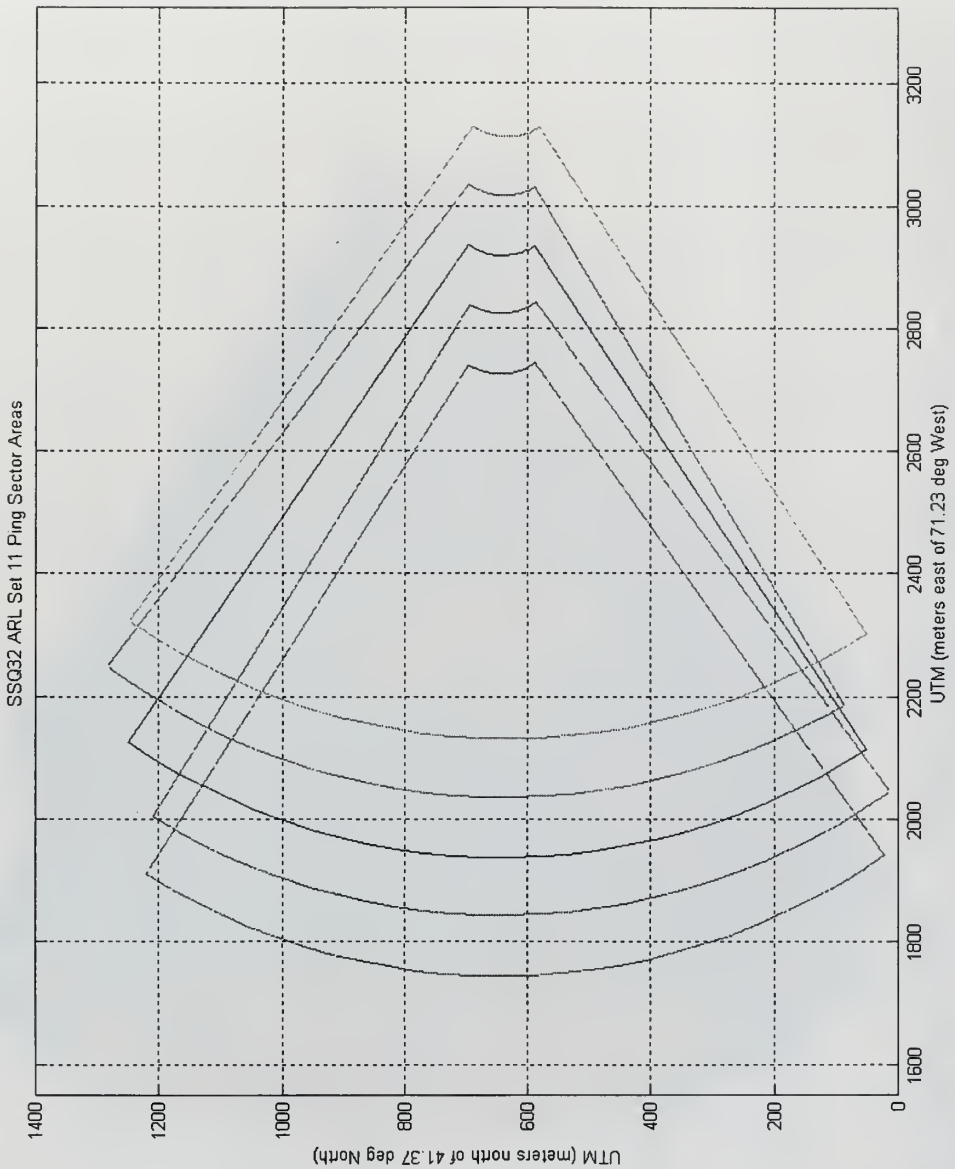

Figure 24. Sector areas covered by sequence of pings (Set 1) in Event 1.

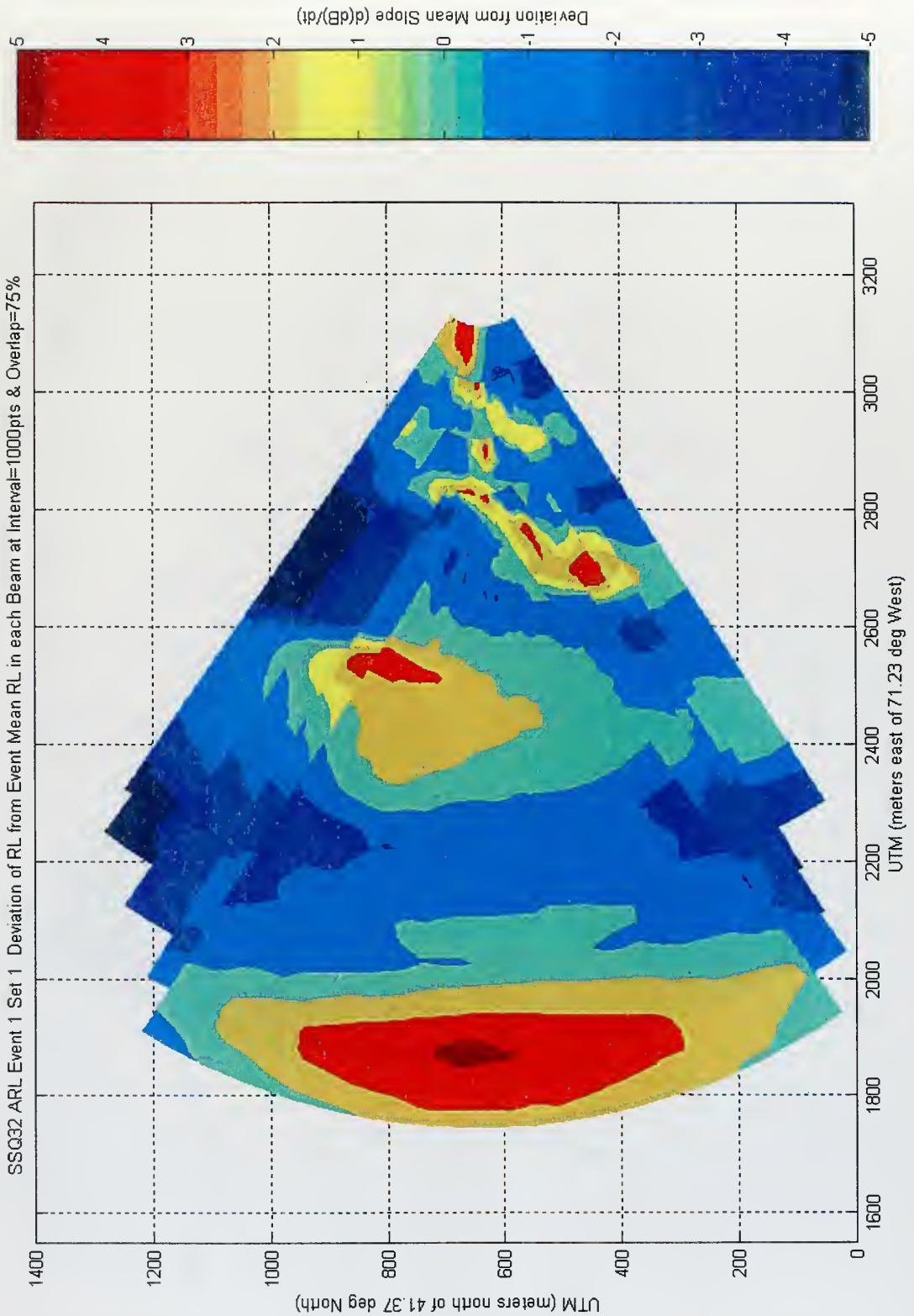

Figure 25. Overlaying contour plots from sequence of five pings (Set 1) from Event 1

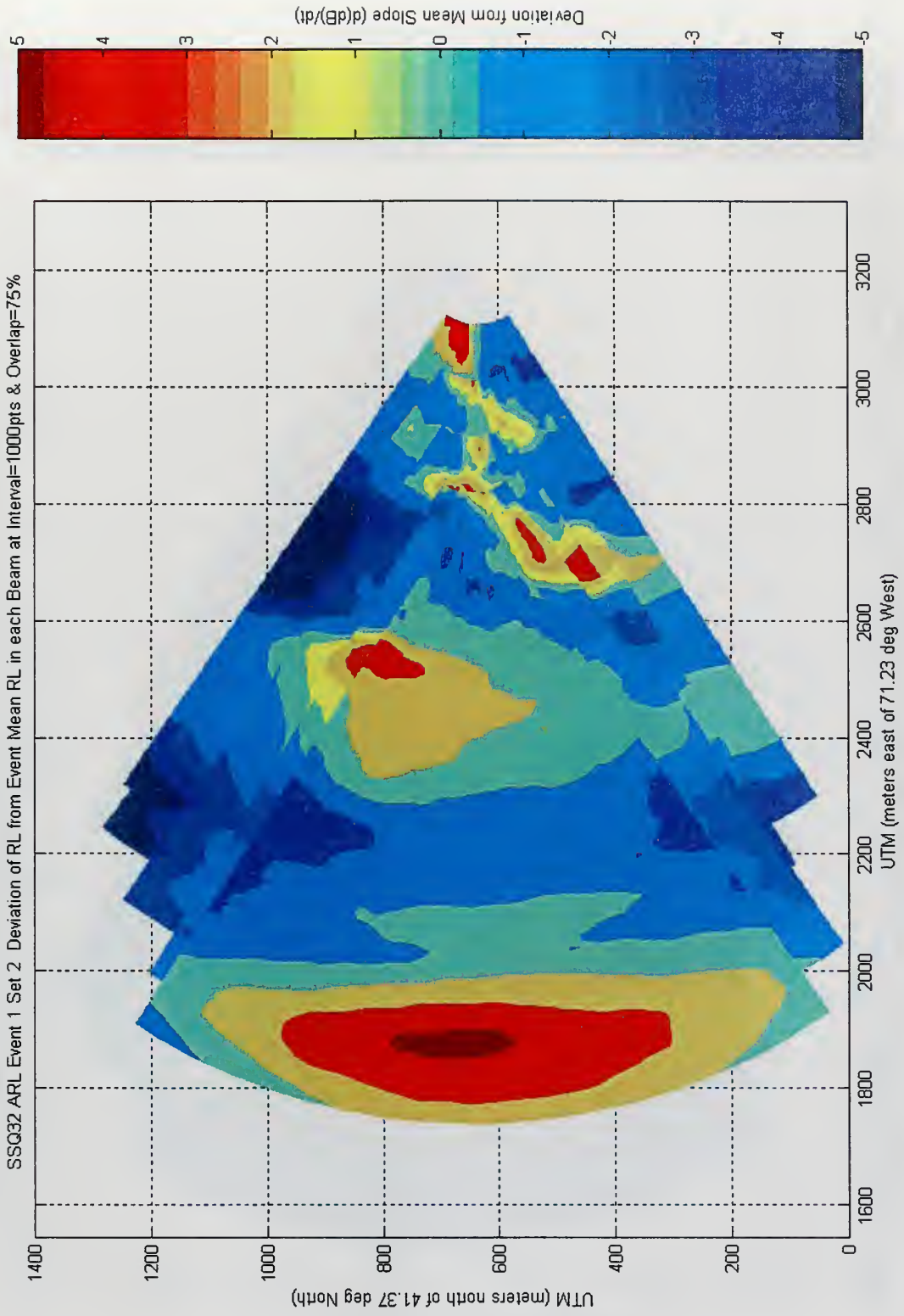

Figure 26. Overlaying contour plots from sequence of pings (Set 2) from Event 1.

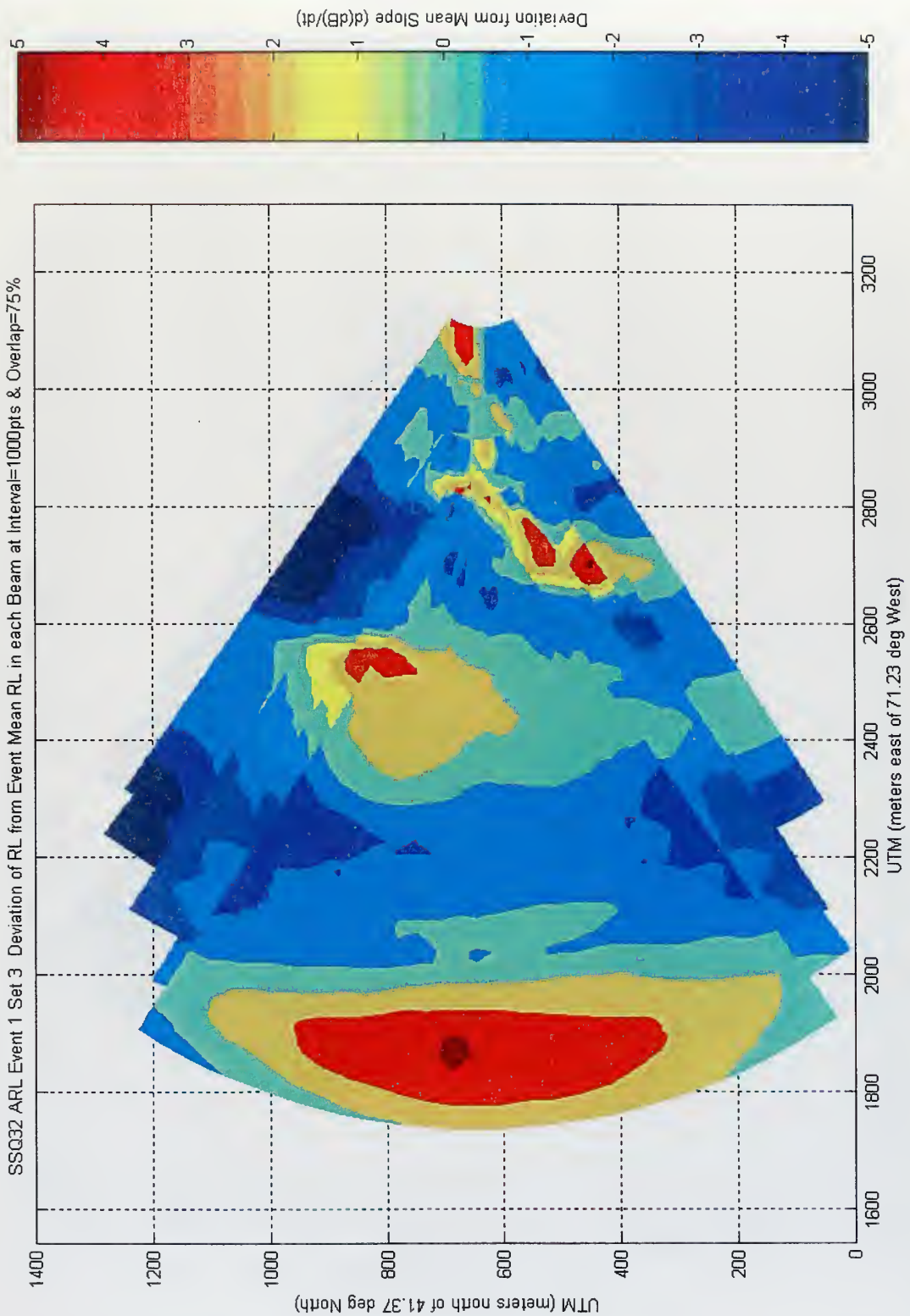

Figure 27. Overlaying contour plots from sequence of pings (Set 3) from Event 1.

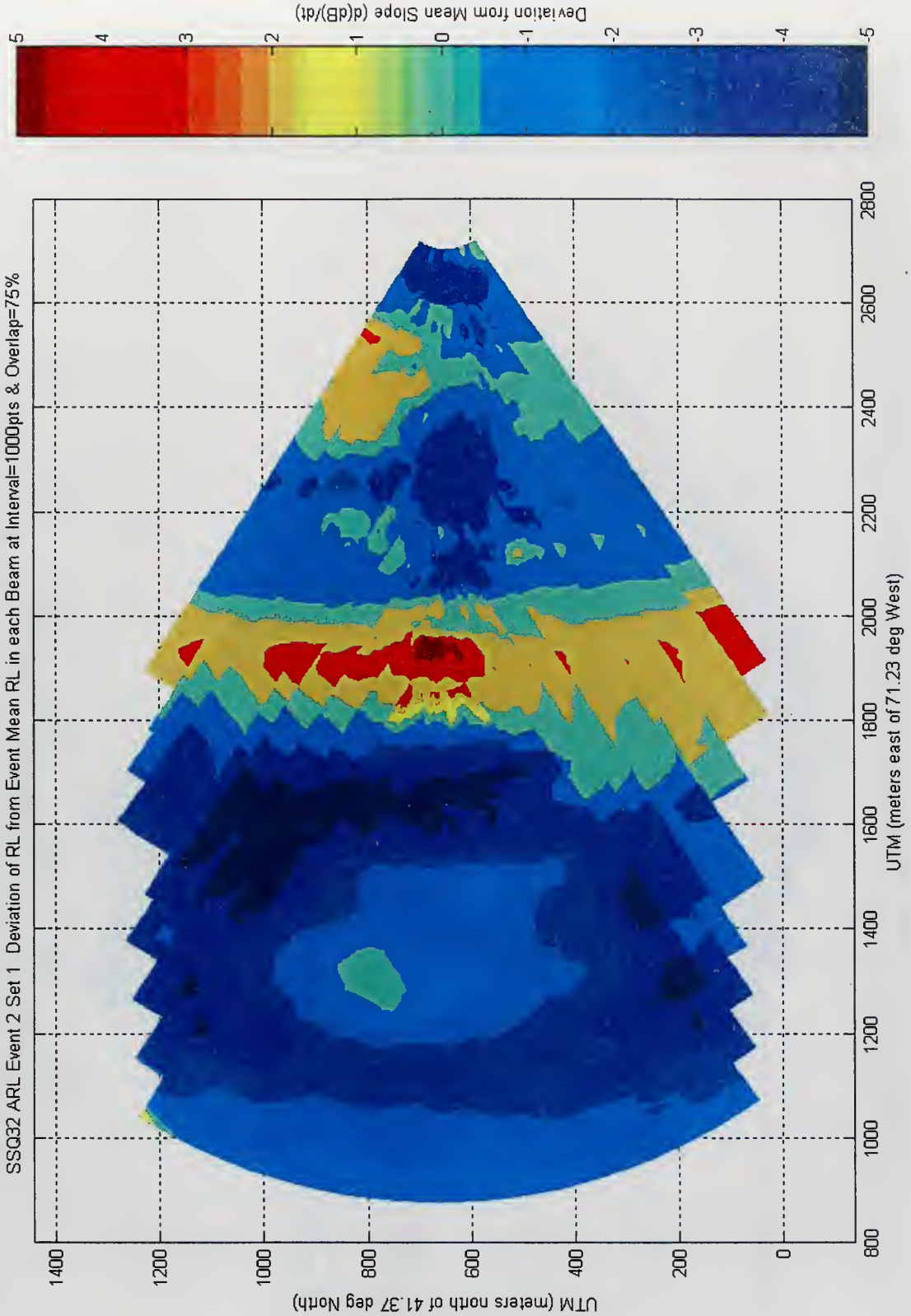

Figure 28. Overlaying contour plots from sequence of pings (Set 1) from Event 2.

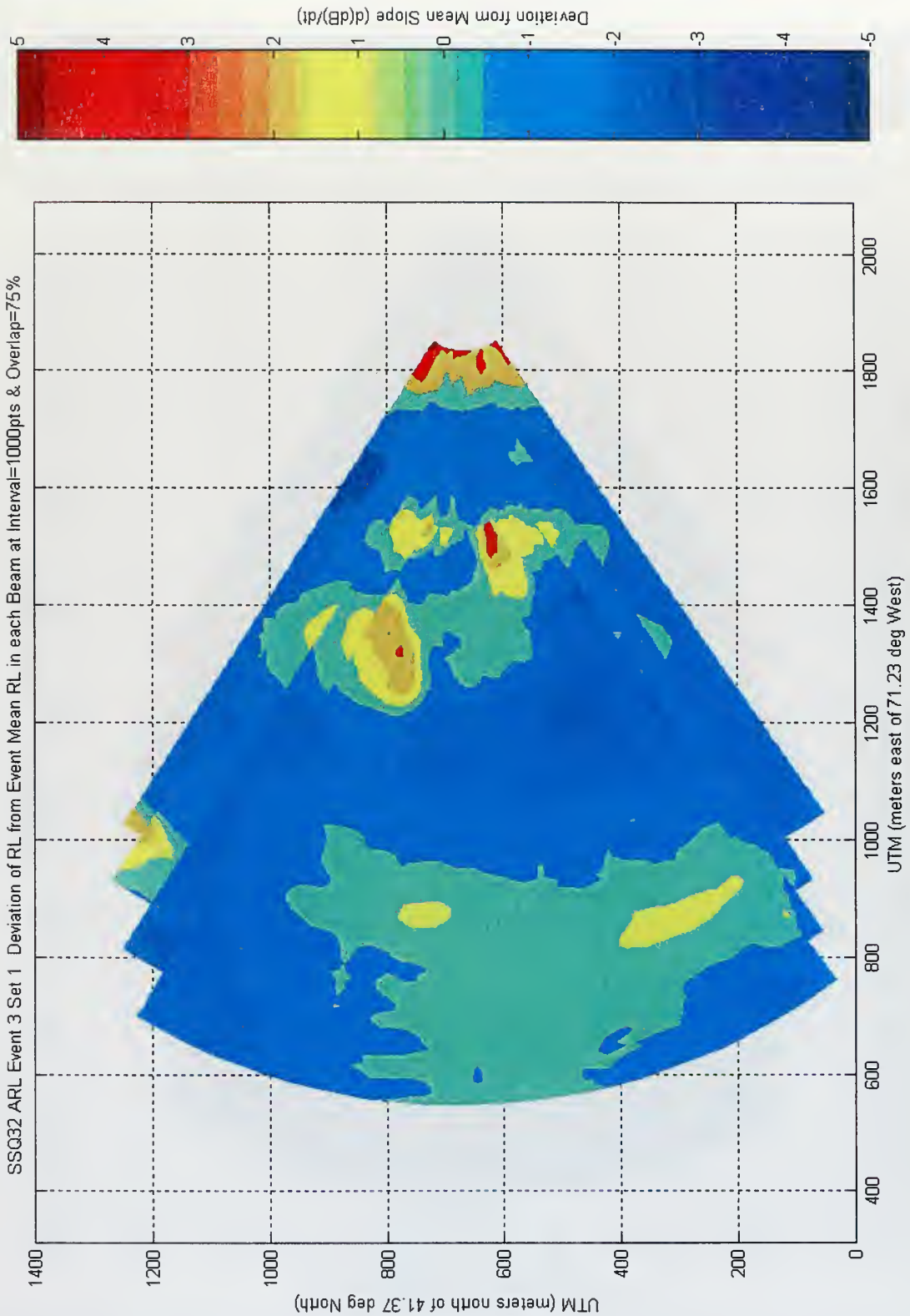

Figure 29. Overlaying contour plots from sequence of pings (Set 1) from Event 3.

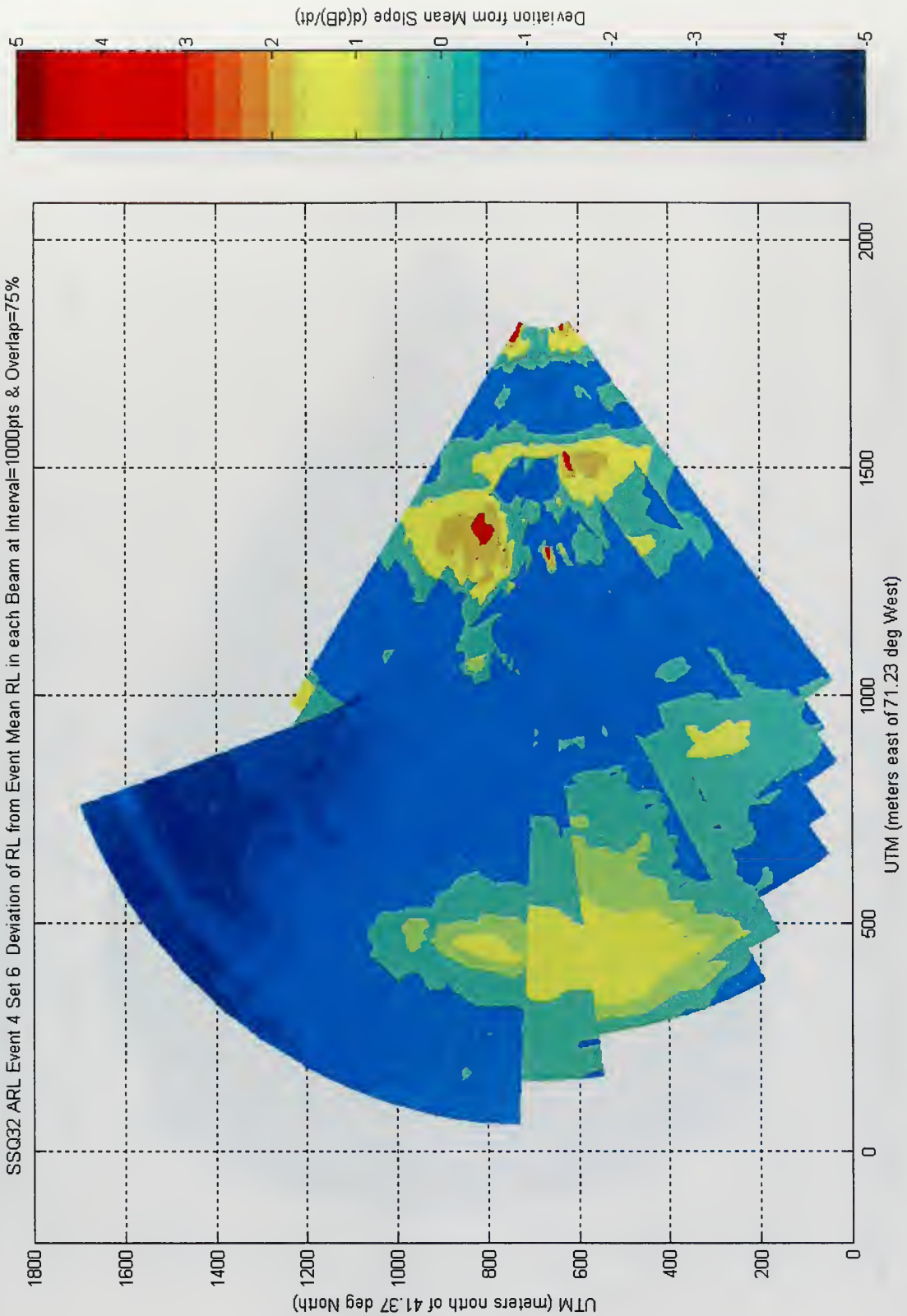

Figure 30. Overlaying contour plots from sequence of pings (Set 6) from Event 4.

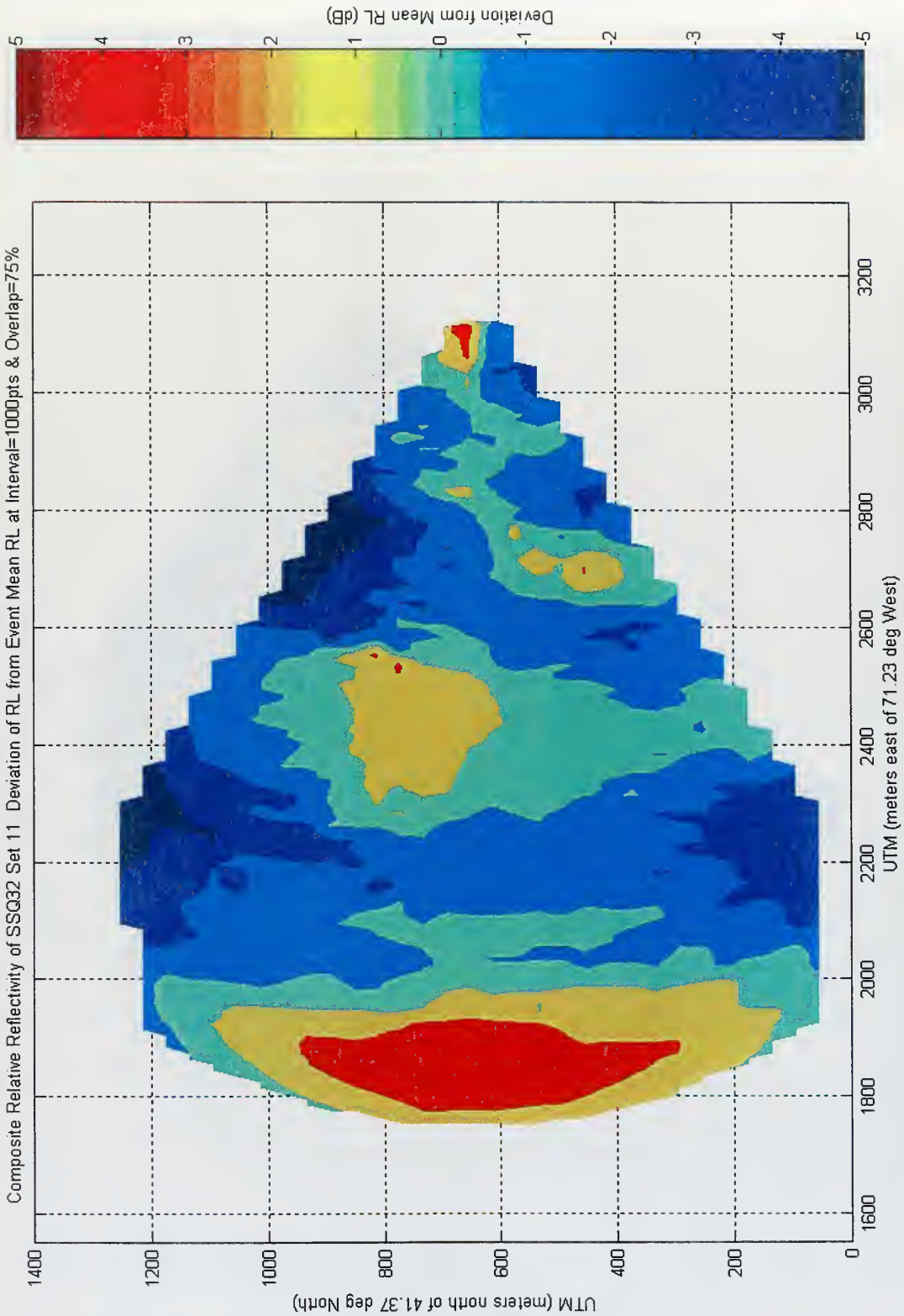

Figure 31. Composite plot of sequence of pings (Set 1) from Event 1.

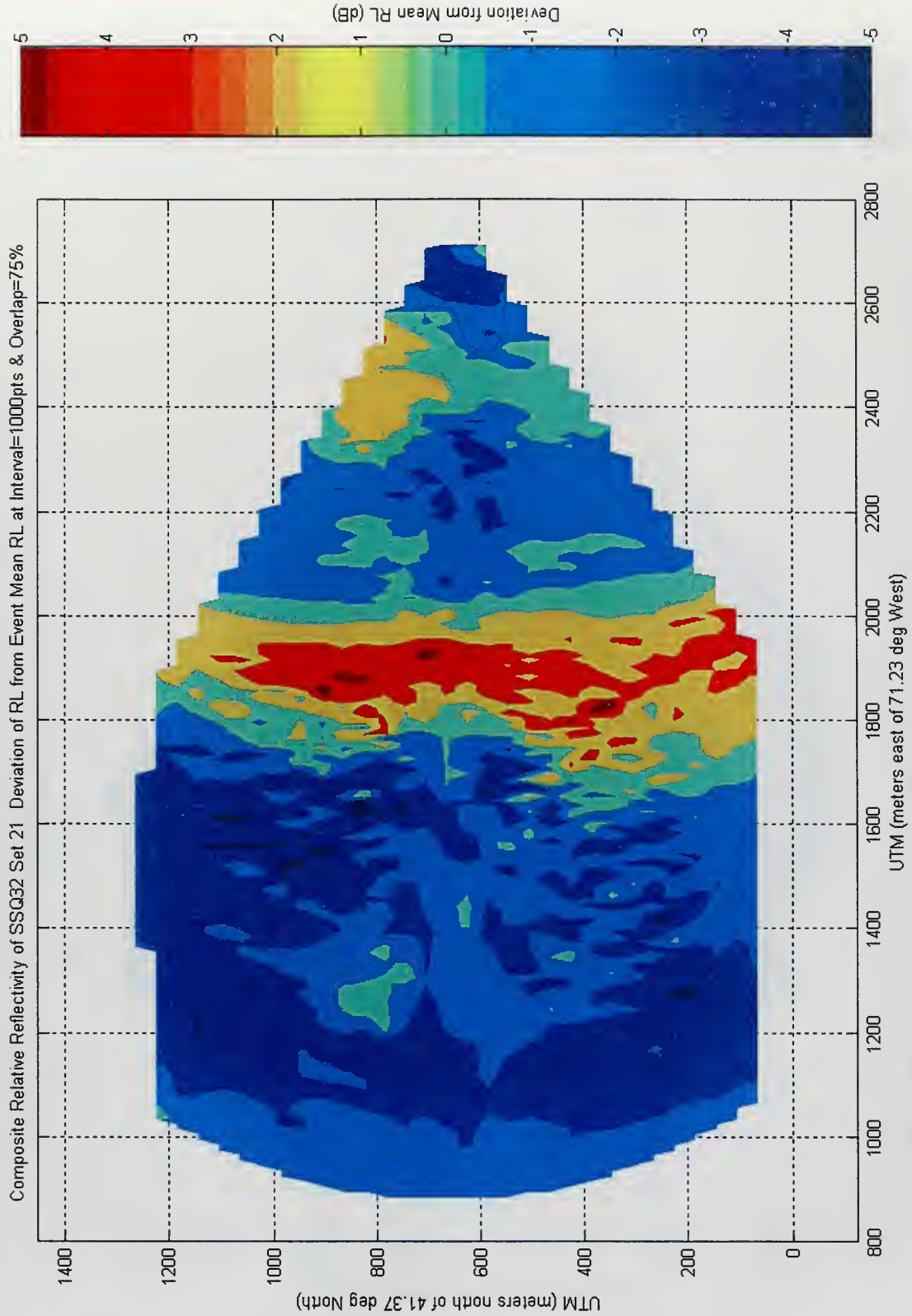

Figure 32. Composite plot of sequence of pings (Set 1) from Event 2.

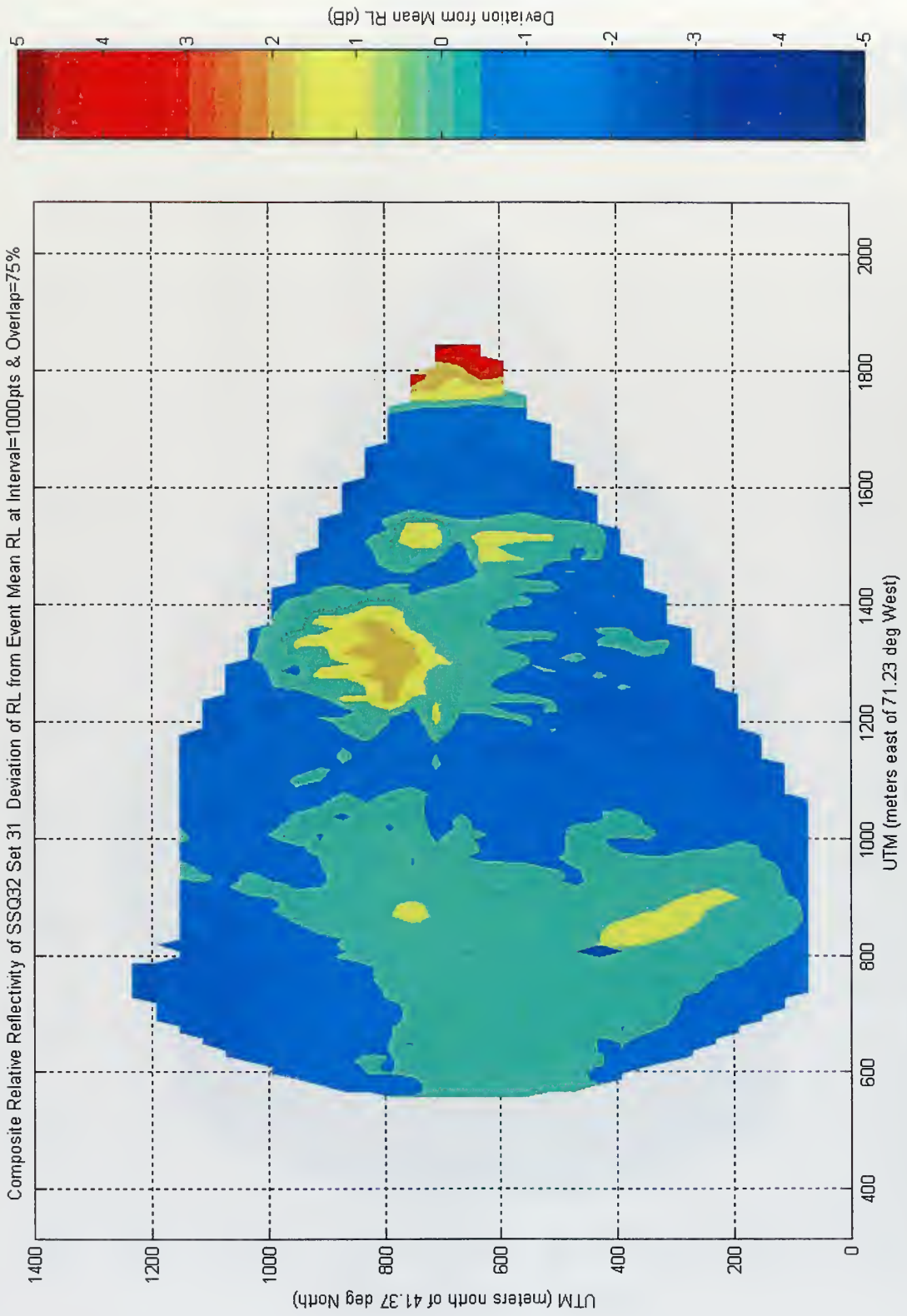

Figure 33. Composite plot of sequence of pings (Set 1) from Event 3.

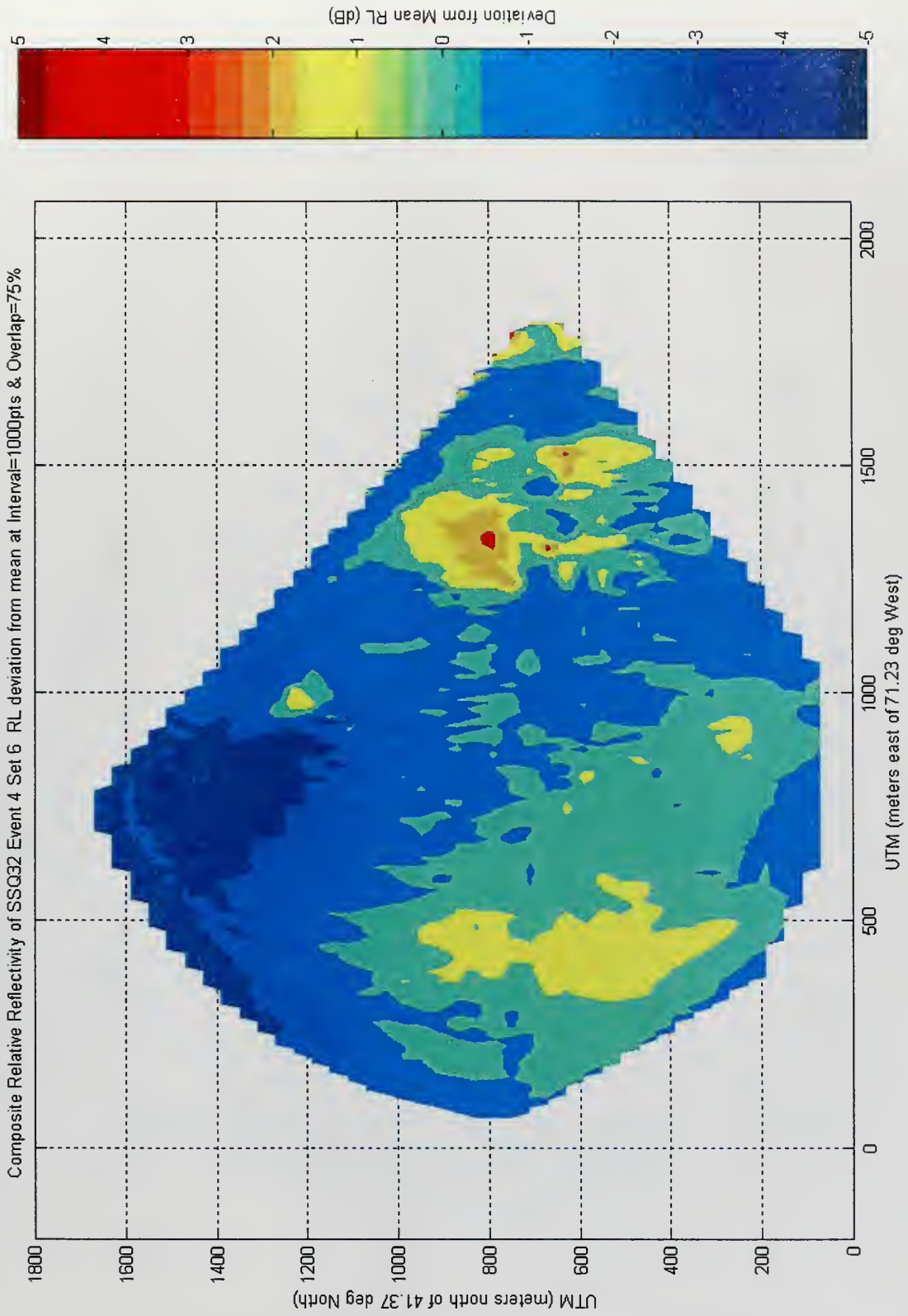

Figure 34. Composite plot of sequence of pings (Set 6) from Event 4.

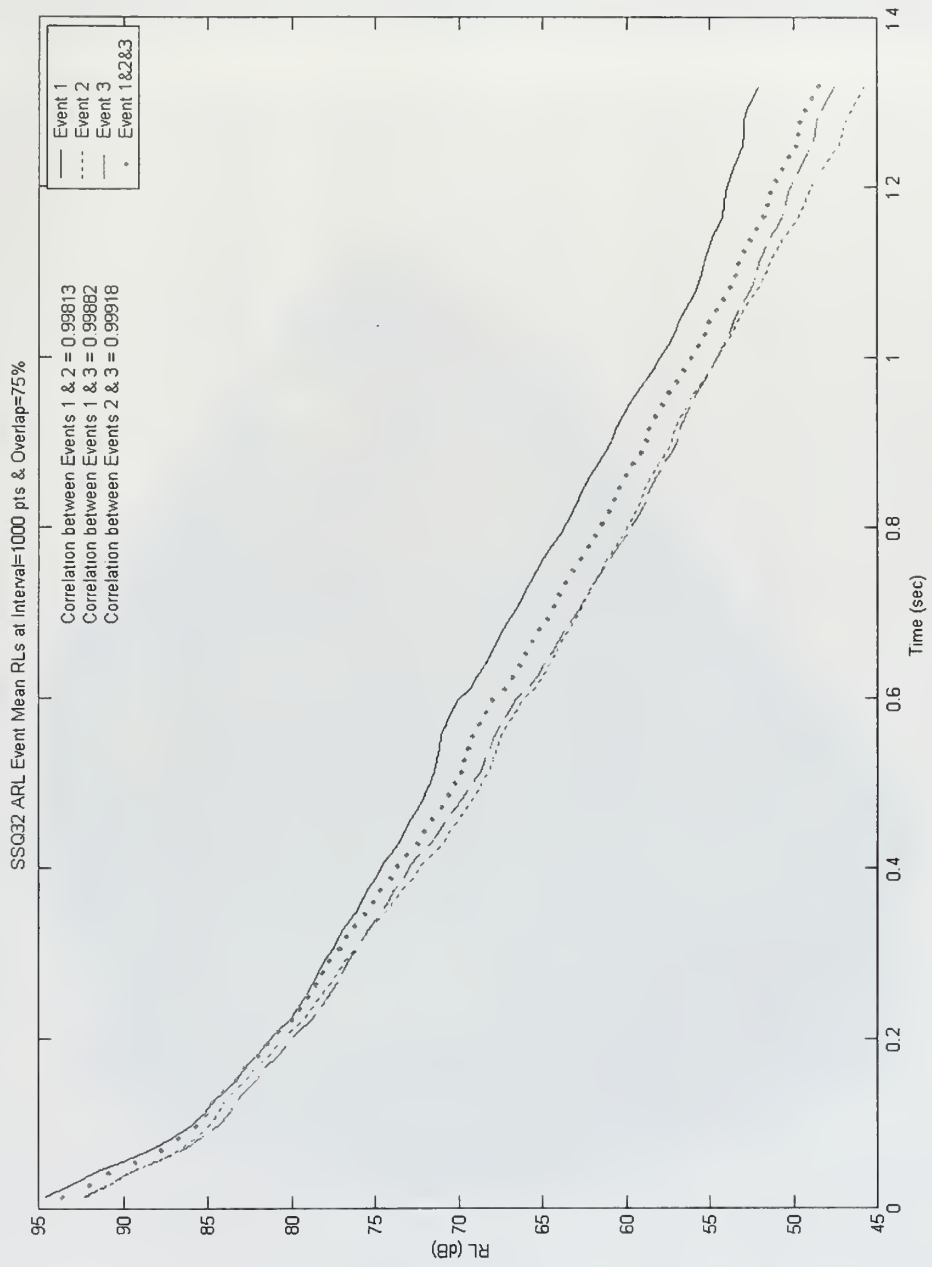

Figure 35. Event non-normalised mean RL curves for Events 1, 2, 3, and all three combined.

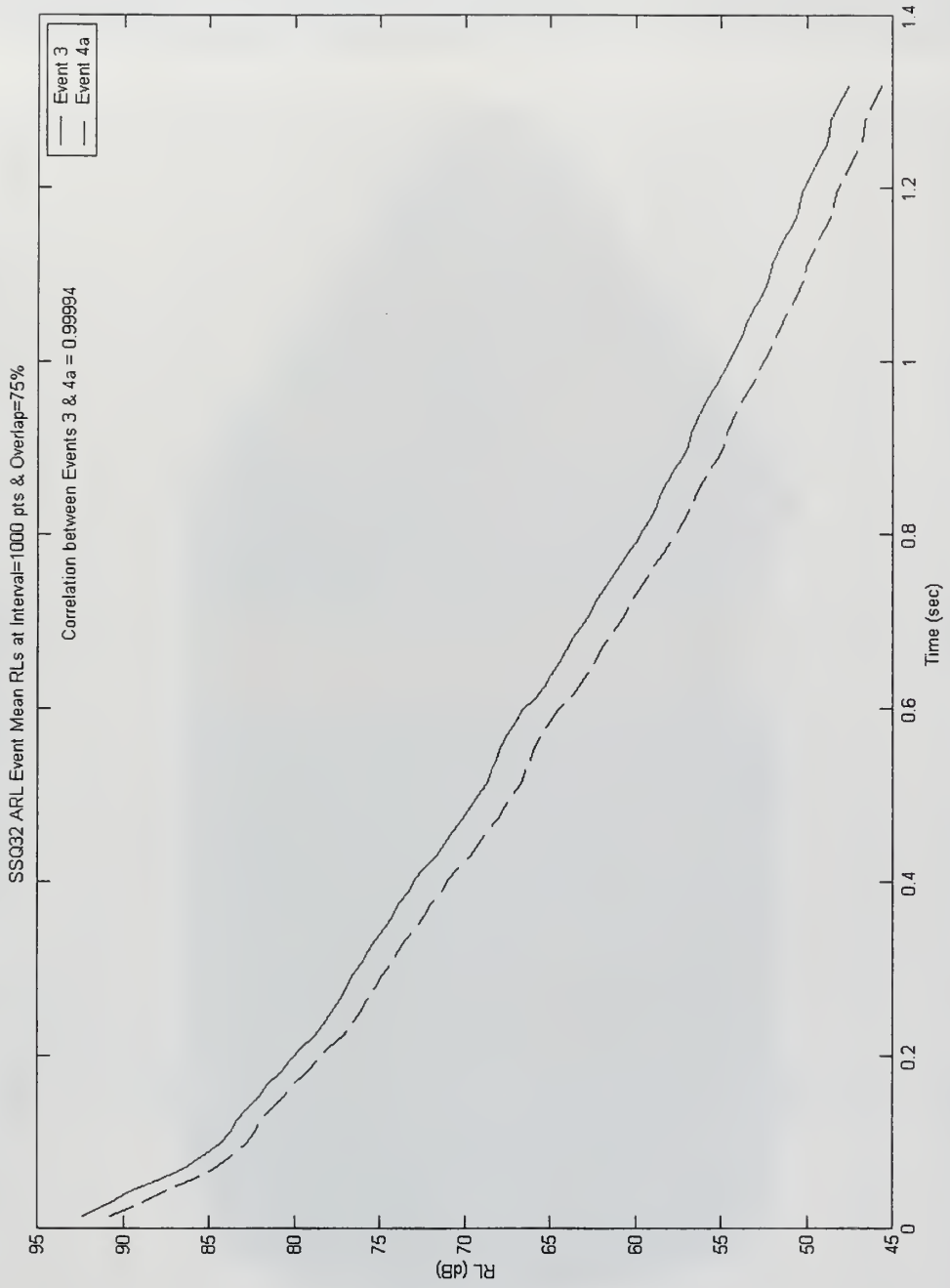

Figure 36. Event mean RL curves for Events 3 (solid) and 4a (dashed).

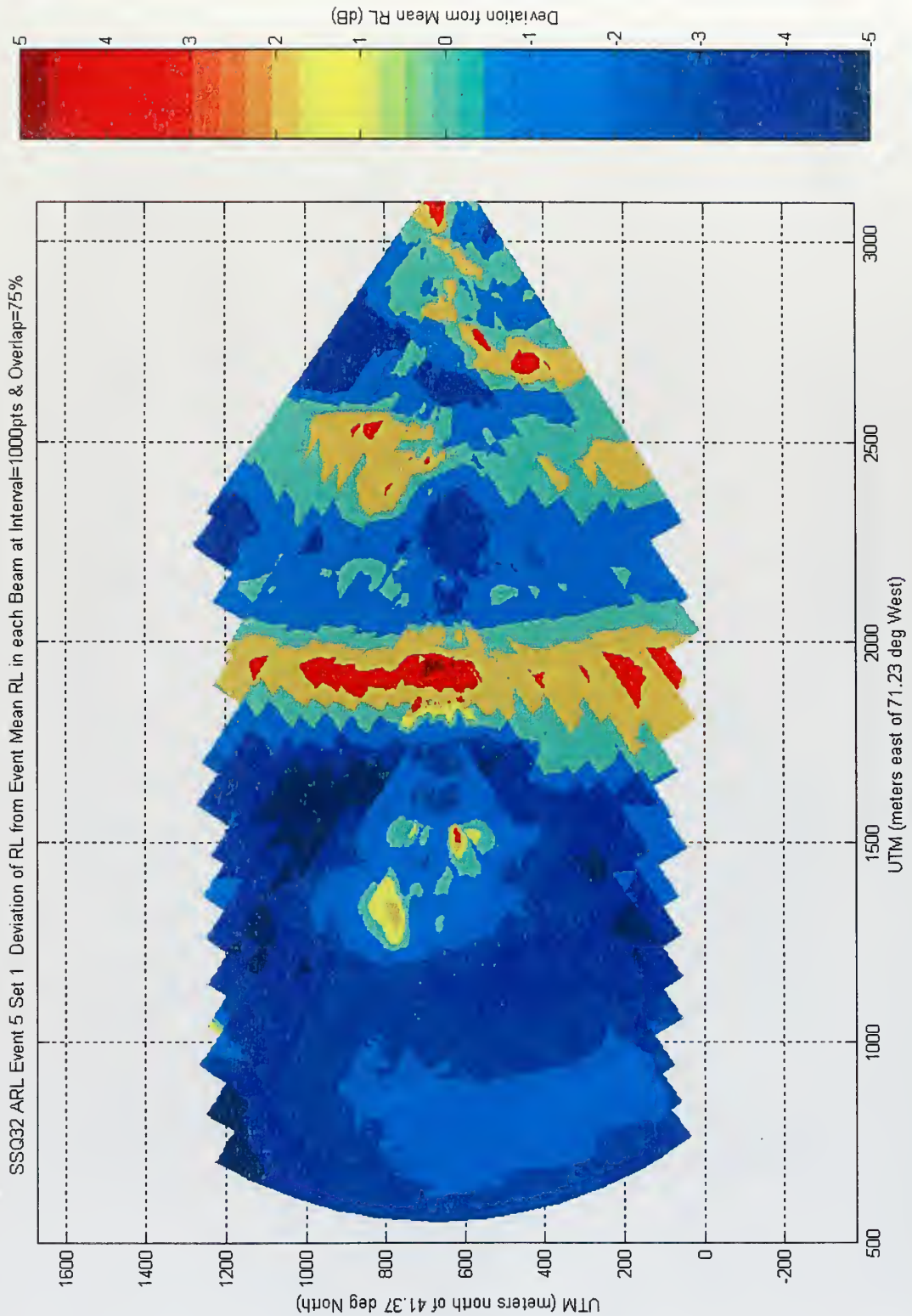

Figure 37. Overlay of contour plots from sequence of pings (Set 1) from Events 1, 2 and 3.

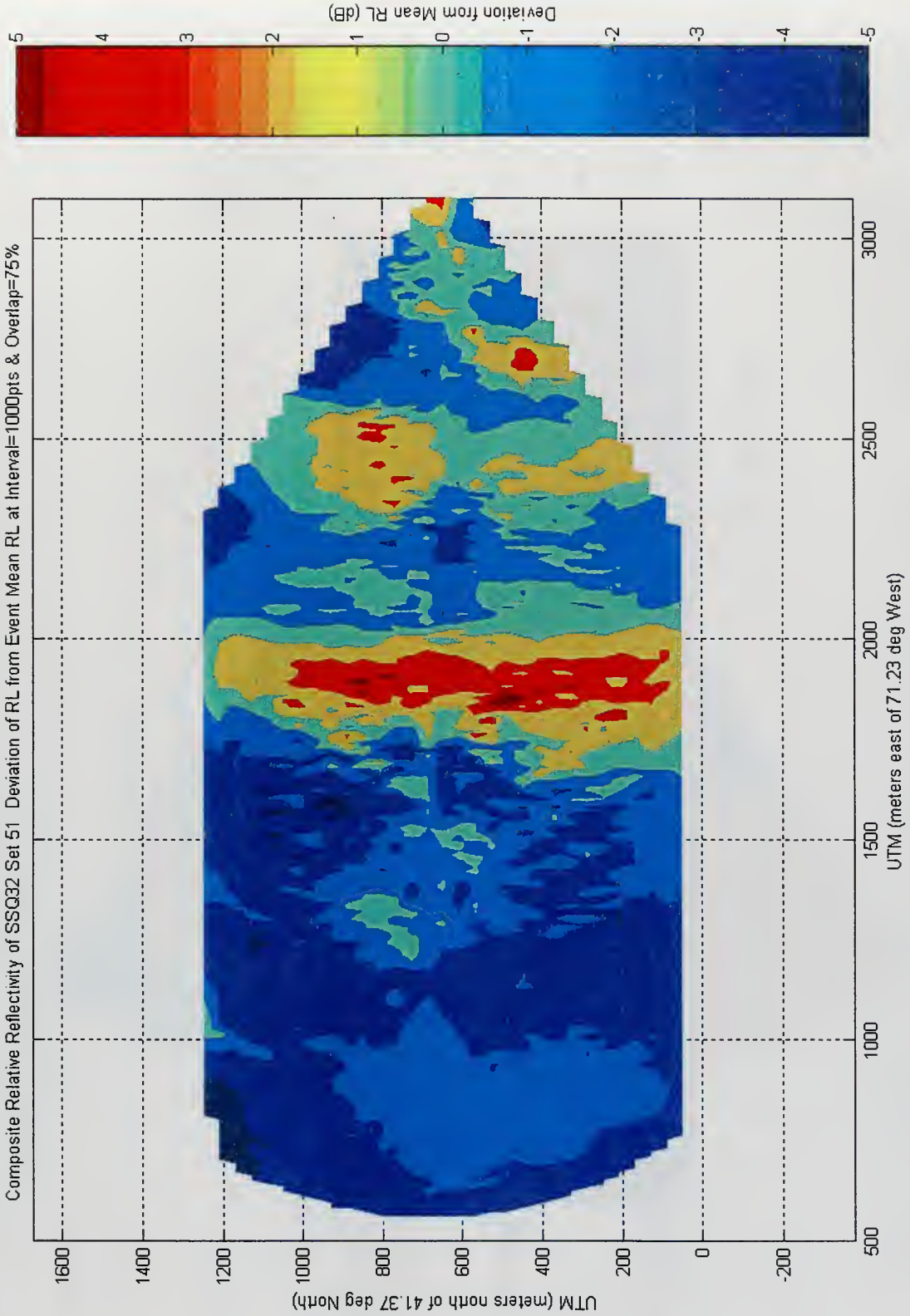

Figure 38. Composite plot of sequence of pings from Events 1, 2 & 3.

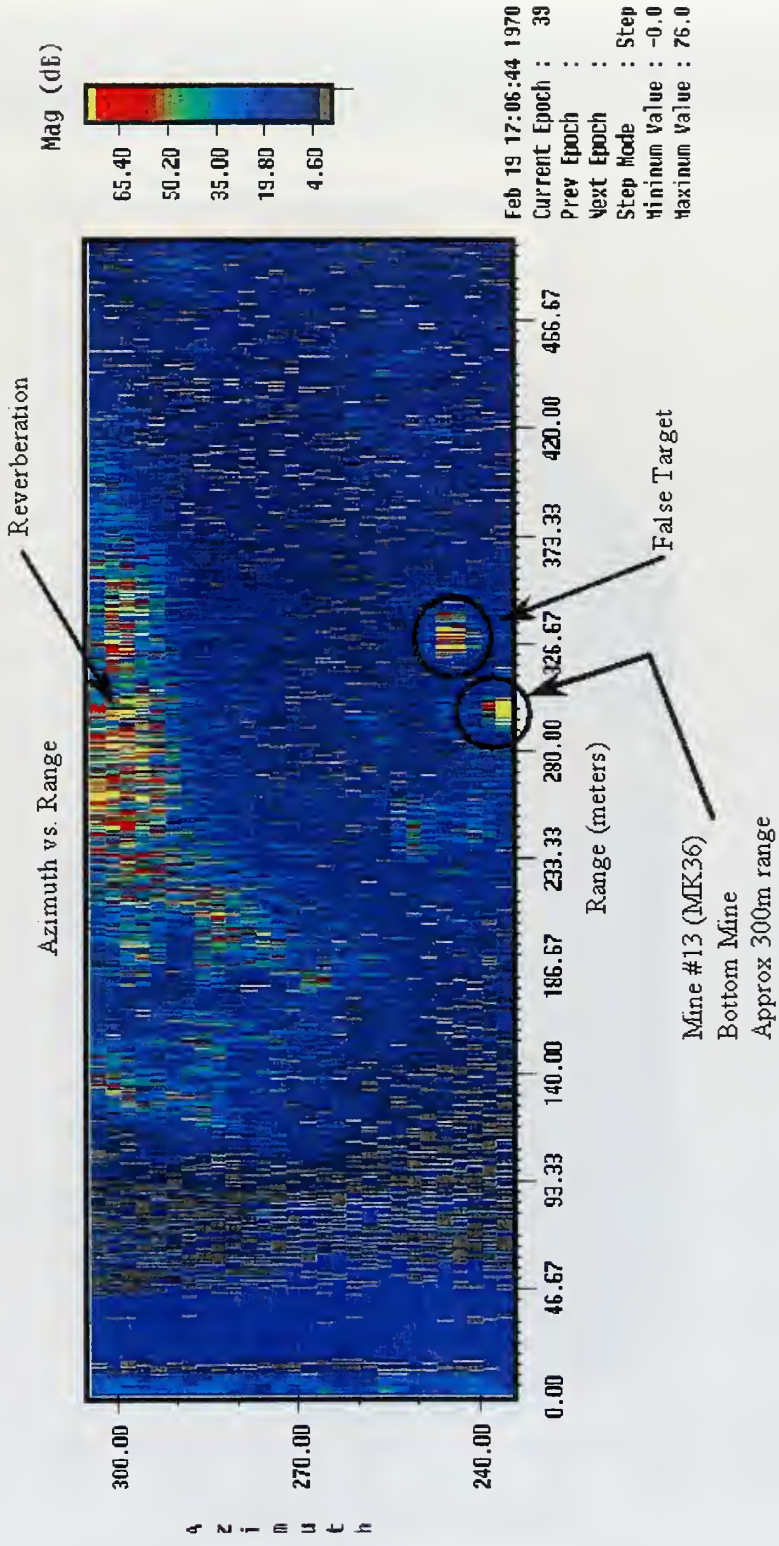

Figure 39 Mine 13 displayed in existing sonar display (from Wilson et al, 1996).

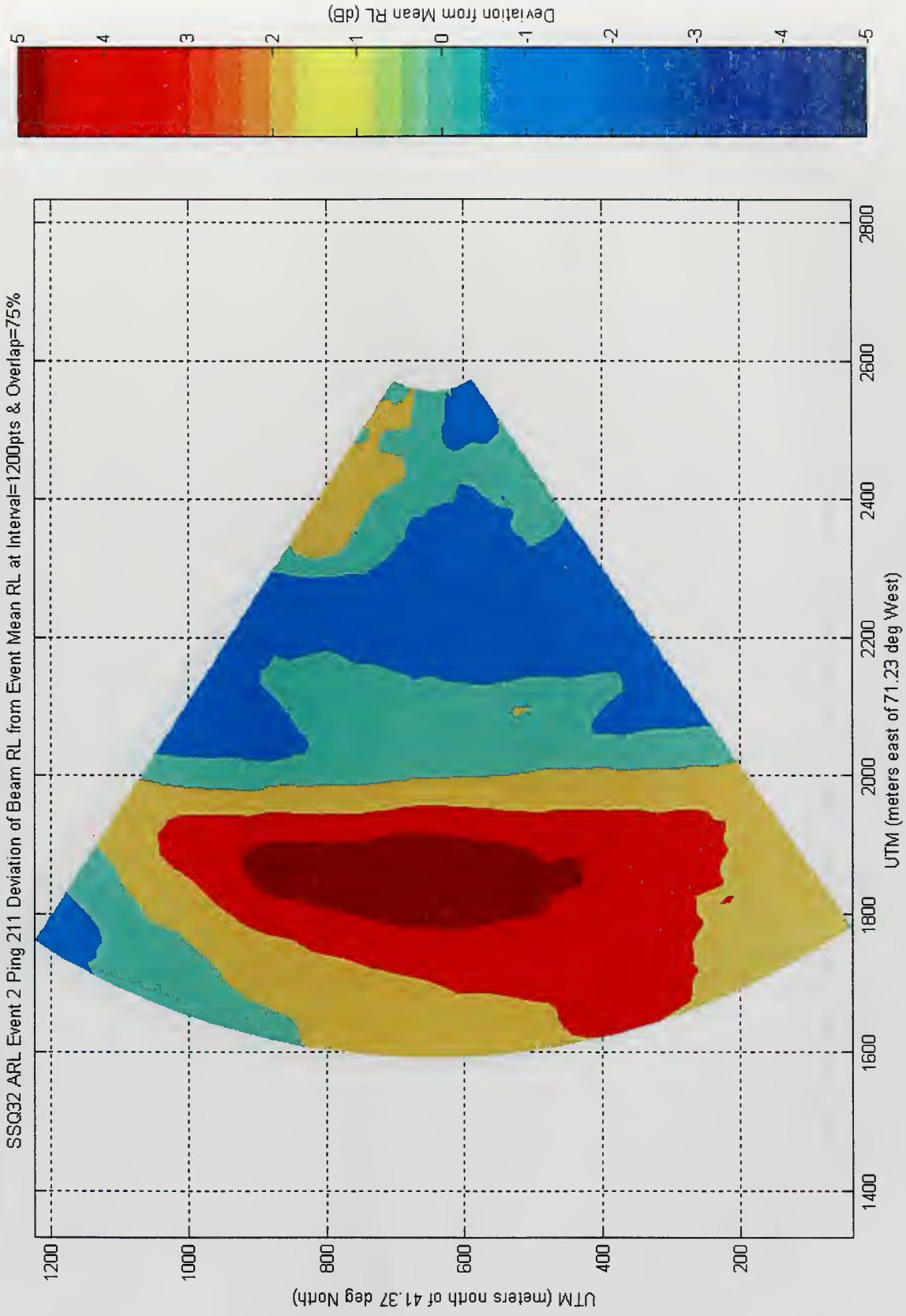

Figure 40 Contour plot of Ping 211's relative reflectivity at interval of 1200.

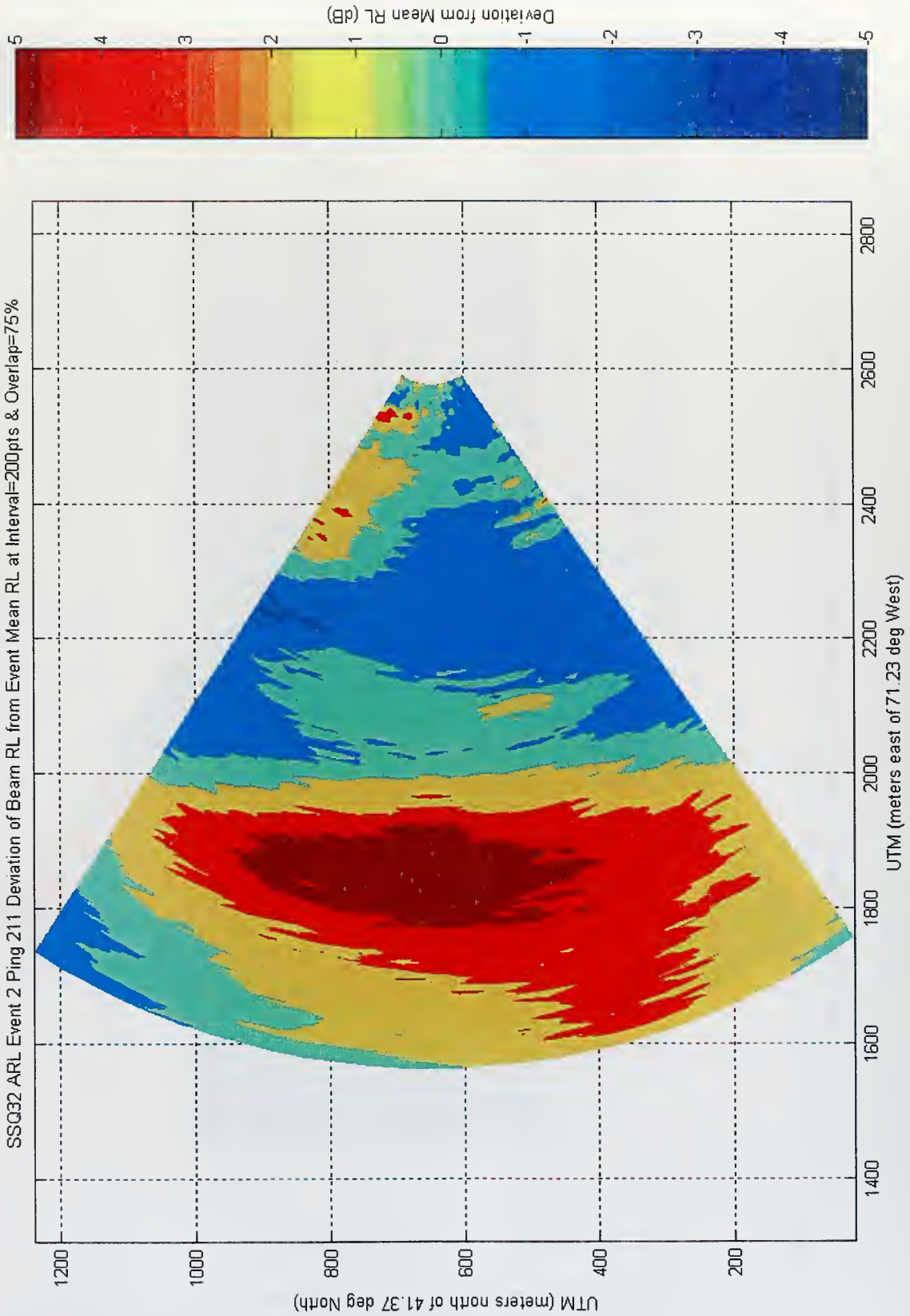

Figure 41 Contour plot of Ping 211's relative reflectivity at interval of 200.

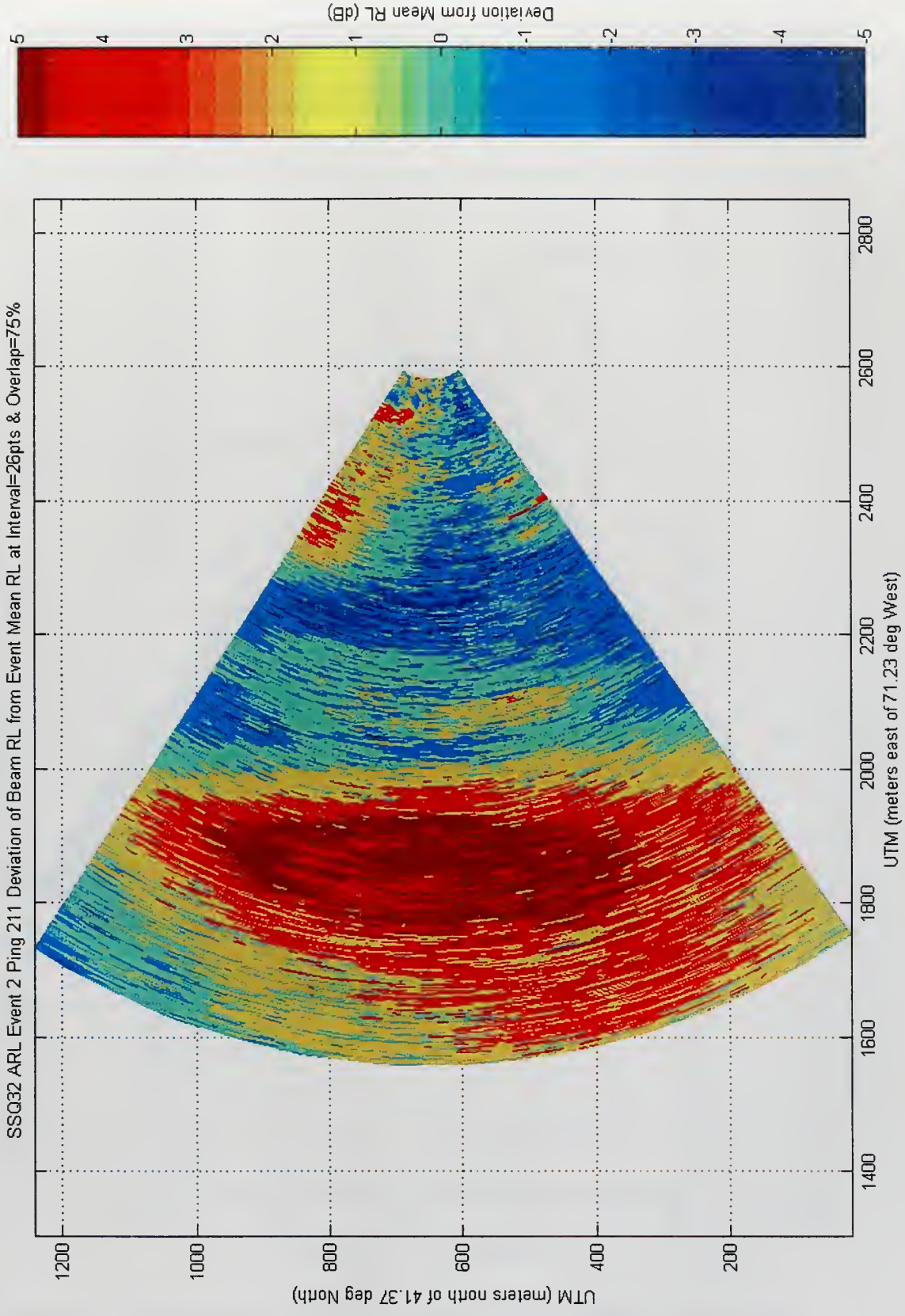

Figure 42 Contour plot of Ping 211's relative reflectivity at interval of 26.

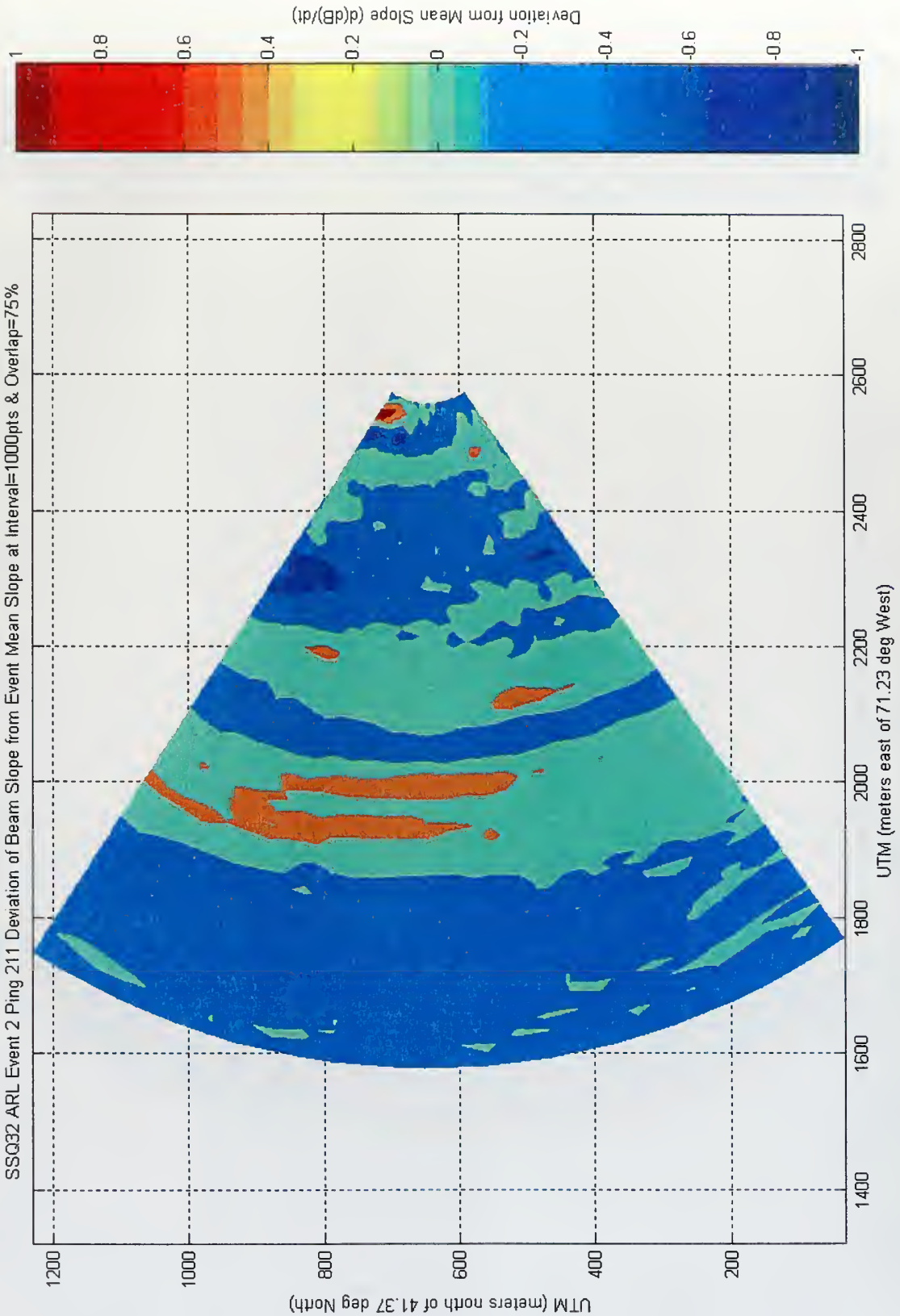

Figure 43 Contour plot of Ping 211's deviation of slope of RL from event-wide (Event 1) mean slope of RL.

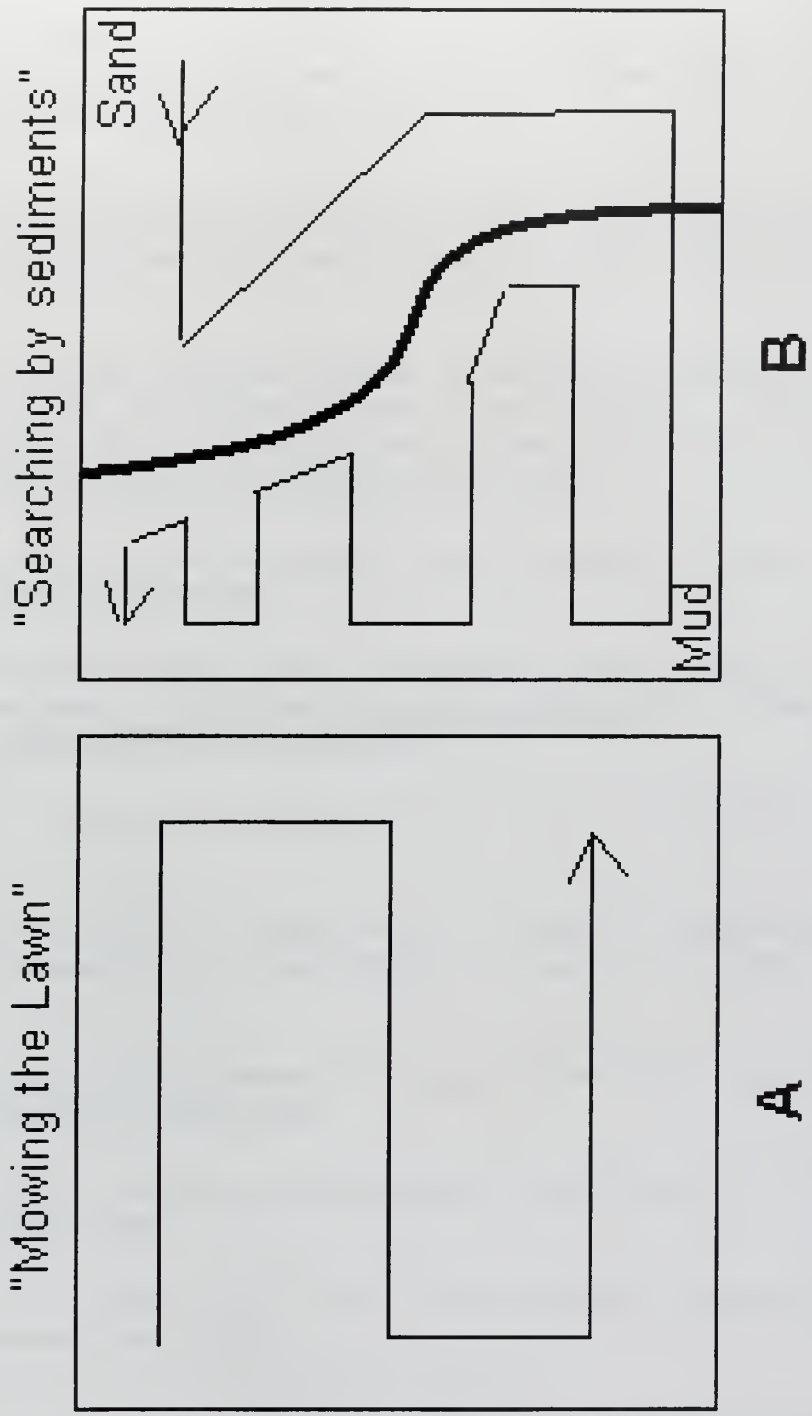

Figure 44. Traditional search plan (A) versus new approach (B) with increased knowledge of environment (from Schlam 1999).

THIS PAGE INTENTIONALLY LEFT BLANK

LIST OF REFERENCES

Applied Oceanography and Meteorology Centre (AOMC), Royal Navy, *Training Publication in Oceanography and Acoustics for Mine Warfare*, unpublished manuscript, HMS DRYAD, Southwick, UK, 1999.

Boehme, H., N. P. Chotiros, L. D. Rolleigh, S. P. Pitt, A. L. Garcia, T. G. Goldsberry, and R. A. Lamb, "Acoustic Backscattering at Low Grazing Angles from the Ocean Bottom. Part I. Bottom Backscattering Strength." *J. Acoust. Soc. Am.*, 77, 962-974, 1985.

Chotiros, N. P., "High Frequency Acoustic Ocean Bottom Backscatter at Shallow Grazing Angles", in Undersea Defence Technology (UDT) 1992 conference proceedings, Wembley Conference Centre, London, 448 – 453, 30 June - 2 July, Microwave Exhibitions and Publishers, London, 1992.

Friedman, N., *The Naval Institute Guide to World Naval Weapon Systems*, p 331, U.S. Naval Institute, Annapolis, 1997.

Gomes, B.R., J.K. Fulford and R. Nero, "Environmental Characterization for the Littoral Warfare Advanced Development Experiment (LWAD 99-1)," Naval Research Laboratory, NRL/MR/7184—99-8218, 1998.

Hamilton, E. L., "Geoacoustic Modelling of the Sea Floor", *J. Acoust. Soc. Am.*, 68(5), 1980.

Jackson, D. R., A. M. Baird, J. J. Crisp, and P. A. G. Thomson, "High Frequency Bottom Backscatter Measurements in Shallow Water", *J. Acoust. Soc. Am.*, 80(4), 1188-1199, 1986.

Jane's Underwater Warfare Systems, Watts, A. J., editor, 12thed., Jane's Information Group, Alexandria, Virginia, 2000.

Komar, P. D., *Beach Processes and Sedimentation,* Second Edition, p 53, Prentice Hall Inc., New Jersey, 1998.

Lathrop, J. D., "High Area Rate Reconnaissance (HARR) and Mine Reconnaissance/Hunter (MR/H)."
[http://www.ncsc.navy.mil/CSS/papers/harrmrhspie.htm]

Mackenzie, K.V., "Bottom Reverberation for 530 and 1030 cps Sound in Deep Water," *J. Acoust. Soc. Am.*, 33, 1498-1504, 1961.

McMaster, R. L., "Sediments of Narragansett Bay System and Rhode Island Sound, Rhode Island", *J. Sedimentary Petrology*, 30, 249-274, 1960.

Medwin, H., "Acoustical Determinations of Bubble-size Spectra", *J. Acoust. Soc. Am.* 62(4), 1041-1044, October 1977.

Medwin, H., and C.S. Clay, *Fundamentals of Acoustical Oceanography*, 1, Academic Press, Boston, 1998.

McCammon, D.F. "Low Grazing Angle Bottom Scattering Strength: Survey of Unclassified Measurements and Models and Recommendations for LFA Use," *US Navy Journal of Underwater Acoustics,* 43, 33-46, 1993.

McKinney, C. M., and C. D. Anderson, "Measurements of Backscattering of Sound from the Ocean Bottom", *J. Acoust. Soc. Am.,* 36, 1, 158-163, 1964.

Milliman, J. D., O. H. Pilkey and D. A. Ross, "Sediments of the Continental Margin of the United States", *Geol. Soc. Bull.,* 83, 1315-1334, 1972.

Milliman, J. D., and R. H. Meade, "World-wide Delivery of River Sediment to the Oceans", *J. Geol.,* 91, 1-21, 1983.

National Data Buoy Centre (NDBC), Station Information
[http://www.ndbc.noaa.gov/station_page.phtml?$station=44025], Aug 2000

National Geophysical Data Center (NGDC), Marine Geology and Geophysics Division, "Marine Trackline Geophysics and Hydrographic Survey Data", CD ROM set U S Department of Commerce, National Oceanic and Atmospheric Administration, National Environmental Satellite, Data and Information Service,. Ver 3.3.

National Oceanic and Atmospheric Administration (NOAA), *Narragansett Bay*, Nautical Chart 13221, U.S. Dept of Com., Washington DC, 1998.

NAVOCEANO, "Mine Warfare Pilot (MWP): New London CT-Newport RI Approaches",
[http:www.navo.navy.smil.mil], Aug 2000.

Neumann, P., and G. Muncill, "Bottom Scattering Inversion, PMW-185 Inversion Technique R&D Kick-Off Meeting," METOC Technology Division, Planning Systems Inc., McLean, VA, 11 August 1999.

Nolle, A. W., "Acoustical Properties of Water-Filled Sands," *J. Acoust. Soc. Am.* 35(9), 1394-1408, Sept, 1963

Null, J. M., "Fleet Battle Experiment Hotel Sensor Data Integration", unpublished manuscript, Neptune Sciences, Inc., San Diego, 2000.

Null J. M., "Perturbative Inversion of Geoacoustic Parameters in a Shallow Water Environment", Master's Thesis, Naval Postgraduate School, Monterey, 1996.

Null, J. M. and J. H. Wilson, "Sediment Classification Using Inversion Techniques (ITs) From Both Mine Warfare (MIW) and ASW Sonar Systems", unpublished manuscript, Neptune Sciences, March, 1999

Osler, J., and C. H. Holland, "High Resolution Geo-Acoustic Models for the Surficial Sediments in the Capraia Basin, Northern Tyrrhenian Sea," SACLANT Undersea Research Centre, Le Spezia, Italy, 1997.

Pitt, S.P., Telephone and E-Mail Communication, ARL-UT, Austin, July-August, 2000

Scanlon, G. A., "Estimation of Bottom Scattering Strength from Measured and Modelled AN/SQS-53C Reverberation Levels", Master's Thesis, Naval Postgraduate School, Monterey, June 1995.

Schalm, D. A., "Inversion of Shallow Water Bottom Sediment Properties using AN/SQS-53C Reverberation Level Data from Exercise LWAD 99-1", Master's Thesis, Naval Postgraduate School, Monterey, September 1999.

Stannic, S., K. B. Briggs., P. Fleischer, R. I. Ray and W. B. Sawyer, "Shallow-water High-frequency Bottom Scattering off Panama City, Florida", *J. Acoust. Soc. Am.*, 83, 6, 2134-2144, 1988.

Stannic, S., K. B. Briggs, P. Fleischer, W. B. Sawyer, and R. I. Ray, "High-Frequency Acoustic Back Scattering From a Coarse Shell Ocean Bottom", *J. Acoust. Soc. Am.*, 85, 1, 125-136, 1989.

Tucholke, B. E., 'Submarine Geology', in "The Marine Environment of the U.S. Atlantic Continental Slope and Rise", J. D. Milliman and W. R. Wright, editors, 56-114, Jones and Bartlett Pub. Inc., Boston, 1987.

Turgut, A., and T. Yamamoto, "Measurements of Acoustic Wave Velocities and Attenuation in Marine Sediments", *J. Acoust. Soc. Am.* 87(6), 2376-2382, 1990.

Urick, R. F., "The Backscattering Strength of Sound from a Harbor Bottom", *J. Acoust. Soc. Am.* 26(2), 231-235, 1954.

Urick, R. F., *Principles of Underwater Sound,* 3d ed., p. 19, McGraw-Hill Inc, 1983.

Westwood, E.K., and P.J. Vidmar, "Eigenray Finding and Time Series Simulation in a Layered-Bottom Ocean," *J. Acoust. Soc. Am.*, 81, 912-924, 1987.

Wilson, J. H. and J. P. Fabre, "Performance Improvement Study, Design and Proposed Testing of Implementation of Inverse Beamforming (IBF) into High Frequency Minehunting Sonar Systems", Small Business Innovative Research Program Topic N94-160, Neptune Sciences, September 1995.

INITIAL DISTRIBUTION LIST

1. Defense Technical Information Center 2
   8725 John J. Kingman Road, Suite 0944
   Ft. Belvoir, VA 22060-6218

2. Dudley Knox Library 2
   Naval Postgraduate School
   411 Dyer Road
   Monterey, CA 93943-5101

3. Chairman (Code OC/GD) 1
   Department of Oceanography
   Naval Postgraduate School
   Monterey, CA 93943

4. Dr. Robert H. Bourke (Code OC/BF) 1
   Department of Oceanography
   Naval Postgraduate School
   Monterey, CA 93943

5. Dr. James H. Wilson 1
   Neptune Sciences, Inc.
   4250 Pacific Hwy., Suite 219
   San Diego, CA 92110

6. Director of Naval Surveying, Oceanography and Meteorology 1
   Room 2384
   Ministry of Defence Main Building
   Whitehall
   London
   SW1A 2HW
   United Kingdom
   Attn: DNSOM/M

7. British Defence Staff 1
   British Embassy
   3100 Massachusetts Ave., NW
   Washington DC 20008-3688
   Attn: SWO(U)

8. Defence Evaluation and Research Agency 1
DERA Bincleaves
Newton's Rd
Weymouth
Dorset
DT4 8SB
United Kingdom
Attn: Head of Innovative Research (Mr G Heald)

9. Cmdre MFP 1
Lancelot Building
Postal Point 29A
HM Naval Base
Portsmouth
Hampshire
PO13 NH
United Kingdom
Attn: SANO

10. COMINEWARCOM 1
325 5th St
NAS Corpus Christi
Corpus Christi
Texas, 78419
Attn: N80 (Scott Burleson)

11. Applied Research Labs 1
The University of Texas at Austin
P.O. Box 8029
Austin
Texas 78753-8029
Attn: Mr S P Pitt

12. Naval Oceanographic Office 1
Stennis Space Center,
Mississippi, 39522
Attn: Mr S Haeger

13. Lt Cdr H R G Howell RN 1
300 Glenwood Circle, #231
Monterey, CA, 93940